Mathematical Modeling of Oxygen Transport, Cell Killing and

Cell Decision Making in Photodynamic Therapy of Cancer

by

Ioannis Gkigkitzis

October 2012

Director of Dissertation: Dr. Xin-Hua Hu

Major Department: Physics

Abstract

In this study we present a model of in vitro cell killing through type II Photodynamic Therapy (PDT) for simulation of the molecular interactions leading to cell death in time domain in the presence of oxygen transport within a spherical cell. By coupling the molecular kinetics to cell killing, we develop a modeling method of PDT cytotoxicity caused by singlet oxygen and obtain the cell survival ratio as a function of light fluence or initial photosensitizer concentration with different photon density or irradiance of incident light and other parameters of oxygen transport. A systems biology model is developed to account for the detailed molecular pathways induced by PDT treatment leading to cell killing. We derive a mathematical model of cell decision making through a binary cell fate decision scheme on cell death or survival, during and after PDT treatment, and we employ a rate distortion theory as the logical design for this decision making proccess to understand the biochemical processing of information by a cell.

Rate distortion theory is also used to design a time dependent Blahut-Arimoto algorithm of three variables where the input is a stimulus vector composed of the time dependent concentrations of three PDT induced signaling molecules and the output reflects a cell fate decision. The concentrations of molecules involved in the biochemical processes are determined by a group of rate equations which produce the probability of cell survival or death as the output of cell decision. The modeling of the cell decision strategy allows quantitative assessment of the cell survival probability, as a function of multiple parameters and coefficients used in the model, which can be modified to account for heterogeneous cell response to PDT or other killing or therapeutic agents. The numerical results show that the present model of type II PDT yields a powerful tool to quantify various processes underlying PDT at the molecular and cellular levels and to interpret experimental results of in vitro cell studies. Finally, following an alternative approach, the cell survival probability is modeled as a predator - prey equation where predators are cell death signaling molecules and prey is the cell survival. The two models can be compared to each other as well as directly to the experimental results of measured molecular concentrations and cell survival ratios for optimization of models, to gain insights on in vitro cell studies of PDT.

Mathematical Modeling of Oxygen Transport, Cell Killing and Cell Decision Making in Photodynamic Therapy of Cancer

A Thesis/Dissertation

Presented To the Faculty of the Department of Physics

East Carolina University

In Partial Fulfillment of the Requirements for the Degree

Doctor of Philosophy

by

Ioannis Gkigkitzis

October, 2012

Mathematical Modeling of Oxygen Transport, Cell Killing and Cell Decision making in Photodynamic Therapy of Cancer

by

Ioannis Gkigkitzis

APPROVED BY:
DIRECTOR OF DISSERTATION/THESIS:_____
Xin Hua Hu, Ph.D.

COMMITTEE MEMBER: _____
Jun Qing Lu, Ph.D.

COMMITTEE MEMBER: _____
Michael Dingfelder, Ph.D.

COMMITTEE MEMBER: _____
Said Said, Ph.D.

COMMITTEE MEMBER: _____
Zhibin Huang, Ph.D.

CHAIR OF THE DEPARTMENT OF _____
John C. Sutherland, Ph.D.

DEAN OF THE GRADUATE
SCHOOL_____
Paul J. Gemperline, Ph.D.

Dedication

This thesis is dedicated to the more honorable than the Cherubim,and beyond compare more glorious than the Seraphim, the Theotokos. “I am the true vine, and my Father is the vinedresser…”(John, 15:1).

Acknowledgements

This work would not have been possible without encouragement of my advisor Dr. Xin Hua Hu, under whose supervision, I chose this topic and began my thesis. I would like to express my sincere gratitude to him for the continuous support of my Ph.D study and research, for his patience, motivation, enthusiasm, and immense knowledge. His guidance helped me in all the time of research and writing of this thesis. I could not have imagined having a better advisor and mentor for my Ph.D study. Besides my advisor, I would like to thank the rest of my thesis committee: Dr. Jun Qing Lu for being a great teacher, the Assistant Chair for Graduate Studies Dr. Michael Dingfelder who has been a wonderful supervisor for all graduate students of the Physics Department, Dr. Said Said, for whom I have very high regards and whom I consider a very close friend of mine, Dr. Zhibin Huang for kindly accepting my invitation and being willing to be a member of my committee, and finally Dr. Sutherland, chairman of the Physics Department, who gave me very valuable advice from his vast experience in the field. Their encouragement and insightful comments were very helpful.

I would like to express my appreciation and respectful gratitude towards Dr. Paul J. Gemperline, Dean of the Graduate School, and Associate Dean Heather Ries, for being so understanding and supportive at some very important and critical moments of my graduate studies. I thank my collaborator Dr. Carlos Austerlitz for the stimulating discussions, for the sleepless nights we were working together before deadlines, and for all the fun we have had, for all the things he taught me and for his valuable friendship. Also, I thank my officemate in the Physics Department Marina Moran for our friendship and mutual support.

I would like to express my very sincere gratitude to Dr. Michael Spurr, Brenda Mortion, Marhatta Pragya and Gwen Hardin for the support to make this thesis possible. These persons have been abundantly helpful and have assisted me in numerous ways, opening for me the road to success. I am also very thankful to Dr. Thomas Mc Connel and Dr. Johannes Hattingh, Chairmen of the Mathematics Department, for their continuous willingness to help me complete my degree and constant encouragement. I am very grateful to both of them.

Finally, I take this opportunity to express the profound gratitude from my deep heart to my my father Αναστασιο, my brother Τεο and my sister Κατερινα, τον γεροντα μου Πατέρα Νεκτάριο and my beloved γερόντισσα Αγνή και τη συνοδεία αυτής, especially αδερφή Χρυσοβαλάντου (my adopted mother) and Μισέλ for their love and continuous support – both spiritually and materially, for their generous care and the home feeling whenever I was in need during my studies. Without their “ευλογία” this work would not have been possible. Their unflinching courage will always inspire me.

TABLE OF CONTENTS

LIST OF SYMBOLS OR ABBREVIATIONS

$^3O_2$	Triplet state oxygen
$^1O_2$	Singlet oxygen state
D_d	Diffusion coefficient in depletion zone
D_s	Diffusion coefficient inside spheroid
∇^2	Laplace operator
$C(r,t)$	Oxygen concentration
$\partial/\partial t$	Time derivative
$\Gamma(r,t)$	Rate of oxygen consumption
r	Radial distance
R_d	Radius of depletion zone
R_s	Radius of spheroid
Γ_{PDT}	Rate of oxygen consumption due to PDT
Γ_0	Rate of oxygen consumption constant
k_{ot}	Monomolecular decay rate of excited sensitizer triplets to their ground state
k_p	Bimolecular rate of triplet sensitizer quenching by ground state oxygen
$[A]$	Concentration of intracellular targets
I_a	Photon absorption
ϕ_t	Photosensitizer triplet yield
S_Δ	Photosensitizer triplet quenching
$\partial/\partial r$	Radial derivative
C_m	Consumption of oxygen in the medium far from the sphere
D	Fluence
a	Bleaching coefficient
ρ	Density
σ_{psa}	Absorption cross-section
δ	Survival ratio
N_s	Concentration of the substratum
X	The concentration of intact (alive) cells
a_0	Sensitivity of cells of a particular type to the photodynamic action
t_{ox}	Sensitivity of cells of a particular type to the photodynamic action
k_{ox}	Coefficient of the sensitivity
K_m	Michaelis-Menten constant

V	Maximum reaction rate
M	Cell permeability coefficient
x , y	Amount of molecular species
v_i	Production/consumption rates of self-organized criticality model
V_i	Michaelis Menten coefficient for the bistable switch model
M_i	Michaelis Menten coefficient for the bistable switch model
$R(D)$	Rate-distortion function
A_M	Alphabet
X	Random variable
$E(f)$	Expected value of density function f
$i(j)$	Self-information
$P(j)$	Probability distribution
$P(j,k)$	Joint probability distribution
$A_M \times A_N$	Product space
$P(j\|k)$	Input conditional probability distribution
$Q(j\|k)$	Output conditional probability distribution
$i(j\|k)$	Conditional self-information
Y	Random variable
$i(j,k)$	Mutual information
$d(j,k)$	Distortion measure
$d(Q)$	"Average" distortion associated with this conditional probability
$I(Q)$	"Average" mutual information associated with this conditional probability
D	Upper bound of distortion
Q_D	set of all D admissible strategies
$J(Q)$	Mutual information augmented functional
s	Lagrange multipliers
μ_j	Lagrange multipliers
E	Molecular species for the mass action paradigm
S	Molecular species for the mass action paradigm
k_i	Interaction coefficient for the mass-action paradigm
κ_i	Interaction coefficient for the mass-action paradigm
γ_i	Coefficient of timescale
F	Sigmoidal function
W_i	Net effect on molecule i of all molecules in the network
σ	Parameter that controls the steepness of the sigmoidal function
ω_{ij}	Coefficients of net effect

p_X	Stimulation probability
q	Cell survival probability
$Q_{Y\|X}$	Conditional probability (“strategy”)
$I(X,Y)$	Average mutual information
$H(Y)$	Prior uncertainty of Y the receiver has about the sender's signal X
$H(Y\|X)$	Uncertainty of Y after receiving information about the sender's signal X
η_ε	“Bump function” mollifier
c	Updating factor for the survival probability in the Blahut Arimoto algorithm
T_U	Upper bound for the accuracy of the Blahut Arimoto algorithm
T_L	Lower bound for the accuracy of the Blahut Arimoto algorithm
L	Lagrange function
λ	Lagrange multiplier
g	Constraint of the Lagrange Multipliers
$V_{potential}$	Potential of the Lagrange multipliers
p	Probability of survival
v	Constant that measures the deviation of the functional response from linear
b	Linear coefficient in the survival probability
ϕ	Michaelis Menten response of significance of prey size to survival probability
H	Prey size for which the predation rate is half-maximum
r	Predation rate
σ_{x_i}	Standard deviation
$f(x_i)$	Probability density function
N	Probability of survival (cell)
V_i	Maximum predator attack rate
K_i	Prey density where the attack rate is half-saturated

LIST OF TABLES

LIST OF FIGURES

- **Figure 3.8.2** Time dependence of the solution vector at the cell boundary $(r = r_0)$ using two spatial meshes of 10-step and 40-step: (a) and (c): normalized concentrations of ground-state molecules; (b) and (d): normalized concentrations of excited molecules. All parameters and coefficients are of the same values as those in Fig. 3.8.1.
- **Figure 3.8.3.** Time dependence of the solution vector at the middle of the cell $(r = \frac{r_0}{2})$ using the 40-step mesh and $D = 8 \times 10^{-6} (cm^2 / s)$ and $D' = 2.00 \times 10^{-5} (cm^2 / s)$ for different initial oxygen concentration: (a) and (b): $[^3O_2]_i = 5.0 \times 10^{17} (cm^{-3})$; (c) and (d) $[^3O_2]_i = 7.0 \times 10^{16} (cm^{-3})$. All other coefficients are of the same values as those in Fig. 3.8.1.
- **Figure 3.8.4.** The decay constants of (a) t_S and (b) t_R versus the initial photosensitizer concentration $[S_0]_i$ and photon density ρ at the cell center $(r = 0)$. The values of parameters are given by $D = 8 \times 10^{-6} (cm^2 / s)$, $D' = 2.00 \times 10^{-5} (cm^2 / s)$, $M = 2.00 \times 10^{-2} (cm / s)$, $[^3O_2]_i = 7.0 \times 10^{16} (cm^{-3})$ and $V_m = 2.9 \times 10^{18} (cm^{-3} s^{-1})$ with all other coefficients given in the Appendix A.
- **Figure 3.8.5.** The decay constants of t_S and t_R versus the initial photosensitizer concentration $[S_0]_i$ and photon density ρ at the cell center $(r = 0)$ for (a) and (b); at the cell boundary $(r = r_0)$ for (c) and (d). The values

of other parameters and coefficients are the same as those in Fig. 3.8.4 except the following: $D = 8 \times 10^{-7} (cm^2 / s)$, $D' = 2.00 \times 10^{-6} (cm^2 / s)$.

- **Figure 3.8.6.** The decay constants of t_S and t_R versus the initial photosensitizer concentration $[S_0]_i$ and photon density ρ at the cell center $(r = 0)$ for (a) and (b); at the cell boundary $(r = r_0)$ for (c) and (d). The values of other parameters and coefficients are the same as those in Fig. 3.8.5 except the following: $M = 2.00 \times 10^{-5} (cm / s)$.
- **Figure 3.8.7.** The cell survival ratio curves calculated with $V_m = 2.9 \times 10^{18} (cm^{-3} \cdot s^{-1})$ and different photon densities ρ, initial photosensitizer concentrations$[S_0]_i$ and oxygen parameters. From (a) to (d): $\rho_1 = 2.0 \times 10^6 (cm^{-3})$, $\rho_2 = 7.0 \times 10^6 (cm^{-3})$, $\rho_3 = 2.0 \times 10^7 (cm^{-3})$, $[S_0]_i = 7.0 \times 10^{13} (cm^{-3})$. For (e) and (f): $[S_0]_{i1} = 1.0 \times 10^{15} (cm^{-3})$, $[S_0]_{i2} = 7.0 \times 10^{12} (cm^{-3})$, $[S_0]_{i3} = 1.0 \times 10^{12} (cm^{-3})$, $\rho = 5.0 \times 10^6 (cm^{-3})$. Other parameters in (e) and (f) are the same as those in (a) except the following: (f) $D = 8 \times 10^{-7} (cm^2 / s)$, $D' = 2 \times 10^{-6} (cm^2 / s)$. All other coefficients are given in the Appendix A. Each set of curves marked with either ρ or $[S_0]_i$ consists of three lines calculated at different cell locations: solid: $r = 0$; dot: $r = \frac{r_0}{2}$; dash: $r = r_0$.

- **Figure 3.8.8.** Comparison of two calculated cell survival curve sets with the measured data represented by the symbols by Qin *et al*. All parameters used in the numerical calculations are the same as those in Fig. 8(a) except the following: $\beta_0 = 8.0 \times 10^{-2} (s^{-1})$ and $[^3O_2]_i = 4.0 \times 10^{17} (cm^{-3})$. Note that the photon density $\rho = 6.25 \times 10^5 (cm^{-3})$ and $\rho = 2.50 \times 10^6 (cm^{-3})$ corresponds respectively to fluence $F = 75 (mJ/cm^2)$ and $F = 300 (mJ/cm^2)$ while $[S_0]_i = 4.0 \times 10^{12} (cm^{-3})$ corresponds to $20 (\mu g/ml)$ using the molecular mass of Photofrin as $3000 (g/mol)$. Each set of curves marked with ρ consists of three lines calculated at different cell locations: solid: $r = 0$; dot: $r = \frac{r_0}{2}$; dash: $r = r_0$.
- **Figure 4.2.1.** Morphological features of autophagic, apoptotic and necrotic cells. (a) Normal, (b) autophagic, (c) apoptotic (d) and necrotic cells. Whereas the morphologic features of apoptosis are well defined, the distinction between necrotic and autophagic death is less clear. The scale bar represents 1 μm.
- **Figure 4.2.2.** Transmission electron micrographs of monolayer R3327-AT cells treated by in vitro PDT. (a) Non-treated cell with normal appearing

mitochondria, and (b) PDT-treated cell with matrix swelling of mitochondria.

- **Figure 4.3.1.** A schematic representation of the known molecular pathways and biochemical events induced by PDT treatment leading to cell death.
- **Figure 4.6.1.** The dynamic evolution of the stimulus probability vector in the concentration space.
- **Figure 4.6.2.** The time dependent Blahut Arimoto Algorithm
- **Figure 4.7.1.** PARP activation is an immediate cellular response to metabolic, chemical, or radiation-induced DNA SSB damage. Upon DNA cleavage by enzymes involved in cell death (such as caspases), PARP can deplete the ATP of a cell in an attempt to repair the damaged DNA. ATP depletion in a cell leads to lysis and cell death. PARP also has the ability to directly induce apoptosis, via the production of PAR, which stimulates mitochondria to release AIF. This mechanism appears to be caspase-independent.
- **Figure 4.7.2.** Singlet Oxygen is the most important cytotoxic agent generated during PDT(it decays after photo irradiation time). Singlet oxygen is produced during PDT via a triplet-triplet annihilation reaction between

ground state molecular oxygen (which is in a triplet state) and the excited triplet state of the photosensitizer.

- **Figure 4.7.3.** ROS initiates the degradation process of Bcl-2 that could bind to Bax to prevent its activation. At a later time after the photo-irradiation a post-treatment increase of Bax is observed.
- **Figure 4.7.4.** Actived Caspase 3 is potent effector of post-treatment cell apoptosis: For the intrinsic cell death pathway, apoptosis is triggered by intracellular events such as DNA damage and oxidative stress. For the extrinsic cell death pathway, apoptosis is triggered by extracellular stimuli such as TNF and TRAIL. A sharp increase in the levels of Caspase 3 indicates the beginning of apoptosis.
- **Figure 4.7.5.** A sample of a survival probability curves as predicted by the Blahut Arimoto algorithm for the cell model. Value of the parameter $s = -10^{-2}, -10^{-3}, -10^{-4}$ Photon density $\rho = 10^{6} cm^{-3}$. Photo sensitizer (Photofrin) concentration in a cell $[S_0] = 5 \times 10^{13} cm^{-3}$. Single cell oxygen concentration $[^3O_2] = 6.06 \times 10^{17} cm^{-3}$.
- **Figure 5.2.1.** A schematic representation of the idea of survival units modeling. Cell life as a sum of survival (life) units (quantums) , and a life quantum (a “survival probability quantum”) contains life in an embryonic

form that might or might not develop to a 100% probability of survival depending on the state cell (for example, recovery after photo-chemo therapeutic treatment, stress, hyperthermia, etc.).

- **Figure 5.2.2.** The existence of threshold as the link between different aspects of the modeling process.
- **Figure 5.2.3.** Logical design of the steps that may lead to an organic connection of different components of modeling (information, axioms, rate equations) as the new approach to current issues in the foundations of mathematics.
- **Figure 5.2.4.** Cell as a programmable device. The compiler translates the high level language into assembly language. The assembler translates assembly language into object code. The linker builds an executable program from object modules and any library modules required.
- **Figure 5.3.1.** Survival curve (a) $V_1 = 10^{-2}, V_1 = 10^4$, $V_3 = 10^{-6}, R = 10^{-10}$, $K_1 = 10$, $K_2 = 10, K_3 = 10^{-7}$, $w_1 = 10^{-15}, w_2 = 1$, $w_3 = 2 \times 10^4$. Survival curve (b) $V_1 = 10^{-1}$, $V_1 = 10^4$, $V_3 = 10^{-6}$, $R = 10^{-10}$, $K_1 = 10$, $K_2 = 10$, $K_3 = 10^{-7}$, $w_1 = 10^{-15}$, $w_2 = 1$, $w_3 = 2 \times 10^4$. Survival curve (c) $V_1 = 10^{-3}, V_1 = 10^4$, $V_3 = 10^{-6}, R = 10^{-10}$, $K_1 = 10$,

$K_2 = 10$, $K_3 = 10^{-7}$, $w_1 = 10^{-15}$, $w_2 = 1$, $w_3 = 2 \times 10^4$. Survival curve (d) $V_1 = 10$, $V_2 = 1$, $V_3 = 10^{-3}$, $R = 10^{-8}$, $K_1 = 10^{-2}$, $K_2 = 10^{-3}$, $K_3 = 10^{-4}$, $w_1 = 1$, $w_2 = 1$, $w_3 = 1$.

- **Fig.5.3.2.** An logical design application of the Predator-Prey equations for different time domains where different cell death inducers are activated. In a cellular automaton, it will be possible to determine the route of damage. Necrotic and apoptotic cell death proceed in different time scales. Necrosis is a form of cell death that occurs rapidly (minutes) in response to severe insult. Apoptosis is a slower form of death lasting for many hours or days.

License Agreement between Ioannis Gkigkitzis and "John Wiley and Sons"

Licence Numbers:

- 3006210217117 for use (print and electronic) of the graphs,
- 3015140021238 for use (print and electronic) of text extract (8 pages)
- 3015131100615 for use (print and electronic) of the full article

of Gkigkitzis, Y.M. Feng, C.M. Yang, J.Q. Lu, X.H. Hu, Modeling of Oxygen Transport and Cell Killing in Type-II Photodynamic Therapy, Photochemistry and photobiology, 88 (2012) 969-977.

Licennce Number: 3010490498154 for use of the graphs/figures of *Hu, X. H., Y. Feng, J. Q. Lu, R. R. Allison, R. E. Cuenca, G. H. Downie and C. H. Sibata (2005) Modeling of a Type II Photofrin-Mediated Photodynamic Therapy Process in a Heterogeneous Tissue Phantom. Photochem. Photobiol. 81, 1460-1468.*

License Agreement between Ioannis Gkigkitzis and Elsevier

Licennce Number: 3020590563324 for use of one figures (Figure 7 of the reference) of *Moore, R.B., Xiao, Z., Tulip, J., and Chapman, J.D.: 'A comparison of susceptibility to photodynamic treatment between endothelial and tumor cells in vitro and in vivo', Photodiagnosis and Photodynamic Therapy, 2007, 4, (3), pp. 160-169.*

Licennce Number: 3020600074446 for use of figures (Figure 1 of the reference) of *Edinger, A.L., and Thompson, C.B.: 'Death by design: apoptosis, necrosis and autophagy', Current Opinion in Cell Biology, 2004, 16, (6), pp. 663-669.*

CHAPTER 1: INTRODUCTION

1.1 Motivation

The goal of the study of cell decision processes according to National Institute of General Medical Sciences of NIH, is to understand how molecular signaling networks regulate cell life-death decisions in tissues and to apply this understanding to the design and use of therapeutic drugs[1]. Research in this directions aims at proper application of mathematical modeling and experimental techniques that will yield quantitative understanding of cellular decision making processes and their correlations with cellular biochemistry. The validity of mathematical models can only be established by rigorous analysis and comparison with experimental results. Photodyamic therapy (PDT) is a unique case study of system biology in which cell repair and death in response to combined stimulations of photosensitizer and light can be quantitatively investigated and modeled. Therefore, , modeling study of cell killing by PDT serves as an interesting cross point at which information theory of decision making can be combined for analysis of a complex biological system.

PDT uses a photosensitizer, light, and oxygen to create tissue damage. PDT photochemistry depends on the presence of oxygen and tissue oxygen is consumed through photochemical reactions [1] [2] [3]. This phenomenon has been studied by numerous authors and models of in vitro PDT studies are available for cultured cells and multicellular tumor spheroids [4], in relation to light propagation and heat transfer [5], for oxygen levels

[1] Center for Cell Decision Processes (MIT), National Centers for System Biology
http://www.systemscenters.org/centers/center-for-cell-decision-processes/

surrounding a given capillary in relation to the transient behavior of PDT process [6], for PDT in a heterogeneous tissue phantom [7] and others. The oxygen diffusion as an important component of oxygen transport in a single cell spherical model, as well as a detailed intracellular molecular PDT model that would result in biochemical states observed in the principal mechanisms of PDT cell killing, need to be investigated. A complete PDT treated single cell model will not only provide a system that can be used in the design of cellular automata to describe tumor dynamics through the coupling among vascular, cellular and subcellular scales, but will also serve as the background for the stimulation of a goal oriented decision making about cell fate determination during PDT treatment, as described in later chapters.

Living cells posess the striking ability to process information and make decisions[8] [9]. In response to signals from the environment and from other cells, a cell may modulate its behavior either continuously (e.g., changing the level of a molecular concnentration) or in a discrete manner, choosing among a discrete set of predefined behaviors [8]. The motivation of this dissertation is to develop a quantitative and accurate model that describes the behavior of a cell as an information processing system, that will arise not only from a detailed molecular pathway understanding but also from a signal processing approach. This has been the subject of investigation of a growing numbers of researchers and has been characterized as a great challenge of physics today.

1.2 Signicance of this research

This research examines for the first time the effects of oxygen diffusion and transport on the observed kinetics during Photodynamic Therapy in a spherical cell model and also provides a theoretical background for the qualitative and quantitative characterization of different aspects of basic cellular decision making processes. The logical design and computational algorithms consider the decision-making process of a single cell in response to PDT treatment, and can be adjusted to accommodate and provide important insights for other cellular response to other treatments, such as radiation, chemotherapy, neurodegeneration, etc. , by applying the principles introduced here. Moreover, this study includes the introduction of predator prey dynamical systems for the study of PDT survival curves in the time domain and points towards an axiomatic foundation of biological behavior of PDT treated cells, according to the current line of research in the field, that will assess various experimental data.

1.3 Major results

In this dissertation research we:

I. Study and analyze the oxygen diffusion with a spherical cell model in type II PDT taking into account the spatial heterogeneity by adding diffusion and metabolism terms for the investigation of different oxygen diffusion mechanisms through the cell membrane and inside the cell within the context of PDT.

II. Develop a system biology model that includes 70 types of molecules and their detailed pathways and biochemical events induced by PDT treatment leading to cell death and can occur through a multiplicity of different mechanisms such as apoptosis, autophagy, and necrosis.

III. Develop a model of tumor cell decision making in response to PDT by employing rate distortion theory and designing a time dependent three dimensional Blahut-Arimoto algorithm where the source input is a stimulus vector composed by time dependent concentrations siganling molecules as these are determined by the system of the molecular rate equations through interactions, and the output is the probability of cell decision for survival or death.

IV. Develop a theory of cell survival probability in the framework of a predator-prey interaction, employed using the cellular survival density as the prey and potential cell death inducing molecules as the predators.

1.4 Structure of thesis

This thesis contains five chapters.

Chapter 2 presents some basic background. After first providing a brief review of cancer and the history of PDT, it discusses mathematical modeling of the biochemical processes involved in PDT and the historical development. This is then followed by a presentation of

oxygen diffusion in a spherical cell and Michaelis-Menten oxygen uptake kinetics. The section concludes with a discussion of cellular decision making and source coding theory.

Chapter 3 presents the model of oxygen diffusion and its effect on cellular response to type II PDT. The first section presents a brief general introduction to clinical application and modeling, and then the focus shifts to the actual study of the oxygen diffusion in type II PDT. This topic is dealt with using a rate equation group, appropriate boundary conditions, decay constants and a cell killing model. A positive definite test of the solution vector in time-domain is presented.

Chapter 4 presents a model of cellular decision making in response to type II PDT. The first section focuses on the rate distortion theory, as the foundation for consideration of the signal transmission within the cell. The following sections then take up the study of the biochemical events induced by PDT, the mathematical modeling scheme for the formulation of these events, and the logical design for cell decision making that uses the Blahut arimoto algorithm. The chapter concludes with a presentation of simulations results and a discussion of their implications.

Chapter 5 presents the a Predator Prey cell killing model for comparison with the previous rate distortion theory model and available experimental results in the time domain. The chapter contains a discussion on the concection between current mathematical and biological modeling systems in response to the main research need for the development of a new mathematical theory for study of survival curves of PDT treated cell populations. . A discussion of suggested future research direction is included.

Chapter 6 is a summary of the analysis presented in this study. It presents a discussion on conclusions and implications of the modeling techniques developed in the previous chapters.

CHAPTER 2: BACKGROUND

2.1 Cancer and Photodynamic Therapy

The focus of this dissertation lies on a novel clinical treatment modality called the "Photodynamic Therapy" (PDT) which is based primarily on the interaction of light with human tissue and certain cancer-specific agents which can be exploited and utilized in our struggle against cancer.

The World Health Organization defines cancer as "a generic term for a large group of diseases that can affect any part of the body. Other terms used are malignant tumors and neoplasms. One defining feature of cancer is the rapid creation of abnormal cells that grow beyond their usual boundaries, and which can then invade adjoining parts of the body and spread to other organs. This process is referred to as metastasis. Metastases are the major cause of death from cancer".

Cancer is the leading cause of death in economically developed countries and the second leading cause of death in developing countries. About 12.7 million cancer cases and 7.6 million cancer deaths are estimated to have occurred in 2008 worldwide, with 56% of the cases and 64% of the deaths in the economically developing world [10].

Cancers are primarily an environmental disease with 90–95% of cases attributed to environmental factors and 5–10% due to genetics[11], although it is nearly impossible to prove what caused a cancer in any individual, because most cancers have multiple possible causes. The examination of a tissue sample by a pathologist is required for a definite diagnosis of cancer. Medical tests commonly used include blood tests, X-rays, CT scans and endoscopy. The major management options for cancer are surgery, chemotherapy, radiation and palliative care, among others. According to the National Cancer Institute,

radiation therapy uses high-energy radiation to shrink tumors and kill cancer cells. Available methods to kill cancer cells involve x-rays[12], gamma-rays[13], beta rays[14], neutrons[15], high energy electrons[16], protons[17], light and photosensitizers[18], light and gold nanoparticles, surgery, cryosurgery[19], chemicals[20], hyperthermia[21] and thermoablation[22]. Photodynamic Therapy is largely an effort to reduce the use of chemotherapy and radiotherapy for treating cancer. Chemotherapy is considered to impose difficulties because drugs often produce harmful side effects. And radiotherapy is also problematic because x-rays travel through normal tissue to arrive at the tumor site and it is known that the x-rays sometimes damage normal tissue.

The utilization of lasers in medicine has been overwhelming due to the possibility of varying its biological impact via the selection of wavelength, output power and, illumination time and mode. [278]. This thesis focuses on a regimen of utilizing light within medicine referred to as the Photodynamic Therapy (PDT), and considers mathematical modeling techniques to investigate the PDT effect, the mechanism of cell killing and the cell decision making in response to PDT treatment. Compared with conventional cancer therapies such as chemotherapy and radiotherapy, PDT has major advantages, such as: PDT treatment can be repeated in case of recurrence or a new primary tumor in the previously treated area. Such retreatment is extremely difficult for either surgery or radiotherapy, without the risk of severe normal tissue damage[23]. During the past 30 years, PDT has been employed in the treatment of many tumor types, and its effectiveness as a curative and palliative treatment is well documented. Especially for skin cancer, it is becoming an established therapy[23].

In Chapter 3, a mathematical model that involves the major biochemical components of PDT and is based on the cytotoxic character of Reactive Oxygen Species (ROS) generated during treatment is presented and discussed as the first part of our numerical modeling of the PDT processes.

The second part of this study consists of the analysis of cellular decision making which in general is defined as the process whereby cells assume different, functionally important fates with or without an associated genetic or environmental difference. Stochastic cell fate decisions generate nongenetic cellular diversity, which may be critical for cell development but also for disease management and therapeutic treatment as well as optimization studies related to cell survival in a fluctuating, frequently stressful environment[24].

Cellular decision making is a fundamental biological property, and in Chapter 4, a mathematical model that describes this information theoretic phenomenon is presented, with the PDT treatment and cell death/survival as a case study.

2.2 History of PDT

The use of light for therapeutic reasons has been known since antiquity. Phototherapy has its roots in ancient Greece, Egypt, China and India where light was used to treat many diseases such as vitiligo, rockets, psoriasis, skin cancer and even psychosis. Herodotus introduced Heliotherapy (exposure to sun) which was used by the Greeks 2200 years ago for restoration of health [25]. After a long period of time of about 2000 years, physicians revisited the healing effects of the use of light, which its modern form, today, under the name “Photodynamic Therapy”, it was introduced and developed to an effective modality of cancer treatment and a popular science by Oscar Raab, Herman Von Tappeiner and Niles Finsen (18^{th} century). Danish physician Niels Finsen initiated the use of carbon arc phototherapy for lupus vulgaris and won the Nobel Prize in 1903 for his work [25]. Oscar Raab, early in the 20^{th} century was the first to scientifically examine the photo therapeutic effects by experimentally identifying the link between fluorescence product and toxicity. He hypothesized the transfer of energy from light to chemical that could be used as a therapeutic agent in dermatology. Von Tappeiner introduced the name “Photodynamic Therapy”, to describe the phenomenon of oxygen dependent photosensitization (1904).

Hematoporphyrin derivatives were proposed for cancer treatment. A hematoporphyrin derivative is a complex composed of a multitude of different porphyrin molecules and can concentrate specifically in tumors[26]. Such derivatives are photosensitive and yield cytotoxic radicals when activated with light, but are harmless when used alone [27]. This is another definition of PDT (photodynamic therapy). A main advantage of PDT, over classic chemotherapy, relies on the absence of systemic toxicity of photosensitizers alone, and the ability to irradiate and treat the tumor zone specifically. PDT was successfully applied but limited, in most cases, for the treatment of superficial cancers such as esophageal and lung cancers because of the weak light penetration through tissues [28].

Haematoporphyrin (photosensitizer) has been shown to have cytotoxic effects when activated by light and is also tumor localizing, which makes it a desirable target for photo activation and tumor cell damage. Haematoporphyrin was first made by Scherer in 1841[29].”Porphyra” is the Greek name for “red-purple” and was used by Hoppe-Seyler (1871) to describe the purple substance in iron-free haematin as Haematoporphyrin. The biological properties of Haematoporphyrin were analyzed and studied by Haussmann(1908) for the first time. But it was Friedrich Meyer-Betz (1913) , who experimented on himself by injecting in him Haematoporphyrin and noticing pain after controlled light exposure. Selective localization of poprhyrins to tumors was discovered a few years later by Policard (1923)in Lyon, who observed fluorescence in experimental tumors exposed to light and attributed it to accumulation of porphyrin in the tumor [25]. The active photosensitizer used in the clinical PDT trial by Dougherty (treated 113 cutaneous or subcutaneous malignant tumors and observed a total or partial resolution of 111 tumors[26]) in 1978 was an agent called Haematoporphyrin Derivative (HpD), which was first characterized in 1960 by Lipson [30]. In his research, Lipson wanted to find a diagnostic agent suitable for the detection of tumors in patients. With the discovery of HpD, Lipson went onto pioneer the use of endoscopes and HpD fluorescence to detect tumors. The pharmaceutical name of HpD is

Photofrin, as it was introduced on its clinical approval in 1993 for bladder cancer treatment in 1993 in Canada.

PDT has been used for the treatment early carcinomas of the oral cavity, pharynx, and larynx, preserving normal tissue and vital functions of speech [31] head and neck cancer[32], digestive system tumors (Barrett esophagus, esophagus dysplasia), [33-35] various intraperitoneal malignancies[33, 36, 37], prostate[38], bladder cancer[39, 40], mesothelioma[41], lung cancer[42], among several other types of cancer. A complete report can be found in review[43] .

Current strategies use PDT in a combined therapy together with surgery. PDT in this framework has been used as post operational treatment but not only: it is also an exciting area of research to look at the use of PDT along with current therapy to make it more effective. One way to do this may be to use PDT *during* surgery to help keep cancer from coming back on large surface areas inside the body, such as the pleura (lining of the lung) and the peritoneum (lining of the belly or abdomen). These are common sites of spread for some types of cancer.

The exciting future of PDT involves combinations of new innovative methodologies [43] such as the two photon PDT to achieve deeper tissue penetration and better photon absorption by the photosensitizer[44], metronomic PDT to deliver drug and illumination at very low dose rates over an extended period [45], nanoparticle PDT for photosensitizer delivery and energy trunsucing [46], among others.

As part of a brief historic review of PDT action and PDT agents, it is important to adress the question why do photosensitizers localize selectively in tumors. According to current opinion and research results, the selective tumor uptake is probably not due to special properties of tumor cells[47] [48] but rather to the differences in the physiology between tumors and normal tissues[48-50]:

- tumors have a larger interstitial volume than normal tissues,
- tumors contain a larger fraction of macrophages than normal tissues,
- tumors have a leaky microvasculature,
- tumors have poor lymphatic drainage,
- the extracellular pH is low in tumors,
- tumors contain a relatively large amount of newly synthesized collagen,
- tumors contains many receptors for lipoproteins.

It is stated that some sensitizers localize in both the nucleus and the mitochondria, lipophilic ones tend to stick to membrane structures, and water soluble drugs are often found in lysosomes. In some cases, light exposure leads to a relocalization of the sensitizers [51]. From the biochemistry point of view, PDT action is linked to the intracellular localization of the photosensitizers since the main active photoproduct singlet oxygen $^1O_2$ lifetime is short in cells (μseconds) with a short range of range of diffusion from the site of production[52] [29]. This has been suggested to be the reason for the low mutagenic potential of PDT, since most photosensitizers are localized outside the nucleus. On the other hand, it has been observed that PDT has a strong effect on cell division which is probably mainly due to microtubule damage and may contribute significantly to PDT induced cell death [48],[53].

2.3 Mathematical Modeling of Biochemical Processes

Mathematical modeling is essential to clearly reveal and understand the fundamental processes underlying the properties of living biophysical systems. Often modeling can be implemented with systems of differential equations which allow the qualitative study of biological processes and interpretation of regular and irregular behaviors of different quantities represented by corresponding variables. This modeling of biophysical processes includes the study of growth, interaction between

variables (species, molecules, micro-organisms, etc.), oscillations, trigger, and other biological mechanisms. With the use of appropriate algorithms that numerically solve a differential equation system, it is possible to describe the behavior of a complex biological system on the basis of its major components and the main features of their interactions. The processes of molecular dynamics and the molecular interactions can be investigated with the use of information system theory and then compared to experimental data. Complex inhomogeneous structures resulting from the miraculous variations of qualitative and quantitative characteristics of living systems, that regulate the corresponding bio- environments in which bio-molecular processes take place, cannot, in principle, be formalized in a mathematical equation. Mathematical modeling allows the abstraction, idealization, and description of major characteristics depending upon the interest of the research. Intracellular molecular interactions can be studied with the purpose of extracting useful conclusions, by using computational methods. For example, the mathematical formulation of biochemical reactions of enzyme catalysis [54] [55] [56] has been used as a standard reference in molecular dynamics with a number of applications beyond enzymatic physics. In particular, in the area of system modeling at the cell level, the theory of metabolic control is actively studied, and targets towards the determination of controllable stages in complex metabolic cycles of intracellular reactions.

All that said, and in anticipation of the analysis that will follow, one more important matter needs to be discussed. There might indeed be a general belief in mathematics (and in physics, and in biology) that with time essentially any problem of "mathematical interest" will be solved. According to Wolfram though, there is ,in a sense, "genuine impossibility" and If all of physics can successfully be reduced to mathematics, then mathematical impossibility in a sense becomes physical impossibility. Models of physical systems have indeed very frequently been set up like traditional digital computations, with discrete variables, and explicit progression with time. But even traditional physical models are in many senses computational for even though there are continuous variables and equations to solve, we use

computer softwares[57, 58], to extract valuable information. We will be discussing about cellular processes such as cellular decision making. How can we know whether a computational model actually is the appropriate model for cell decision making? The complexity of such a program-algorithm is expected to be very high, and If the model is computationally irreducible, we can only hope to find enough computational reducibility to identify known physical or biological laws within the cell model. if the model reproduces any reasonable number of features of biophysical processes, and is relatively simple, then there is a good chance that within its class of simple models we can find an accurate initial modeling approach. Beyond well-known reducible features, there lies an infinite frontier of computational irreducibility and if we take the alternative pathway and try to reduce physics and biology to mathematics we expect to run into phenomena like Gödel's theorem of incompletness. Therefore, the constraints in cell decision making and predictive modeling in general are not ones of physics, but rather ones of a deeper nature. According to the Principle of Computational Equivalence[2], the constraints on what is possible will be abstract features of the general properties of mathematical or computational environments.

Of course one has to keep in mind of the limitations of computability of an algorithm. According to the Church-Turing conjecture, a function is algorithmically computable if and only if it is computable by a Turing machine. A Turing machine is a theoretical device[57] that consists of a line of cells known as "tape" that can be moved back and forth, an active element known as the "head" that possesses a property known as "state" and that can change the property "color" of the active cell underneath it, and a set of instructions for how the head should modify the active cell and move the tape. At each step the

machine may modify the color of the active cell, change the state of the head, and then move the tape one unit to the left or right (Stephen Wolfram "A New Kind of Science",2002, Wolfram Media).

To overcome the limitations of a Turing algorithm, Burgin discovered the super recursive algorithms. Super-recursive algorithms are generalizations of ordinary algorithms that are more powerful, that is, compute more than Turing machines[59, 60]. According to Burgin, "the super recursive class of algorithms is a class in which it is possible to compute functions not computable by any Turing machine". A Turing machine indeed can process any number of different patterns with the option to accept or reject the input or to update cells on the tape and it is a theoretical construct rather than a computer. The universal Turing machine, can emulate any other Turing machine. More precisely, it can(Mike Deehan, "The Universal Turing machine is a Turing Machine emulator", March 2012):

1. Define the symbols that the specific Turing machine will use.

2. Define the symbols that encode the states and transition rules for the specific Turing machine.

3. Encode the rules for that specific Turing machine onto the input tape.

A universal Turing machine therefore, can emulate even itself and examples of the capabilities is the use of the Universal Turing machine in solving Hilbert's Decision problem" and the "Halting problem". What we need to notce here is that Turing machines (computers) use functions whose values are algorithmically computable and therefore any features or entities coming from sources that do not belong in this category, will require a new framework . For example, although it is known that questions about the behaviour other Turing machine, there are are undecidable, meaning that the function in question cannot be calculated mechanically ("Halting Problem"). A Turing machine can be simulated by a universal turing machine, but a universal Turing machine cannot be simulated by a simple Turing machine. This is a critical piece of information. In the later chapters, we will be discussing about the

survivability of the cell. One may be tempted to use the language of bio-computing to describe the entity of a cell. Indeed, the first steps towards the design of programmable molecular computing machines based on Turing theory have already been taken. A DNA computer coupled with an input and output module which would theoretically be capable of diagnosing cancerous activity within a cell, and release an anti-cancer drug upon diagnosis were presented in[61]. The analogies in this study were hardware-enzymes and software-DNA. An extension of this initial design was presented in[62] in 2012, where the device was shown to operate on three-dimensional building blocks by applying mechanical analogues of polymer elongation, cleavage and ligation, movement along a polymer, and control by molecular recognition unleashing allosteric conformational changes. The invention of this mechanical device that embodies the theoretical computing Turing machine was awarded a US patent in 2001. Earlier, the authors in[63] used specially prepared pieces of DNA in a test tube to input data of a computation and then left the molecules to their natural inetractions which included limking up to form sequences of DNA which could be chemically decoded to give the results of the computation[3]. Attractive as it seems to borrow ideas from DNA based computers and try to use Turing like models in molecular biology to analyze life mechanisms with DNA processors, these innovative and perhaps useful ideas are not sufficient to describe the living entity of a cell. Cellular life requires a different description, a description that will be able to accommodate wondrous and challenging phenomena, such as cell survival under adverse circumstances and cell fate decision making.

John Von Neumann posed and solved the following question: what kind of logical organization is sufficient for an automaton to control itself in such a manner that it reproduces itself? [64]. A cellular automaton is specified by giving a finite list of states for each cell, a distinguished state called the blank state, and a rule which gives the state of a cell at time t+1 as a function of its own state and the states of its neighbors at time t. It consists of a cellular space and a transition function defined over this space.

[3] Toby Howard, "Computing with DNA", appeared in Personal Computer World magazine, April 2000"

Finite automata consititute the basis of Turing machines[64]. Von Neumann was the first provide an algorithmic model of a self-reproducing automaton, the Universal Constructor, a self-replicating machine in a cellular automata environment and (in a brief summary), he proved that the construction of this sort of automaton would necessitate the solution to three fundamental problems [64, 65]:

α. to store instructions in a memory;

β. to duplicate these instructions;

γ. to implement an automatic factory ("Universal Constructor"), able to read the memory instructions, and, based on them, to construct the components of the system;

δ. to manage all these functions by means of a central control unit.

A self-reproducing system must contain the program of its own construction. This program is a sort of consistent and complete abstract image of the system. In other words, self-reproduction needs programming and processors (software -for information based replication- and hardware)[4]. The solution to these problems mentioned above may be found in living things as observed by modern biology. An efficient mechanism of information storage and an elegant mechanism of duplication of the DNA molecule may be the one and only perfect solution to the twin problems of information storage and duplication for self-replicating automata[65]. But more importantly, Von Neumann understood that any information-based replicator must contain inside itself (among other indispensable things) a symbolic representation of itself, an "image" of itself. The relation between the replicator (hardware) and the image (a structure of symbols, the software) is a functional relation of dependence, since the symbolic representation consists of directives and instructions that must be interpreted by the replicator machinery for constructing a copy of itself. According to[5] Von Neumann proposed this scheme before the structure of the DNA molecule was uncovered by Watson and Crick[66] , though after the Avery-

[4] http://www.uncommondescent.com/biology/john-von-neumann-an-ider-ante-litteram/

[5] Rocha, L.M. " Von Neumann and Natural selection" Biologically inspired computing lecture notes, chapter 6

MacLeod-McCarty experiment[67] which identified DNA has the carrier of genetic information. According to Brenner[68] "The concept of the gene as a symbolic representation of the organism–a code script–is a fundamental feature of the living world and must form the kernel of biological theory."

As a final remark on Von Neumann's Universal Constructor we need to notice first that the four principles (α,β,γ,δ) mentioned above are irreducible in complexity (irreducible incomplexity are the principles of a Turing machine as well) and secondly that the concept of the symbolic representation-based self reproduction implies a language (a symbol system, a syntactic code to be used to map instructions into construction commands for replication. In copying a description, the syntactic aspects are replicated[6]).

[6] Rocha, L.M. " Von Neumann and Natural selection" Biologically inspired computing lecture notes, chapter 6

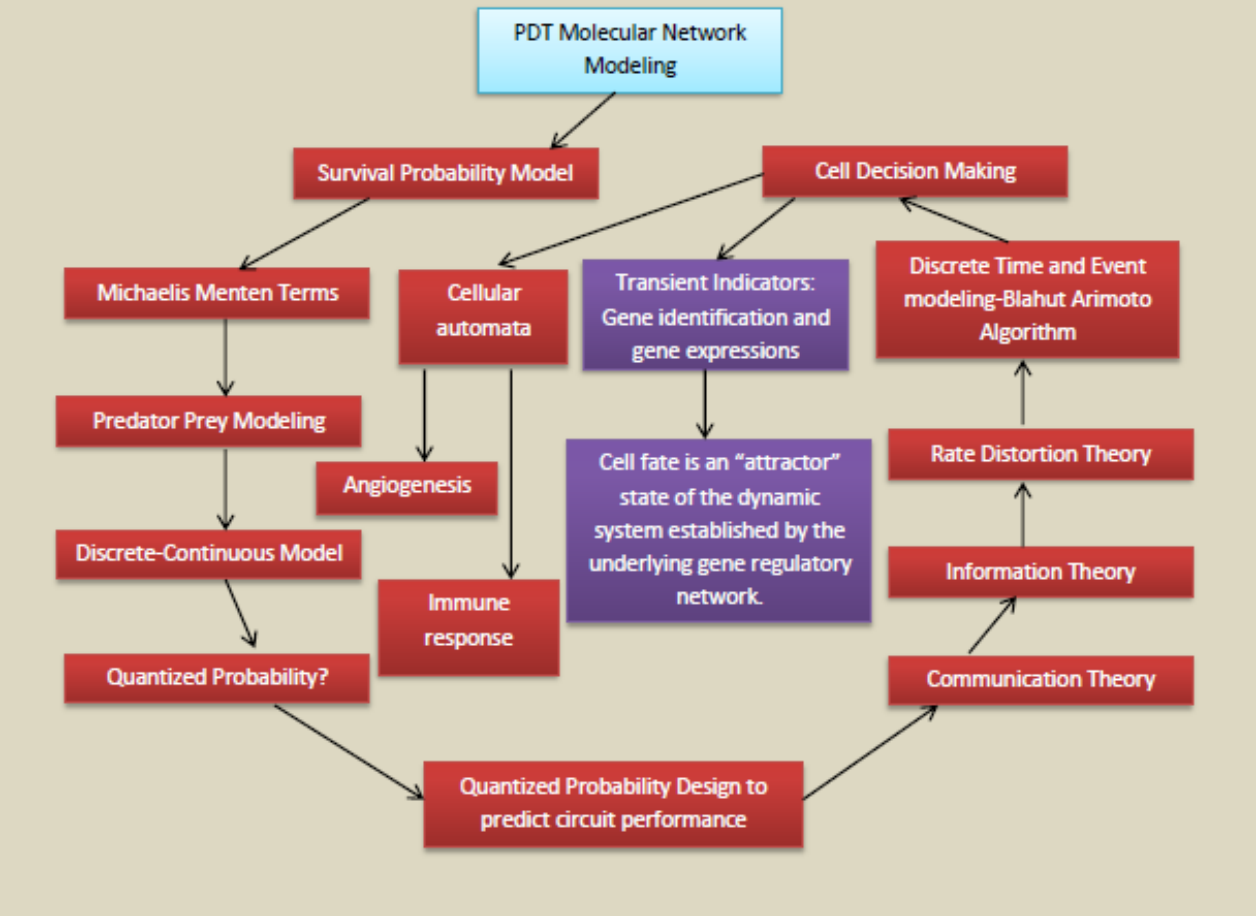

Figure 2.3.0. The research direction of this study

2.4 Type I and type II reaction in photodynamic therapy (PDT)

There are two types of reaction during PDT, two mechanisms by which the triplet (excited) state photosensitizer can react with biomolecules, known as the Type I and Type II reactions. Following the absorption of light, the sensitizer is transformed from its ground state into an excited state. The activated sensitizer can undergo two kinds of reaction[69]:

- Type I reaction: Type I involves electron/hydrogen transfer directly from the photosensitizer, producing ions, or electron/hydrogen abstraction from a substrate molecule to form free radicals. These radicals then react rapidly, usually with oxygen, resulting in the production of highly reactive oxygen species (e.g. singlet oxygen, the superoxide and the peroxide anions). These radicals then attack cellular targets[7]. The Type I reaction is a radical or redox reaction in which a photosensitizer, excited to the triplet state, interacts with a neighbouring molecule (A) by exchange of an electron or a hydrogen atom:

$$T + A \rightarrow T^{-} + A^{+} \quad (2.4.1)$$

$$A^{+} + {}^{3}O_2 \rightarrow A_{ox} \quad (2.4.2)$$

Or

$$S^{-} + O_2 \rightarrow S_0 + O_2^{-} \quad (2.4.3)$$

$$O_2^{-} + A \rightarrow A_{ox} \quad (2.4.4)$$

in both cases giving an oxidized biomolecule. Alternatively:

$$T + {}^{3}O_2 \rightarrow T^{+} + O_2^{-} \quad (2.4.5)$$

$$T^{+} + A \rightarrow S_0 + A^{+} \quad (2.4.6)$$

- Type II reaction: Type II involves the direct interaction of the excited triplet state photosensitizer with molecular oxygen (triplet ground state) which results in the photosensitizer returning to its singlet ground state and the formation of singlet oxygen, a highly reactive oxygen species. These species oxidize various substrates. This is an energy transfer process.

$$T + {}^{3}O_2 \rightarrow S_0 + {}^{1}O_2 \quad (2.4.7)$$

[7] The Leeds Centre for Photodynaic Therapy (PDT) website, School of Biochemistry and Molecular Biology, University of Leeds.

$$^1O_2 + A \rightarrow A_{ox} \quad (2.5.8)$$

Most photosensitizer (PS) drugs used in clinical studies of PDT achieve tumor eradication by generating highly reactive oxygen molecules in the singlet excited states through a Type II process[7]. It also known that there are three main mechanisms by which PDT mediates tumor destruction[69, 70]:

- Direct tumor-cell killing, which depends on the non-homogenous distribution of the photosensitizer within the tumor, the availability of oxygen within the tissue that is targeted by PDT, and the time of illumination.
- Vascular damage, which reduces the amount of nutrients supplied by the blood vessels to the tumor cells and causes severe tissue hypoxia and vascular effects associated with a delay in tumor growth.
- Immune response, which refers to the infiltration of lymphocytes, leukocytes and macrophages into PDT-treated tissue. PDT generated tumor-sensitized immune cells that could be recovered from lymphoid sites distant to the treated tumor at different time intervals after PDT have been reported[71].

In this study, we will focus on the PDT process that involves the excitation of photosensitizer (PS) by photons and a cascading chain of reactions leading to cytotoxicity (necrosis, apoptosis, autophagy) , since we will be mainly interested in modeling cell killing through different bio molecular mechanisms, and cell survival probabilities based on a cell model, as well as cell decision making as a result of PDT stimulation.

2.5 Mathematical Modeling of PDT

There are several factors that can affect dosimetry during PDT. The initial interactions involving the photosensitizer, light, oxygen and various biological targets within the tissue, as well as the dynamic changes in these parameters during treatment need to be taken into consideration. The analysis of these factors is of crucial importance for the design of useful dosimetric models [280] .

The effects of photochemical $^3O_2$ depletion on the efficacy of PDT have been analyzed in the case of photosensitized multicell tumor spheroids in [3]. A time dependent theory of $^3O_2$ diffusion with consumption was introduced to quantitatively determine the rate of photodynamic $^3O_2$ consumption as a function of the incident fluence rate and several other parameters that describe $^3O_2$ transport in this system. With these parameters and knowledge of the properties of $^1O_2$ in a cellular environment, the diffusion-consumption model was shown to be potentially useful in the calculation of the amount and distribution of reacting $^1O_2$ molecules in a multicell tumor spheroid during PDT. By comparing the calculations with the results of previous experiments, the authors were able to estimate the threshold dose of reacting $^1O_2$ necessary to kill cells in the special cases of tumor spheroids. To model the Type II photodynamic process, the following time dependent diffusion with consumption equations were numerically solved, in the region of interest:

$$D_d \nabla^2 C(r,t) = \frac{\partial C(r,t)}{\partial t} \quad , \quad R_s \le r < R_d \tag{2.5.1}$$

$$D_s \nabla^2 C(r,t) - \Gamma(r,t) = \frac{\partial C(r,t)}{\partial t} \; 0 \le r < R_s \tag{2.5.2}$$

where $C(r,t)$ is defined as the local $^3O_2$ concentration, r as the radial distance from the center of the spheroid, t is the time from irradiation of PDT, R_s, R_d were the radius of the spheroid and the outermost radius of the depletion zone respectively, and D_d, D_s are the corresponding diffusion coefficients for $^3O_2$ and $\Gamma(r,t)$ is the total rate of $^3O_2$ consumption within the spheroid. It was noted that $^3O_2$ will be consumed within the spheroid by photodynamic as wells as metabolic processes:

$$\Gamma(r,t) = \Gamma_m(r,t) + \Gamma_{PDT}(r,t), \quad 0 \le r < R_s \tag{2.5.3}$$

Where

$$\Gamma_{PDT}(r,t) = \frac{\Gamma_0 \cdot k_{ot} \cdot [^3O_2]}{k_{ot} \cdot [^3O_2] + k_p} \tag{2.5.4}$$

And

$$\Gamma_0(r,t) = \frac{S_\Delta \cdot \phi_t \cdot I_a \cdot k_{oa} \cdot [A]}{k_{oa} \cdot [A] + k_d} \tag{2.5.5}$$

In these equations $[A]$ stands for the concentration of intracellular targets of $^1O_2$ reaction (acceptor concentration), I_a is the photon absorption, ϕ_y denotes the photosensitizer triplet yield, and S_Δ denotes the photosensitizer triplet quenching. The interpretations of all other constants can be found in [3]. The PDE system was solved subject to the boundary conditions

$$C(r = R_s^-, t) = C(r = R_s^+, t) \tag{2.5.6}$$

$$D_s \frac{\partial C(r = R_s^-, t)}{\partial r} = D_d \frac{\partial C(r = R_s^+, t)}{\partial r} \tag{2.5.7}$$

Specifying that at the edge of the spheroid the $^3O_2$ concentration and the $^3O_2$ flux will be continuous across the boundary, expressing mathematically the fact that the system is open to the environment. Together with the boundary conditions, a set of initial conditions for the numerical solution of the system was provided:

$$C(r,0) = C_m - \Gamma_{met}\frac{R_s^3}{3D_d}\left(\frac{1}{R_s} - \frac{1}{R_d}\right) - \Gamma_{met}\frac{(R_s^2 - r^2)}{6D_s} \quad , \quad 0 \le r < R_s \tag{2.5.8}$$

$$C(r,0) = C_m - \Gamma_{met}\frac{R_s^3}{3D_d}\left(\frac{1}{r} - \frac{1}{R_d}\right) \qquad R_s \le r < R_d \tag{2.5.9}$$

Where C_m denotes the $^3O_2$ consumption in the medium far from the sphere. To solve this system of equations, the space and time coordinates were discretized and placed on a radial lattice. The equations were then discretized following a Crank-Nicolson scheme to insure stability and second-order accuracy in both time and space[72]. $^3O_2$ microelectrode measurements established the validity of the model and provided values for the parameters that constitute it. Useful conclusions were drawn such as that the magnitude of the spheroid-cell surviving fraction was correlated with the extent of anoxia induced by the therapy.

In contrast to this model where the depletion radius was assumed to be constant throughout PDT, a model that allowed the depletion radius to vary dynamically as a function of the spatially averaged rate of $^3O_2$ consumption was presented in [280]. Upon the onset of irradiation, the depletion zone boundary was forced to move further away from the spheroid edge in response to the increases $^3O_2$ consumption in the spheroid. In this model, as the $^3O_2$ concentrations reach a quasi-equilibrium state, the depletion radius reaches its maximum value. It then decreases as gradually as photo bleaching effects become significant and the photochemical $^3O_2$ consumption decreases. This is considered

necessary for the proper analysis of the $^3O_2$ measurements that demonstrate the effect of photo bleaching [280]. In this study, the rate $\Gamma_{PDT}(r,t)$ was modified to accommodate photo bleaching, according to a simple exponential bleaching term $e^{-a\cdot D}$ where D is the fluence $(J\cdot cm^{-2})$ and a is a bleaching coefficient $(J^{-1}\cdot cm^2)$:

$$\Gamma_{PDT}(r,t)=\frac{\Gamma_0\cdot k_{ot}\cdot[^3O_2]}{k_{ot}\cdot[^3O_2]+k_p}\cdot e^{-a(t)\cdot D} \tag{2.5.10}$$

In the same reference, a second possible mechanism that implicates the $^1O_2$ as the direct mediator of sensitizer bleaching was investigated, suggesting that the photosensitizer is degraded by chemical reaction with $^1O_2$. Assuming that $^1O_2$ reacts only with ground state of the photosensitizer S_0, and considering that in the absence of photo bleaching the concentration of S_0 remains constant, and moreover that loss of ground absorption proceeds much slower than the rates associated with the primary photochemical reactions occurring during treatment, a simple ordinary differential equation was derived:

$$\frac{d[S_0]}{dt}=-k_{os}[S_0][^1O_2] \tag{2.5.11}$$

and further considerations led to an expression describing $^1O_2$ mediated sensitizer degradation as:

$$[S_0](t)=[S_0](0)\cdot\exp\left(-\frac{k_{os}}{k_{os}[A]}\int_0^t S_\Delta\cdot\phi\cdot_t I_a(t')\cdot\frac{k_{ot}[^3O_2](t')}{k_p+k_{ot}[^3O_2](t')}\cdot\frac{k_{oa}[A]}{k_d+k_{oa}[A]}\right) \tag{2.5.12}$$

In this study, it was assumed that the photosensitizer can be modeled as uniformly distributed throughout the spheroid. The rate equations used in this study for the sensitizer excited singlet and the sensitizer triplet excited concentrations are:

$$\frac{d[S_1]}{dt} = I_a(t) - k_m[S_1] - k_{isc}[S_1] - k_{as}[A][S_1] \tag{2.5.13}$$

$$\frac{d[T]}{dt} = k_{isc}[S_1] - k_p[T] - k_{ot}[T][A] - k_{at}[A][T] \tag{2.5.14}$$

Where the interpretation of the constants can be found in this reference.

A rate equation approach used to solve the time dependence of the molecular concentrations in a Type II PDT process as a consequence of the local photon density ρ with six coupled, first order differential equations was presented in [7, 73]. The PDT process takes place in a cell spheroid and it is started by the absorption of photons by S_0, with an absorption cross-section σ_{psa}. The system equations of this model are:

$$\frac{d[S_0]}{dt} = -k_{pb}[^1O_2][S_0] - \nu\rho\sigma_{psa}[S_0] + \frac{\eta_{30}}{\tau_1}[S_1] + \frac{\eta_{30}}{\tau_3}[T] + \frac{\alpha_S}{\tau_3}[T][^3O_2] \tag{2.5.15}$$

$$\frac{d[S_1]}{dt} = -\frac{1}{\tau_1}[S_1] + \nu\rho\sigma_{psa}[S_0] \tag{2.5.16}$$

$$\frac{d[T]}{dt} = -\frac{\eta_{30}}{\tau_3}[T] - \frac{\alpha_s}{\tau_3}[T][^3O_2] + \frac{\eta_{13}}{\tau_1}[S_1] \tag{2.5.17}$$

$$\frac{d[^3O_2]}{dt} = -\frac{\alpha_s}{\tau_3}[T][^3O_2] + \frac{\eta_0}{\tau_0}[^1O_2] + P \tag{2.5.18}$$

$$\frac{d[^1O_2]}{dt} = -k_{pb}[S_0][^1O_2] - k_{cx}[R][^1O_2] - \frac{\eta_0}{\tau_0}[^1O_2] + \frac{\alpha_s}{\tau_3}[T][^3O_2] - k_{sc}[C]_i[^1O_2] \tag{2.5.19}$$

$$\frac{d[R]}{dt} = -k_{cx}[R][^1O_2] + U \tag{2.5.20}$$

Where R are the intracellular receptors for $^1O_2$. The first and second terms on the right-hand side of (Eq. 2.19) are the rates of $^1O_2$ consumption in oxidization and photo bleaching of intracellular receptors. In addition, (Eq. 2.19) also includes the reaction of $^1O_2$ with various oxygen scavengers with an average rate k_{sc} and concentration $[C]$. The values of coefficients and parameters and a detailed discussion on the selection of these coefficients are presented in reference[7] . This model accommodates the assumption that PDT process is caused primarily by the oxidization of various intracellular receptors at the PS binding sites. Various repair mechanisms can be activated within a cell to undo the cytotoxic damage. When the concentration of cytotoxic agents exceeds a certain threshold in a cell, irreversible apoptosis or necrosis occurs[74]. This is the justification why the time evolution of unoxidized receptors $[R]$ is determined by its reaction rate with singlet oxygen and a repair rate U .

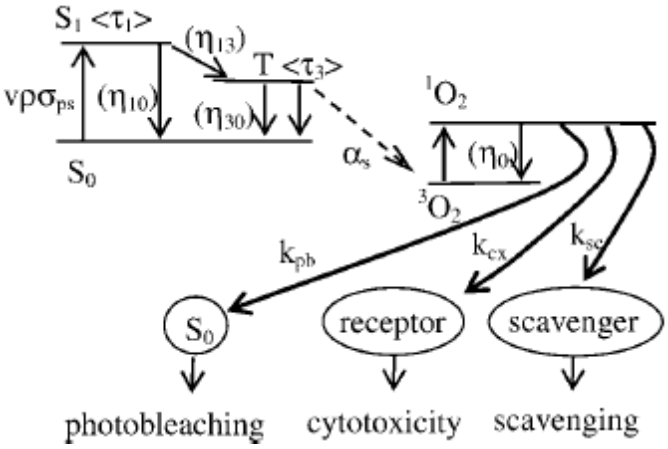

Figure 2.2.1. A schematic representation of the PDT process[7]. The symbols in angled brackets are relaxation times of the excited states, symbols in parentheses are quantum efficiencies and symbols with dashed lines are reaction constants.

The authors in this report, calculated the steady-state light distributions using a Monte Carlo method in a heterogeneous tissue phantom model and showed that the photon density differs significantly in a

superficial tumor of only 3 mm thickness. Then, they went on to define respective decay times and quantitatively study the effects of photon density, drug dose and oxygen concentration on photobleaching and cytotoxicity of a photofrin-mediated PDT process. Comparison of the dependences of the receptor decay time on photon density and drug dose at different concentrations of oxygen clearly showed an oxygen threshold under which the receptor concentration remains constant or PDT exhibits no cytotoxicity[7]. Although this model is considered to be useful toward the understanding of clinical PDT treatment (and a short discussion of treatment of chest wall recurrence of breast carcinoma was presented), the time dependence of $[R]$ and its relation to cell survival in the time domain with a cell-killing model remained to be determined in the future.

An elementary model that provides estimates for the rate of oxidation and the necessary irradiation dose has been presented in[75] . The dose curve of cell damage was calculated and the calculation results were compared with the experimental data. In particular, the authors consider lipids of the external membrane of a cell as the vitally important substratum of the cell and singlet oxygen attacks this substratum, oxidizing it. The cell damage was therefore associated with the oxidation of membrane lipids. In their biological tissue model, the authors used a system of kinetic equations similar to the system proposed in [7] and briefly discussed above, to describe the photodynamic fullerene–oxygen action and corresponding chemical reactions in tissue. In this model, the new component is X the concentration of intact (alive) cells and it was also assumed that the rate of damage of cells is proportional to the fraction of the oxidized substratum:

$$\frac{d\delta}{dt} = -\frac{\delta}{t_{ox}}\ ,\ \delta(0) = 1 \qquad (2.5.21)$$

$$\frac{dX}{dt} = -\alpha_0 \cdot (1-\delta) \cdot X\ , \qquad X(0) = X_0 \qquad (2.5.22)$$

Where

$$\delta(t) = \frac{N_s(t)}{N_s(0)} \tag{2.5.23}$$

Is a dimensionless variable, and N_s is the concentration of the substratum, $t_{ox} = \frac{1}{k_{ox}[^1O_2]}$ and the constant α_0 describes the sensitivity of cells of a particular type to the photodynamic action and its value is unknown; however, it can be found from measured dose curves. The solution of this system yields the dependence of the number of surviving cells on time, i.e., the so-called dose curve:

$$\ln(\frac{X}{X_0}) = -\alpha_0 \cdot \{t_{ox}[1 - \exp(-\frac{t}{t_{ox}})] - t\} \tag{2.5.24}$$

However, the receptor-independent contributions to the rate of cell killing as a result of ROS (reactive oxygen species) stress were not discussed in this study, although their contribution is significant as the fluence rises, and therefore accurate modeling of cell killing by PDT remained a challenging task because of the complexity of the process.

As a concluding remark here, it is necessary to mention that it has been observed and demonstrated that PDT has significant immunological effects[76] and that it also causes significant vascular damage[77]. The immunological effects of PDT play a role in tumor destruction as well as the prevention of tumor recurrence [78], but more experimental data are necessary before any modeling scheme is applied.

2.6 Oxygen diffusion in a spherical cell - Michaelis-Menten oxygen uptake kinetics

Cell membranes act as barriers to most, but not all, molecules. The cell membrane functions as a semi-permeable barrier, allowing a very few molecules across it while fencing the majority of organically

produced chemicals inside the cell. Oxygen is among the few simple molecules that can cross the cell membrane by diffusion[79]. Diffusion is one principal method of movement of substances within cells, as well as the method for essential small molecules to cross the cell membrane. For example, metabolic processes in animals and plants usually require oxygen, which is in lower concentration inside the cell, thus the net flow of oxygen is into the cell (M.J. Farabee, online biology book). Diffusion of oxygen is considered to be a "passive" transport that requires no energy from the cell. A mathematical-numerical approach to the modeling of oxygen diffusion in a spherical cell was initiated in [80] with a spherical cell model that consists of a surface membrane and protoplasm and where external diffusion effects are neglected. In this model, enzymes are compartmentalized in the protoplasm and act as catalysts for the metabolic reactions which provides the energy for the cell [80], while oxygen is acting as a substrate for metabolic reactions. A Michaelis-Menten type term for the oxygen uptake kinetics is assumed:

$$\frac{\partial[O_2]}{\partial t} = D \cdot \nabla^2[O_2] - \frac{V \cdot [O_2]}{[O_2] + K_m} \tag{2.6.1}$$

With boundary conditions

$$\frac{\partial[O_2]}{\partial r} = 0, \quad r = 0 \tag{2.6.2}$$

$$M[O_2] + D\frac{\partial[O_2]}{\partial r} = M[O_2]_0, \quad r = r_0 \tag{2.6.3}$$

and with initial condition

$$[O_2](r,0) = 0 \tag{2.6.4}$$

(2.28)where r is the spatial coordinate measuring the distance from the center of the cell, t is the time coordinate, D is the diffusion coefficient of oxygen in the cell, V is the maximum reaction rate,

K_m is the Michaelis-Menten constant, r_0 is the radius of the cell, and M is the permeability of the cell membrane of $r = r_0$. The numerical results were obtained using the "random choice" type method which was developed for reaction diffusion equations in [81] for the construction of solutions of systems of nonlinear hyperbolic conservation. laws.

Equations above are presented in the context of transport and uptake of oxygen in a spherical cell, they in fact have wider biological applicability. It is well-known that the apparent behavior of many biological and biochemical processes is well represented by diffusive mass transport coupled with the Michaelis-Menten reaction rate expression[82]. Thus these equations are appropriate for a wide variety of biological applications, ranging from applied enzyme catalysis to cellular reactions [83] and other diffusionally influenced biological systems[83]. Therefore, since diffusion of O_2 in cells has attracted research interests in consideration of cellular metabolism and other biochemical processes, quantitative modeling is to be pursued in order to consider the rate of oxygen uptake by molecules in the metabolism and processes unrelated to PDT, using a nonlinear Michaelis–Menten term of probably two adjustable parameters. All the above models consider a spherical configuration in which a spherical symmetry of oxygen distribution of O_2 was assumed to simplify mathematical treatment.

2.7 Cellular Decision Making

Cell communication, or signal transduction, has at least been thought to be an "automatic" cascade of biochemical events. However, some studies report that even before a message makes it through the outer cell membrane to the inner nucleus, the cell is busy activating a molecular switch to guide how the message will be delivered in the first place [84]. Linking cellular decisions making with the

biochemical dynamics in signal transduction can be a very challenging task[8]. These dynamics span a wide range of temporal and spatial scales. The method of stochastic or deterministic bistable switches has been suggested as a viable biochemical mechanism to implement decision processes on long time scales[85] where an external stimulus is required to induce changes in the switch's state. It is interesting to observe that a bistable switch model is based on a positive feedback loop between two or more components. For example, consider a biochemical reaction network involving the two molecular species X and Y. Mathematically, the temporal evolution of the amounts of the two species is described with the ordinary differential equations[85]

$$\frac{dx}{dt} = v_1 + v_2 - v_3 = k_1 + \frac{V_1 y}{M_1 + y} - u_1 x \tag{2.7.1}$$

$$\frac{dy}{dt} = v_4 - v_5 = \frac{V_1 x}{M_2 + x} - u_2 y \tag{2.7..2}$$

Where ultra-sensitivity, which is required to achieve bistability, is generated by the Michaelis Menten type production rates. Other approaches utilize the concept of self-organized criticality, a property that appears in some no equilibrium systems. These models have been developed in the area of stem cell research and propose that stochastic gene expression within a stem cell gene regulatory network self-organizes to a critical-like state, characterized by cascades of gene expression that prime various transcriptional programs associated with different cell fates[86]. Another model again suggests the recapitulation and integration of known biological data from the literature into "influence" diagrams describing the molecular events leading to possible cell fate outcomes and the translation of the diagrams into dynamical Boolean models for simulations.

[8] Johns Hopkins Medical Institutions (2002, July 1). Decision Making At The Cellular Level. ScienceDaily. Retrieved September 20, 2012,

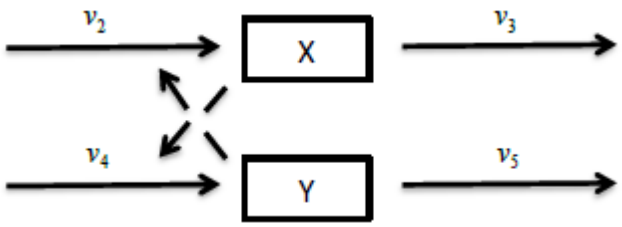

Figure2.4.1: Network schematic for the bistable switch model[85]

A question of major importance is if a cell is damaged, does it repair itself or decide to self-destruct and how does the cell make that decision? These models develop multi-scale approaches of how single molecule events integrate networks to determine cell fate. Indeed, cancer in particular is the result of cell decision-making and deserves special focus. Other activities such as cell maintenance, replication, repair, recombination, programmed cell death —apoptosis, etc. need to be investigated. Cellular decision making is defined as the process whereby cells assume different, functionally important and heritable fates without an associated genetic or environmental difference[24].

However, in biology much attention is focused on mechanisms:

- What is the mechanism by which a biological system works.
- What behavior is produced by a given mechanism.

In contrast, questions about goals need to be addressed[87]:

- What is the goal toward which a biological system works.
- What system behavior best achieves this goal.

This framework of decision making processes assumes that It is impossible or impractical to achieve these goals perfectly due to stochastic fluctuations and It is important to understand how they may be

achieved imperfectly In the most efficient way possible[87]. In a recent research [88] Perkins and Swain characterized cellular decision making as having three main tasks:

- A cell must estimate the state of its environment by sensing stimuli.
- A cell must make a decision informed by consequences of the alternatives.
- A cell must perform these functions in a way that maximizes the fitness of the population (biological units that can make decisions with less information, and therefore less energy, are more efficient and maximize the fitness of the population[87]).

Information theory, which was originally developed for use in telecommunications, has in recent years been increasingly applied to analyzing biological signaling pathways [89] [90] [91] [92] .Rate distortion theory, a branch of information theory has been suggested and presented in several studies as the framework to answer these and related questions. The rate distortion framework provides a perspective on decision making regarding these three tasks as a single process [87]. Indeed, information theory has been used for:

- The determination of the optimal scheme to detect the location of an external chemo attractant source in the presence of noise to direct cell migration[92].
- The quantification of the influence of the topology of a transcriptional regulatory network on its ability to process environmental signals [89].
- An information theoretic approach to understand how reliably biochemical networks can transmit information (how accurately an input signal as a function of time the “input trajectory” can be mapped onto an “output trajectory” [93].
- The study of Information processing and signal integration in bacterial quorum sensing. A mathematical framework for analyzing information processing in cells based on information

theory was derived and used to study the integration of multiple auto inducer signals using the model quorum-sensing bacterium *Vibrio harveyi*[91].

- Reviewing some experiments supporting the view that genetic networks responsible for early development of multicellular organisms might be maximizing transmitted 'positional' information. An interpretation of the specific gap gene circuit, active during early development of the fly embryo, which appears to function close to the limits imposed by noise in gene expression [90].

Rate distortion theory describes how a noisy communication channel can be engineered to transmit a message in a way that simultaneously minimizes error and transmission cost. By regarding a binary cellular decision-making pathway this way, it has been suggested that it is possible to design decision-making strategies that optimally balance accuracy and low metabolic cost[87]. Using this framework, it has been shown that several decision-making motifs observed in natural systems including random strategies, hysteresis, and irreversibility, arise as optimal strategies in various situations[87]. However, in all these studies, discrete, event based techniques have been used. For a dynamic process such as the photodynamic action on biological tissue, event based but also time based modeling is required. The change of the molecular concentrations with respect to given thresholds, and the time variations need to be taken into account.

2.8 Source coding theory and mathematical formulation

The theory of data compression was introduced by Claude Shannon [94] as a mathematical theory of communication, in his foundational work on information theory. Rate–distortion theory is a major branch of information theory which provides the theoretical foundations for lossy data compression. The rate R is usually understood as the number of bits per data sample to be stored or transmitted. Shannon showed that, for a given source (with all its statistical properties known) and a

given distortion measure, there is a function $R(D)$, called the rate-distortion function. If D is the tolerable amount of distortion, then $R(D)$ is the best possible compression rate.

The basic elements of communication are

- The Source: Shannon calls it information source, which "produces a message, a “word” or sequence of messages to be communicated to the receiving terminal.
- Sender: Or transmitter, operates on the message in some way to produce a signal suitable for transmission over the channel
- Channel: The medium used to transmit the signal from transmitter to receiver.
- Receiver: It performs the inverse operation of that done by the transmitter, reconstructing the message from the signal.

To set up the foundation for the following studies, we recall the major definitions necessary[95]: It is customary in information theory to refer to a finite set A_M as an alphabet and to call its elements the letters of the alphabet. A probability distribution is a function $P(j)$ defined on A_M with values into $[0,1]$. A function X defined on A_M is called a random variable. In particular, we will be using random variables of the form $X(j) = \frac{j}{\max_j A_M}$ for j in A_M (normalized molecular concentrations). The expected value of a real random variable f is defined as $E(f) = \sum_j P(j) f(j)$. The self-information is denoted by $i(j) = -\log P(j)$ and it is a measure of the information one receives upon being told that the random variable X has assumed the value j . The base of the logarithm determines the information unit. For two alphabets A_M and A_N , a probability $P(j,k)$ distribution defined on the product space $A_M \times A_N$ is called a joint distribution. The marginal distributions are defined as

$$P(j) = \sum_{j} P(j,k) \tag{2.8.1}$$

$$Q(k) = \sum_{k} P(j,k) \tag{2.8.2}$$

And the conditional distributions are

$$P(j|k) = \frac{P(j,k)}{Q(k)} \tag{2.8.3}$$

$$Q(j|k) = \frac{P(j,k)}{P(j)} \tag{2.8.4}$$

The conditional self-information is defined by

$$i(j|k) = -\log P(j|k) \tag{2.8.5}$$

And it is a measure of the information one receives upon being told that the event $X = j$ if one knows already knows the occurrence of the event $Y = k$. The mutual information is defined as

$$i(j,k) = i(j) - i(j|k) = \log \frac{P(j|k)}{P(j)} = \log \frac{Q(k|j)}{Q(k)} = \log \frac{P(j,k)}{P(j)Q(k)}$$

(2.8.6)

A "word" distortion measure is a nonnegative function that specifies the penalty charged for reproducing a source letter or word from the first alphabet by a letter or word from the second alphabet, $d(j,k)$. With each conditional probability $Q(j|k)$ there is an associated average distortion:

$$d(Q) = \sum_{j,k} P(j) \cdot Q(k|j) \cdot d(j,k) \tag{2.8.7}$$

And an average mutual information

$$I(Q) = \sum_{j,k} P(j) \cdot Q(k|j) \cdot \log \frac{Q(k|j)}{Q(k)} \tag{2.8.8}$$

A conditional probability assignment is said to be D admissible if and only if $d(Q) \leq D$ and the set of all D admissible conditional probability assignments is denoted by Q_D. Then the rate distortion function is defined as

$$R(D) = \min_{Q \in Q_D} I(Q) \tag{2.8.9}$$

For a given source with probability $P(j)$, a distortion measure $d(j,k)$ and a maximum permissible value of average distortion D, the problem is to minimize the average mutual information $I(Q)$ by appropriate choice of the conditional probabilities $Q(k|j)$ subject to the constraints

$$Q(k|j) \geq 0 \tag{2.8.10}$$

$$1 = \sum_{k} Q(k|j) \tag{2.8.11}$$

$$\sum_{j,k} P(j) \cdot Q(k|j) \cdot d(j,k) = D. \tag{2.8.12}$$

The problem has been solved in [95] using the method of Lagrange multipliers, by forming the augmented functional

$$J(Q) = I(Q) - \sum_{j} \mu_j \cdot \sum_{k} Q(k|j) - s \sum_{k,j} P(j) \cdot Q(k|j) \cdot d(j,k) \tag{2.8.13}$$

Where the Lagrange multipliers are the parameters μ_j and S. In particular, the critical points will satisfy the equation

$$Q(k|j) = \frac{Q_k e^{s \cdot d(j,k)}}{\sum_l Q_k e^{s \cdot d(j,k)}} \tag{2.8.14}$$

For a particular negative value of the parameter S we can generate D and R parametrically from the equations

$$D = \sum_{j,k} [\frac{1}{\sum_k Q_k e^{s \cdot d(j,k)}} \cdot P_j Q_k e^{s \cdot d(j,k)} \cdot d(j,k)] \tag{2.8.15}$$

$$R = s \cdot D + \sum_j P(j) \log[\frac{1}{\sum_k Q_k e^{s \cdot d(j,k)}}] \tag{2.8.17}$$

The minimization problem is a quite technical problem and a complete mathematical analysis can be found in [95] .

In this study our aim is to try to interpret the cellular biochemical reaction network as a noisy communication channel and the cell as an information quantizer and understand how a cell decision is made upon processing of information through biochemical signaling. This might be useful in the effort to assess deviations and/or controversial data from cell survival studies, understand the reliability of a molecular cell death stimulus controlling the survival of a cell and use probability distributions of the form stimulus/decision, instead of a deterministic function that represents a “noiseless system”. Our case study will be the photodynamic action on a single cell. Mathematical modeling of biological problems has focused on the integration of the most crucial properties of the phenomenon under study into a model formulated in terms of continuum ordinary or partial differential equations. In this study, we develop an individual-based framework for modeling PDT reaction and cell processes, that can be used in integrated biology to accommodate biological complexity in cancer as well as other phenomena, through multiple scale techniques such as hybrid cellular automata [96].

CHAPTER 3: OXYGEN TRANSPORT IN TYPE II PDT

3.1 Clinical application and mathematical modeling

Conventional cancer therapies include radiation and chemotherapies, surgery, and a combination of any or all of those therapies. The treatments themselves have important side effects, even life-threatening. Photodynamic therapy offers an alternative, less invasive treatment for such illnesses such as several types of cancers, and has been recognized as an effective option for treatment of cancers and other diseases[43]. It involves the use of three basic components [97]: a photosensitizer, a light-absorbing molecule that is activated by the second element, light of a corresponding wavelength, and third, molecular oxygen is consumed during the photochemical reaction to produce cytotoxic agents, thus destroying neoplastic tissue. Clinically used photosensitizers associate with plasma membrane or intracellular membranes of the mitochondria, lysosomes and endoplasmic reticulum (ER) and a significant difference between PDT and chemotherapy or radiotherapy is that it is considered to be less geno-toxic since the major site of photosensitizers' localization are the above factors and not the nucleus [98].

Mathematical modeling is essential to clearly reveal and understand the fundamental processes underlying the properties of living biophysical systems in general, and the reaction of photodynamic therapy with biological tissue, in particular. It is accepted that cell photo-killing (induced in cultured cells) may involve all three main cell death morphologies described, i.e. apoptotic, necrotic and autophagy cell death [99]. Dynamic modeling of cell fate exist, for apoptosis/necrosis [100] and for autophagy [101], in a single cell model. In a previous work [102] we established a model of oxygen transport and cell killing in Type II PDT. This model can be directly linked to these cell fate models, to

provide a coherent model of the major biochemical events in PDT on the basis of major components and the main features of the intracellular interactions. Identifying major components of the Type II PDT bio molecular network and interactions and then deriving cell survival/death models, by using computational methods, is the goal of the analysis in the following chapters.

3.2 Study of oxygen diffusion in type II PDT

The therapeutic effects of PDT *in vivo* are realized through different mechanisms which include direct killing of target cells, vascular shutdown and induction or modification of immune response[103]. Investigations of PDT under *in vivo* conditions are critical to understand and improve clinical applications. On the other hand, *in vitro* studies of the very complex PDT processes with cultured cells have attracted significant attention for multiple reasons [104] [105] [106]. Detailed study of PDT *in vitro* within a controlled cellular environment is essential to analyze the multiple signaling pathways underlying the cell killing effect of PDT[103]. Secondly, cell killing through PDT yields a unique case study of system biology in which cell repair and death in response to combined stimulations of photosensitizer and light can be quantitatively investigated and modeled. In response to a type II PDT treatment, cell death can be initiated by production of singlet oxygen and other reactive oxygen species (ROS) with optically excited photosensitizers in the presence of oxygen molecules[107]. In addition oxygen functions as the essential molecules for cellular metabolism and other biochemical processes, such as membrane transport, growth, cellular repair and maintenance processes, a series of activities essential for cell survival. Most cellular activities require energy in the form of oxygen, primarily obtained from the degradation of adenosine triphosphate[108]. Oxygen must be present in sufficient amounts in the mitochondria to maintain effective concentrations of ATP in the electron transport system[108]. If oxygen availability is limited, functions such as contractility, electrolyte or protein transport, motility and various biosynthetic activities can no longer be maintained and irreversible alterations may occur[108].

Therefore, oxygen and associated transport play critical roles in the survival and death of PDT treated cells[103]. Thus a systematic study of oxygen transport in a single cell by taking into account of various molecular interactions and pathways can yield critical insights to understand the cytotoxicity and other effects of PDT.

The effects of oxygen consumption in photodynamic therapy (PDT) have been considered theoretically and experimentally by other authors, and mathematical models of the mechanism of photo-oxidation have been used to calculate and estimate the sensitizer and light dose delivered to a tumor undergoing PDT as well as oxygen depletion due to reaction with intracellular substrate [73, 109]. Experimental studies have shown that low fluence rates or fractionation of the exposure may improve the PDT effects[110]. Indeed, several studies demonstrating the variability in time and/or space of ground-state oxygen $^3O_2$ concentration[111, 112], sensitizer availability[113, 114] and light delivery to the treatment area [112] during typical therapy protocols suggest that the dynamic character of these quantities should be incorporated in PDT dosimetry[109]. For example, it has been proposed that the fact that the reaction of singlet oxygen can be monitored by measuring $^3O_2$ consumption, could be used to screen photosensitizers in vitro for desirable photophysical properties [115].

Our analysis is based on a previously established numerical model [7], that was introduced in order to study the molecular interaction involved in type II PDT processes in time domain and to describe the cascade of events that is believed to lead to potentially cytotoxic reactive oxygen species reactions(ROS). That model was based on a method of rate equations proposed by Foster and others [43] [73] [116]. The concentrations of key molecules in both ground and excited states were solved as functions of illumination time with a group of coupled rate equations. By defining two decay constants to characterize the loss of ground-state photosensitizer and receptor oxidation, the authors have investigated the dependence of photo bleaching and cytotoxicity on the initial concentrations of

photosensitizer and incident light irradiance at the molecular level. The existing model, however, does not account for the oxygen transport inside and outside of the cell and provides no direct link to the observable cell survival curves. In this study, we present a significantly improved PDT model which allows detailed examination of the roles played by oxygen and associated transport in a spherical cell configuration [117]. Furthermore, this model includes a rate equation of cell killing probability via two molecular "death effectors" of single oxygen molecules or ROS and their receptors for calculation of cell survival ratio as a function of incident light fluence or initial photosensitizer concentrations. Numerical results are obtained with this model to demonstrate its utility for relating the cell survival curves to various parameters of molecular interactions that are critical to understand cell killing by PDT. As a result, the present model provides for the first time a powerful tool to quantify the effects of oxygen in terms of cell survival curves that can be compared to the measured data.

3.3 Rate equation group

We have developed a rate equation based model[117] to quantify the time evolution of the following molecule species in a type II PDT process: photosensitizers in the singlet ground state S_0, photosensitizers in the singlet and triplet excited states S_1 and T, oxygen in triplet ground and singlet excited states ${}^3O_2$ and ${}^1O_2$, and receptor R. Even though the singlet excited oxygen molecules ${}^1O_2$ my play a critical role, it is well known that other ROS species are also involved in the cytotoxicity of PDT directly or indirectly at mitochondria as the source and target sites (first reactive oxygen species formed during photodynamic therapy (PDT) is ${}^1O_2$ but other ROS are formed downstream including superoxide anion $\bullet CO_2^-$,hydrogen peroxide, H_2O_2, and hydroxyl radical $\bullet OH$)[118]. Consequently, ${}^1O_2$ here should be interpreted as the ROS molecules including the singlet oxygen. We mainly consider two

pathways in modeling of cytotoxicity (the studies described in the next chapters involving a group of molecules should expand and elucidate the understanding of mechanisms of PDT cytotoxicity). One is the designation of the R receptors as the representation of those molecules that reside on mitochondria membranes and becomes oxidized by $^1O_2$ to initiate cell death or apoptosis processes through various pathways. Another relates to the presence of $^1O_2$ which drive a cell to start apoptosis if the concentration of ROS becomes high. With these guidelines in mind, we employ 6 rate equations to describe the time evolution of the key molecular concentrations leading to the accumulation of oxidized receptors represented by R involved in the cytotoxicity through a type II PDT mechanism as the following[117]:

$$\frac{d[S_0]}{dt} = -k_{pb}[^1O_2][S_0] - \nu\rho\sigma_{psa}[S_0] + \frac{\eta_{30}}{\tau_3}[T] + \frac{\alpha_S}{\tau_3}[T][^3O_2] \tag{3.3.1}$$

$$\frac{d[S_1]}{dt} = -\frac{1}{\tau_1}[S_1] + \nu\rho\sigma_{psa}[S_0]$$

(3.3.2)

$$\frac{d[T]}{dt} = \frac{\eta_{13}}{\tau_1}[S_1] - \frac{\eta_{30}}{\tau_3}[T] - \frac{\alpha_s}{\tau_3}[T][^3O_2] \tag{3.3.3}$$

$$\frac{d[^3O_2]}{dt} = -\frac{\alpha_s}{\tau_3}[T][^3O_2] + \frac{\eta_0}{\tau_0}[^1O_2] + D\nabla^2[^3O_2] - \frac{V_m[^3O_2]}{[^3O_2] + K_m} \tag{3.3.4}$$

$$\frac{d[^1O_2]}{dt} = -k_{pb}[S_0][^1O_2] - k_{cx}[R][^1O_2] - \frac{\eta_0}{\tau_0}[^1O_2] + \frac{\alpha_s}{\tau_3}[T][^3O_2] - k_{sc}[C]_i[^1O_2] \tag{3.3.5}$$

$$\frac{d[R]}{dt} = -k_{cx}[R][^1O_2] + U \tag{3.3.6}$$

The definitions of coefficients and their values used in the above equations have been detailed in[7] and are provided in the Table 1 for completeness. Use of the efficiency factor α_s for the bimolecular energy transfer from the excited photosensitizer PS to oxygen allows study of the effect of relaxation time τ_3 on the excitation of oxygen [7]. Equation (3.3.5) describes the photochemical processes that produce and consume $^1O_2$ molecules. For example, the first and second terms on the right-hand side of (Eq.3.3.5) are the rates of $^1O_2$ consumption in photo bleaching and oxidization of intracellular receptors. In addition, this equation also includes the reaction of $^1O_2$ with various oxygen scavengers with an average rate k_{sc} and concentration $[C]$. In this model it is also assumed that the cytotoxicity induced in a Type II PDT process is caused primarily by the oxidization of various intracellular receptors at the PS binding sites, including those of the vasculature in the tumor, with the highly active $^1O_2$ molecules [70]. In response, various repair mechanisms can be activated within a cell to undo the cytotoxic damage. When the concentration of cytotoxic agents exceeds a certain threshold in a cell, irreversible apoptosis or necrosis occurs[74, 119]. Consequently, the time evolution of unoxidized receptors $[R]$ should be determined by its reaction rate with $^1O_2$ and a repair rate U as in equation (3.3.6)[7]. The photo bleaching or destruction of the PS can occur by photochemical reaction of S_0 with $^1O_2$ in a first simplified approach, which can be described by a reaction rate k_{pb} in (Eq. 3.3.5). It is also possible that multiple types of intracellular receptors exist that react with 1O2 at different rates. Therefore, k_{cx} and $[R]$ should be regarded as the averaged values over different species of receptors involved in the PDT process[7]. The relaxation time of PS from S_1 to S_0 is given by τ_1, which has been estimated to be about 10 ns due to the fast transitions between the singlet states. The relaxation time of the PS for intersystem crossing from T to S_0, is given by τ_3, and has been estimated to be in the

range of microseconds to milliseconds [7]. Fast relaxation of the singlet oxygen τ_0 has been estimated to be about less than 1 μs [52, 120]. The quantum yields of the S_1 to S_0, T to S_0 for the PS and the $^1O_2$ to $^3O_2$ are η_{10}, η_{30} and η_0 respectively as found in the literature [121] [122]. Because no experimental data could be found, a small value of $k_{sc}[C]_i$ is used, which has minimal influence on $[^1O_2]$ and $[R]$ over the time.

Conditions at an initial time from which the system of the 6 rate equations describing the physical system of the PDT treated cell evolves. The initial value problem needs to be specified and the initial conditions of Eq. (3.3.1) to (3.3.6) at the beginning of illumination ($t = 0$) are given by an initial concentration vector of $([S_0],0,0,[^3O_2],0,[R]_i)$.The spatial variation of the oxygen concentration is limited to the interior of a cell, i.e., $0 < r < r_0$, with r_0 as the radius of the spherical cell. The second term U on the right hand side of Eq. (3.3.6) is set to be a very small positive constant at 1($cm^{-3}s^{-1}$) for avoiding appearance of negative concentrations in numerical calculations. It is verified that the small valued U has no effect on calculations of decay constants and cell survival ratio[117].

Among the six equations listed above, the first three and last two remain the same as presented in a previous publication[7] and the corresponding species can be assumed not to diffuse. These species have very short lifetimes after their formation and are not expected to diffuse a significant distance before their transition[123] or, in the case of singlet oxygen, react with cellular substrates[124]. More precisiely: in these equations, we do not consider spatial dependence of concentrations for these molecules for two reasons. First, the molecules of photosensitizers and receptors are much larger and more massive than the small molecules of $^3O_2$ and therefore the related diffusion will take much longer time to become significant on PDT process. This argument should also apply to the excited

photosensitizers T acting as a substrate for transferring energy from photons to oxygen molecules (with a relaxation time τ_3 as discussed before). With respect to S_1 and $^1O_2$, these highly chemically active molecules have very fast relaxation rates to ground states. Based on literature, their respective relaxation times of τ_1 and τ_0 are much smaller than τ_3, and thus prevents them from diffusing into locations other than the immediate neighboring sites. With these arguments we consider the effect of diffusion for the ground-state oxygen $^3O_2$ only (Figure 3.3.1).

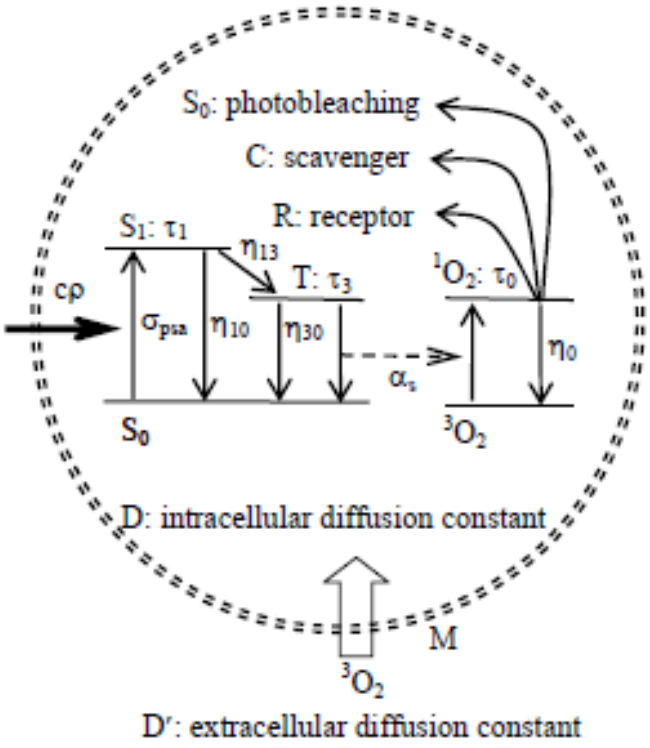

Figure 3.3.1. A schematic diagram to illustrate the molecular interaction and diffusion in a spherical cell model[125].

3.4 Oxygen diffusion and boundary conditions

Having discussed the reactions and rate equations of the photochemical dynamics and the corresponding constraints on the molecular concentrations and constants, we know analyze the boundary conditions, to gain some insight on the requirements that need to be expressed in terms of transport parameters of the problem. Diffusion of $^3O_2$ in cells has attracted research interests in consideration of cellular metabolism and other biochemical processes. Quantitative modeling has been pursued in a spherical configuration in which a spherical symmetry of oxygen distribution or $[^3O_2](\vec{r}) = [^3O_2](r)$ was assumed to simplify mathematical treatment[125]. With this model one considers the rate of oxygen uptake by molecules in the metabolism and processes unrelated to PDT using a nonlinear Michaelis-Menten term of two adjustable parameters: V_m represents the maximum rate of oxygen uptake as $[^3O_2](r) \to \infty$ while K_m yields the value of $[^3O_2]$ for the Michaelis-Menten term to reach a half-maximum uptake rate[125]. We adopt this spherical cell configuration to study oxygen diffusion in a type II PDT process using the equation for molecular oxygen. A word of caution here: A limitation is that Michaelis–Menten kinetics relies upon the law of mass action which is derived from the assumptions of free (Fickian) diffusion and thermodynamically-driven random collision. However, many biochemical or cellular processes deviate significantly from such conditions. For example, the cytoplasm inside a cell behaves more like a gel than a freely flowable or watery liquid, due to the very high concentration of protein (up to ~400 mg/mL) and other “solutes”, which can severely limit molecular movements (e.g., diffusion or collision). This causes macromolecular crowding, which can alter reaction rates and dissociation constants [126] [55] [127].

To establish an appropriate boundary-value problem related to oxygen diffusion, boundary conditions at the cell center ($r = 0$) and membrane ($r = r_0$), [80] are introduced in the following to complement the Eq. (3.3.4):

$$\frac{\partial[^3O_2]}{\partial t} = 0 \text{ if } r = 0 \tag{3.4.1}$$

$$D\frac{\partial[^3O_2]}{\partial t} = M\{[^3O_2]' - [^3O_2]\} \text{ if } r = r_0 \tag{3.4.2}$$

where M is the parameters of oxygen permeability and $[^3O_2]'$ refers to the outside concentration (the membrane allows small molecules like oxygen to pass through easily and it is permeable to this molecule). The oxygen molecules move into the cell and out of the cell at the same rate, and a dynamic equilibrium will exist. Unless, the cell consumes some of the oxygen as it comes into the cell, and therefore more oxygen will move into the cell than out of the cell. If $[^3O_2]'$ distributes outside the cell according to a homogeneous diffusion process with D as the extracellular diffusion constant, one can show that the boundary conditions can be further simplified to the following:

$$\frac{\partial[^3O_2]}{\partial t} = 0 \text{ if } r = 0 \tag{3.4.3}$$

$$D\frac{\partial[^3O_2]}{\partial t} = M\left\{1 - \frac{Mr_0}{D' + Mr_0}\right\} \cdot \{[^3O_2]_i - [^3O_2]\} \text{ if } r = r_0 \tag{3.4.4}$$

Where we assumed $[^3O_2]_\infty = [^3O_2]_i$ as the oxygen concentration far from the cell. In this study the permeability M is used as one of the adjustable parameters to account for the variation of topology of cell membrane due to the presence of microvilli and ruffles. For example, it has been suggested that ruffled cell membrane can reduce its permeability to oxygen because of extended area using a 2D

random walk model[128]. For results presented here, we vary the parameter M from a "classical" value of $2\times10^{-2}(cm/s)$ [129] to $2\times10^{-5}(cm/s)$ to allow a detailed study of oxygen permeability across the cell membrane. Fig. 3.3.1 illustrates schematically various molecular reactions and processes involved in a type II PDT considered here with the coefficients and parameters characterizing the interactions and oxygen transport in a spherical cell.

3.5 Decay constants of photosensitizer and receptor concentrations

The group of differential equations from (1) to (6) can be solved numerically in time domain under the boundary conditions of Eq. (8) to obtain a solution vector of 6 molecular concentrations[117]. The effects of oxygen diffusion within the cell and across the membrane on the solution vector of concentrations are investigated with this model for quantitative understanding of the molecular kinetics related to the type II PDT. We use the partial differential equation (PDE) solver (pdepe) by MATLAB (The MathWorks, Natick, MA) to obtain the solution vector as a function of illumination time t from the start of illumination at t=0 to 3000 (s). Two components of the solution vector, $[S_0]$ and $[R]$, are of particularly interest to our study whose concentration and time dependences can be used to quantify the phenomena of photo bleaching and cytotoxicity in a type II PDT process. Consequently we define two decay constants of t_S and t_R for characterization of the initial decrease of $[S_0]$ and $[R]$, respectively, caused by photon absorption[7]. The two decay times t_S and t_R are defined as the times for $[S_0]$ and $[R]$ to be reduced to 1% of their initial values:

$$[S_0](t_S) = 0.01\cdot[S_0](0) \tag{3.5.1}$$

$$[R](t_S) = 0.01\cdot[R](0) \tag{3.5.2}$$

These decay times are functions of initial drug dose and irradiance of incident light in terms of $[S_0]_i$ and ρ at the binding locations and have been used to quantitatively study the phenomena of photobleaching and cytotoxicity in modeling studies[7]. Utilization of t_S and t_R allows detailed mapping of these decay constants on the grid of the two key parameters mentioned above: photon density ρ proportional to the incident light irradiance and the initial photosensitizer concentration $[S_0]_i$ for inducing cytotoxicity[117]. Effects of other parameters have been studied by mapping the two decay constants at different values of the oxygen diffusion constants D and D', the membrane permeability M and the maximum rate of oxygen uptake V_m.

3.6 Cell killing model

The equation group from (3.3.1) to (3.3.6) can be solved to characterize the main molecular interaction involved in type II PDT. While some of the molecular concentrations are measurable such as $[S_0]$ and $[^3O_2]$, experimental verification of these quantities can be difficult, if not impossible, and they relate indirectly to the ultimate consequence of PDT for cell killing. It is thus highly desired to develop a cell killing model that can link the molecular concentrations to the cell survival ratio which can be measured with an *in vitro* cell model[117]. To build this model we employ survival analysis and we need to define the "cell survival probability N" so that cell biological survival is unambiguous. Cell death (necrosis/apoptosis/autophagy as discussed in later chapters) is considered an event in the survival analysis and only a single event occurs for a single cell model, after which the cell is dead. Recurring event situations are not applicable in this model. We mainly consider two forms of cytotoxicity related to PDT induced by ROS. One is due to the accumulation of oxidized receptors for initiation of apoptosis with the rate of cell killing linearly proportional to the concentration of oxidized receptors [75]. Another is described by a nonlinear term similar to the Michaelis-Menten terms used in

triplet oxygen equation, which represents the receptor-independent contributions to the rate of cell killing as a result of ROS stress[130]. This term becomes significant as the concentration of $[^1O_2]$ or ROS becomes large relative to K_c . The nonlinear term therefore allows the inclusion of the coefficient K_c to simulate the effect of cell repair. We include these two terms into the following equation to quantify the PDT cytotoxicity as

$$\frac{dN}{dt} = -\beta_0 (1 - \frac{[R]}{[R]_i}) N - \frac{V_c [^1O_2]}{[^1O_2] + K_c} \tag{3.6.1}$$

where N can be interpreted as either the cell survival ratio or probability of cell survival with the initial condition given by $N(0) = 1$, the coefficients of β_0 and V_c are parameters that can be adjusted to vary the weights of the two terms and K_c is used for characterization of the cell's ability to resist or repair damage by ROS. This is a first order linear differential equation and the solution can be written as:

$$N(t) = e^{-\int_0^t \beta_0 \left(1 - \frac{[R]}{[R]_i}\right) dt} \cdot \left(\int_0^t \frac{V_c [^1O_2]}{[^1O_2] + K_c} \cdot e^{\int_0^{t'} \beta_0 \left(1 - \frac{[R]}{[R]_i}\right) dt'} dt + 1 \right)$$

(3.6.2)

The values of these coefficients are given in Table 1 for results presented below. The above equation can be solved simultaneously with equations of (3.3.1) to (3.3.6) under the boundary condition of Eq. (3.4.3) and (3.4.4) to obtain the cell survival ratio N as a function of incident light fluence F . The fluence F is obtained from the illumination time t and the irradiance of incident light or the photon density ρ as $F \propto \rho t$.

3.7 Positive definite test of the solution vector in time-domain

Many investigations in the field of partial differential equations has been focused on maximum principles for elliptic and parabolic equations. Weak and strong maximum principles for elliptic and parabolic equations have been proved by several authors that lead to uniqueness theorems especially for linear and nonlinear diffusional equations [131, 132] [133] . Eq. (3.3.1) to (3.3.6) form system of parabolic partial differential equations (PDE) with the boundary condition defined in Eq. (3.4.3-3.4.4). It is therefore of interest to inquire under what conditions the equation group could produce a solution vector of positive definite components to be consistent with their definitions[103]. To derive these conditions, we employ a strong maximum principle recently proved for parabolic PDE [134]. Each of Eq. (3.3.1) to (3.3.3) and (3.3.5) to (3.3.6) in the group can be casted into a parabolic PDE form like Eq. (3.3.4) if we add a Laplace term with a positive diffusion constant of negligibly small value $1\times10^{-15}(cm^2/s)$ [103]. This allows us to use Eq. (3.3.4) as an example for application of the strong maximum principle by replacing $[^3O_2]$ with a function $f(r,t)$ which is assumed to be continuous over the domain of $(0\le r<r_0, 0\le t)$. We first rearrange Eq. (3.3.4) into the following form:

$$\frac{\partial f}{\partial t}-D\nabla^2 f+(\frac{V_m}{f+K_m}+\frac{\alpha_s}{\tau_3}[T])f-\frac{\eta_0}{\tau_0}[^1O_2]=0 \qquad (3.7.1)$$

If $\frac{\eta_0}{\tau_0}[^1O_2]\ge 0$ then the above equation can be turned into an inequality as

$$\frac{\partial f}{\partial t}-D\nabla^2 f+\gamma\cdot f\ge 0 \qquad (3.7.2)$$

where $\gamma(r,t)=\frac{V_m}{f+K_m}+\frac{\alpha_s}{\tau_3}[T]$. The strong maximum principle applies to the above inequality if D and γ are locally bounded and $\gamma\ge 0$, which yields the following conclusion[134]: $f(r,t)=0$ for all

$t \le t_0$ if $f(r,t) = 0$ at $t = t_0$. According to this result a molecular concentration $f(r,t)$ remains positive once it becomes positive as long as the following two conditions are satisfied: (i) other coupling molecular concentrations (such as $[^1O_2]$) stay positive to ensure that Eq. (3.7.1) can be converted into the inequality (3.7.2); (ii) the coefficient γ is positive. A quick examination shows that each of the Eq. (3.3.1) to (3.3.6) can be converted into the form of inequality (3.7.2) and both conditions can be satisfied if the concentrations of the coupling molecules are initially positive or become positive after t=0. One should note that the strong maximum principle applies only to the open domain of the spatial variable r $(0 \le r < r_0)$. At the boundary of spatial domain $r = r_0$, a molecular concentration is not prohibited to become negative [103].

3.8 Results and discussion

***Time-domain results during light illumination for the molecular concentrations*:** We solve the boundary-value problems of molecular concentrations defined by the group of Eq. (3.3.1) to (3.3.6) under the boundary condition of Eq. (3.4.3-4) in the time domain from $t = 0$ to $3000(s)$ with 1000 steps on a logarithmic scale to reduce numerical errors. The spatial domain between the cell center at $r = 0$ to the membrane boundary at $r = 5(\mu m)$ (μm) is divided into a linear mesh of either 10-step or 40-step. Fig. 3.8.1 presents the time dependence of 6 normalized molecular concentrations calculated with the 40-step spatial mesh with the oxygen diffusion shut off by using negligible diffusion constants of D and D' . The concentrations are plotted against the illumination time t in two groups: the ground-state molecules of $[S_0]$, $[^3O_2]$, $[R]$ and the excited ones of $[S_1]$, $[T]$, $[^1O_2]$. Three intracellular locations are chosen to exhibit the spatial variation of concentrations. The lack of oxygen diffusion requires the use of high initial oxygen concentration at $[^3O_2]_i = 5.0 \times 10^{17} (cm^{-3})$ to observe significant decay of $[S_0]$ and $[R]$ for $t \le 3000(s)$. It can be seen easily from the result

presented in Fig. 3.8.1 that the lack of oxygen leads to progressively severe hypoxia for locations away from the cell boundary at $r = r_0$. This in turn affects the production of singlet oxygen so that the maximum values of $[^1O_2]$ decreases from 85.2% at $r = 0.975 \cdot r_0$ to 24.9% at $r = 0$ in comparison to the maximum $[^1O_2]$ at the boundary of $r = r_0$. Similarly the decrease of unoxidized receptor concentration $[R]$ becomes less steep as one moves towards the cell center at $r = 0$. By raising the oxygen diffusion constants towards 10^{-5} to $10^{-6}(cm^2/s)$, the intracellular heterogeneity of oxygen distribution starts to disappear as confirmed by the results calculated at different locations (not shown here). We point out that all of the concentration values shown in Fig. 3.8.1 and other similar results remain positive, as expected based on the strong maximum principle.

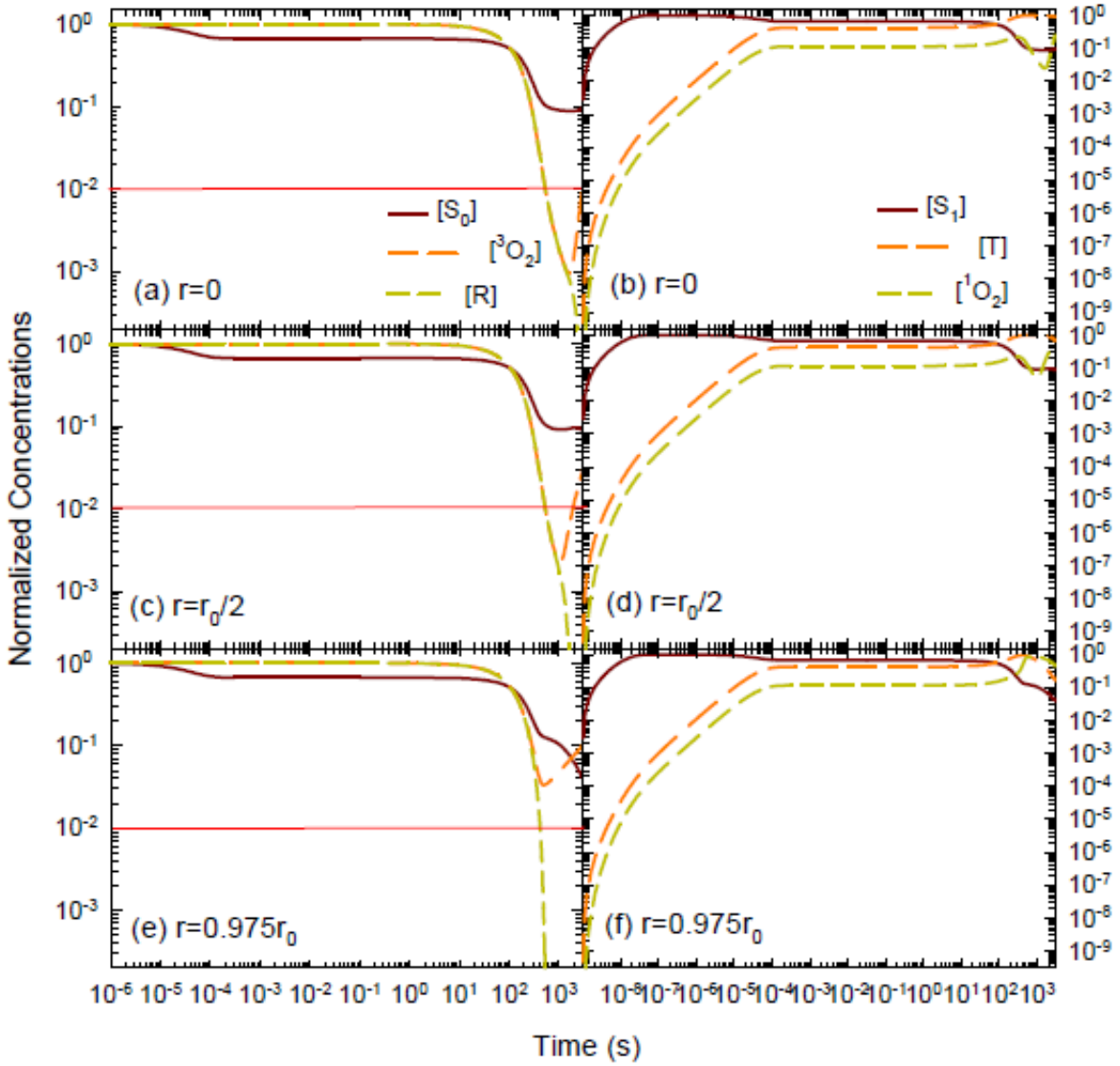

Figure 3.8.1 Time dependence of the solution vector at three intracellular locations using a 40-step spatial mesh and illumination starting at $t = 0$: (a),(c) and (e): concentrations of ground-state molecules normalized by their initial values; (b), (d) and (f): concentrations of excited molecules normalized by their maximum values on the spatial mesh. The values of the parameters are given by: $\rho = 1\times10^{6}(cm^{-3})$, $[S_0]_i = 5.00\times10^{11}(cm^{-3})$, $D = 8.00\times10^{-12}(cm^2/s)$, $D' = 2.00\times10^{-12}(cm^2/s)$, $M = 2.00\times10^{-2}(cm/s)$, $[^1O_2]_i = 5.06\times10^{17}(cm^{-3})$, $V_m = 0$. The values of other coefficients are given in the Appendix A and the red lines indicate the thresholds for the decay constants.

In Fig. 3.8.2 we compare the molecular concentrations calculated at the boundary of $r = r_0$ obtained with different spatial meshes of 40- and 10-step to increase simulation speed. The values of $[R]$ indeed become negative at the cell boundary for $[R]$ at t ~ 500 (s) for both spatial meshes. By increasing the spatial mesh density or the step number from 10 to 40, the number of negative $[R]$ values, however, can be reduced from 20 to 7 among the 1000 data points in the time domain. In all cases the magnitude of negative $[R]$ values are less than 10^{-3} of its initial value. These results suggest that the negative $[R]$ calculated from the boundary-value problem defined here can be attributed to the numerical rounding errors. Furthermore, the appearance of small negative values of $[R]$ does not affect our calculation of the decay constant and use of 10-step mesh can significantly reduce computation time with little reduction in accuracy. Consequently, we adopt the 10-step mesh for the calculation of decay constants presented below.

To illustrate the effect of diffusion, we show in Fig. 3.8.3 the time-domain data with diffusion constants typically used in previous studies of oxygen diffusion[129, 135]. For these high values of D and D', sufficient oxygen is supplied through diffusion so the time evolution of the concentration vector is nearly independent of spatial location. Consequently, Fig. 3.8.3 presents only the results calculated at the middle location of the spherical cell. Because of the efficient diffusion, the influence of initial oxygen concentration $[^3O_2]_i$ is much reduced. In the previous study we proved that the time evolution and decay constants of $[S_0]$ and $[R]$ is very sensitive to the values of $[^3O_2]_i$ without consideration of oxygen diffusion, as shown by Figs. 5 and 6 in [117]. Those data are significantly different from the results presented in Fig. 3.8.3 in which a large difference in $[^3O_2]_i$ leads to similar time evolution of molecular concentrations. Nevertheless, $[^3O_2]_i$ can affect the levels of $[^1O_2]$ and subsequently the cell survival ratio as described by Eq. (2.6.1).

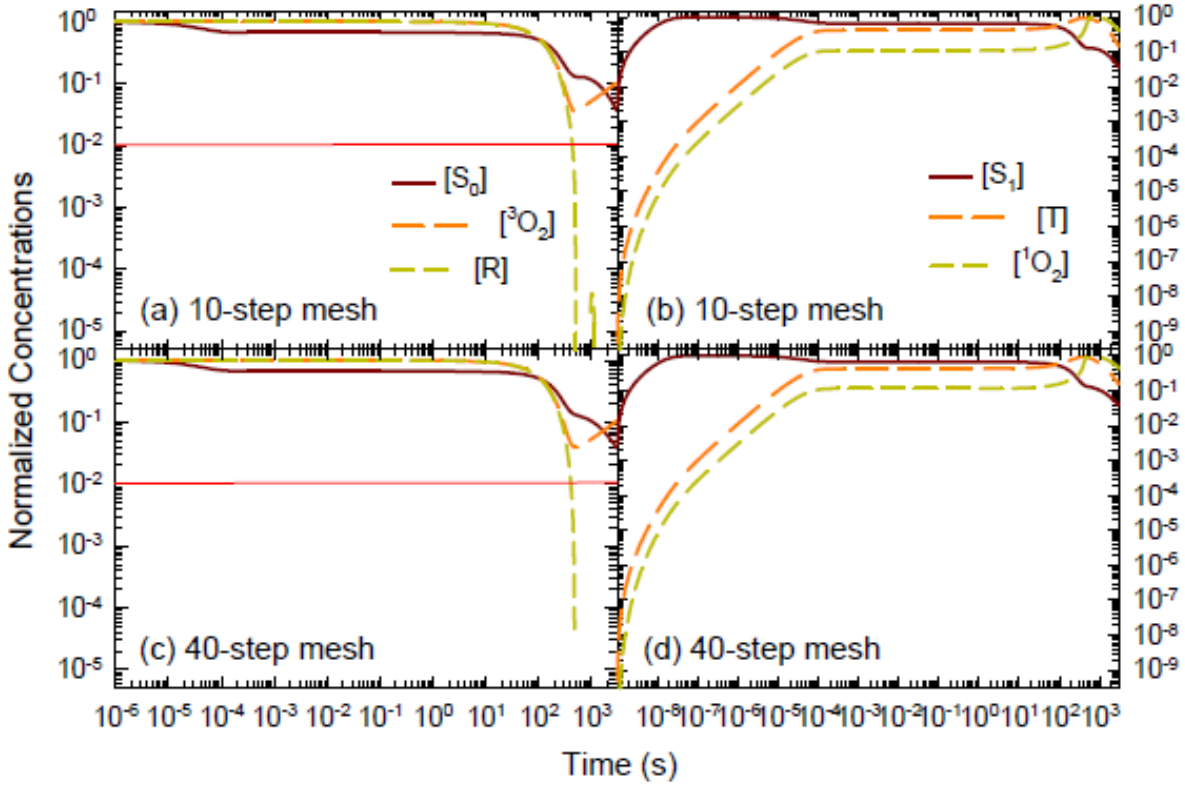

Figure 3.8.2 Time dependence of the solution vector at the cell boundary $(r = r_0)$ using two spatial meshes of 10-step and 40-step: (a) and (c): normalized concentrations of ground-state molecules; (b) and (d): normalized concentrations of excited molecules. All parameters and coefficients are of the same values as those in Fig. 3.8.1.

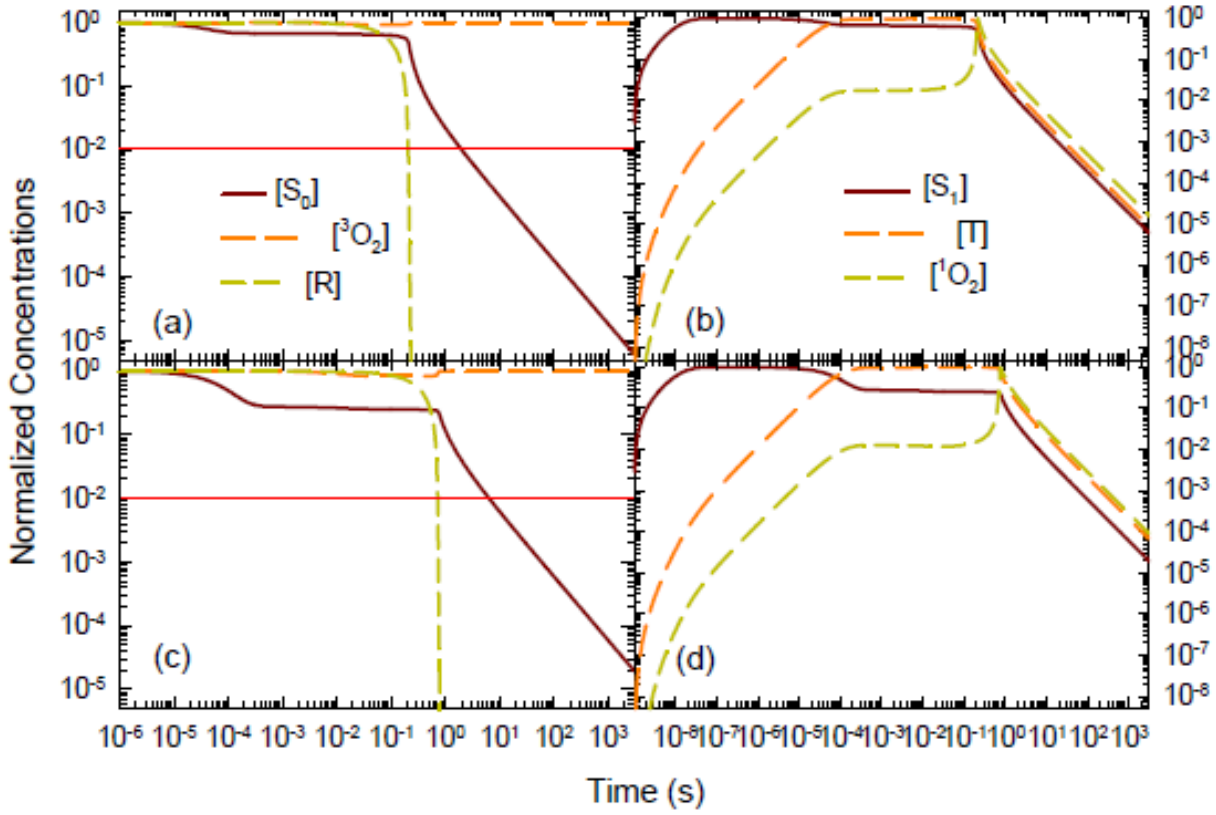

Figure 3.8.3. Time dependence of the solution vector at the middle of the cell $(r = \frac{r_0}{2})$ using the 40-step mesh and $D = 8 \times 10^{-6} (cm^2 / s)$ and $D' = 2.00 \times 10^{-5} (cm / s)$ for different initial oxygen concentration: (a) and (b): $[^3O_2]_i = 5.0 \times 10^{17} (cm^{-3})$; (c) and (d): $[^3O_2]_i = 7.0 \times 10^{16} (cm^{-3})$. All other coefficients are of the same values as those in Fig. 3.8.1.

Mapping of decay constants on the mesh of $[S_0]_i$ ***and*** ρ ***:*** As can be seen from the results in Figs. 3.8.1 to 3.8.3, the time evolutions of photosensitizer concentration $[S_0]$ and unoxidized receptor concentration $[R]$ are often dominated by steep reduction with increasing time of illumination. This prompts us to define two decay constants of t_S and t_R to characterize efficiently the two key processes in the type II PDT at the molecular level: photobleaching related to $[S_0]$ and cytotoxicity related to $[R]$. The group of Eq. (3.3.1) to (3.3.6) is solved in time domain to obtain t_S and t_R as the times for $[S_0]$ and $[R]$ to be reduced to 1% of their initial values at various values of the initial photosensitizer concentration $[S_0]_i$ and photon density ρ. The time-domain calculations and extraction of t_S and t_R are iterated on a 20x20 semi-log mesh of $[S_0]_i$ and ρ with $[S_0]_i$ ranging from 2.0x10^{12} to 1.0x10^{15} (cm^{-3}) and ρ ranging from 1.0x10^5 to 2.0x10^7 (cm^{-3}). The maximum values of the chosen ranges correspond respectively to about 5 (μg/ml) for Photofrin used as photosensitizer and about 80 (mW/cm^2) for the incident light irradiance as it relates to ρ **[7]**. Different values of the oxygen diffusion constants, permeability and strength of the Michaelis- Menten term parameters are employed for the time-domain calculations carried out at two locations of cell center $r = 0$ and boundary $r = r_0$. As a reference, Fig. 3.8.4 presents the results of decay constants obtained with $D = 8.0\times10^{-6}(cm^2/s)$, $D' = 2.00\times10^{-5}(cm^2/s)$, and $M = 2.00\times10^{-2}(cm/s)$ and $V_m = 2.9\times10^{18}(cm^{-3}\cdot s^{-1})$ based on previous reports[129] with a low initial oxygen concentration of $[^3O_2]_i = 7.0\times10^{16}(cm^{-3})$. Since t_S and t_R exhibit similar dependences on $[S_0]_i$ and ρ among all three cell locations, only those at the cell center of $r = 0$ are presented in Fig. 3.8.4. In contrast, the mapping of decay constants are presented in Figs. 3.8.5 and 3.8.6 at both cell center and boundary with different values of D, D', $[^3O_2]_i$ and M.

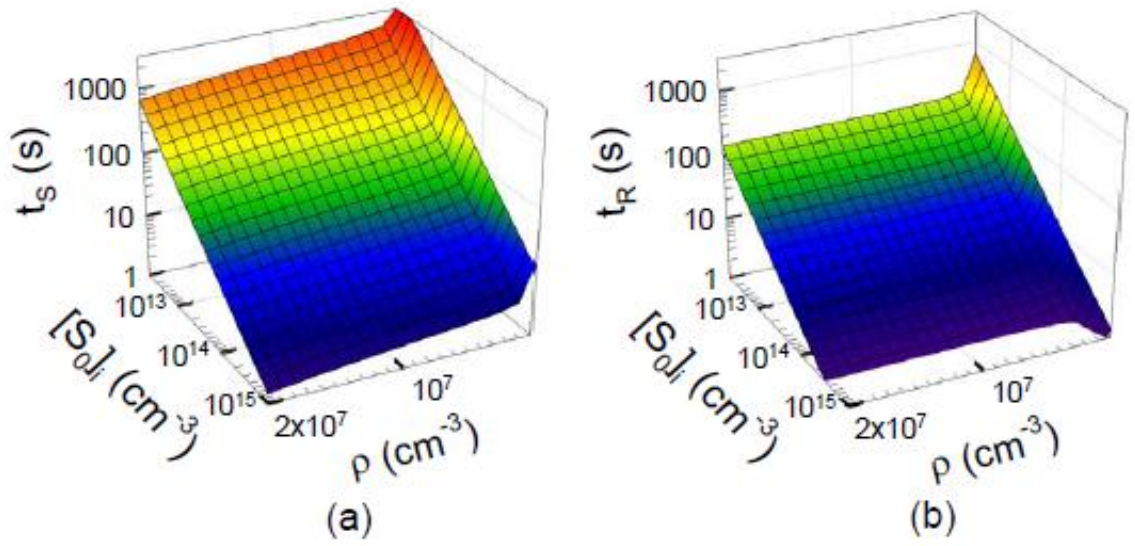

Figure 3.8.4. The decay constants of (a) t_S and (b) t_R versus the initial photosensitizer concentration $[S_0]_i$ and photon density ρ at the cell center $(r = 0)$. The values of parameters are given by D =8$\times$ 10^{-6} (cm^2/s), D' =2$\times 10^{-5}$ (cm^2/s), M =2.00$\times 10^{-2}$(cm/s), $[^3O_2]_i$ =7.00$\times 10^{16}$ and V_m =2.9$\times 10^{18}$ (cm$^{-3}\cdot$s^{-1}) with all other coefficients given in the Appendix A.

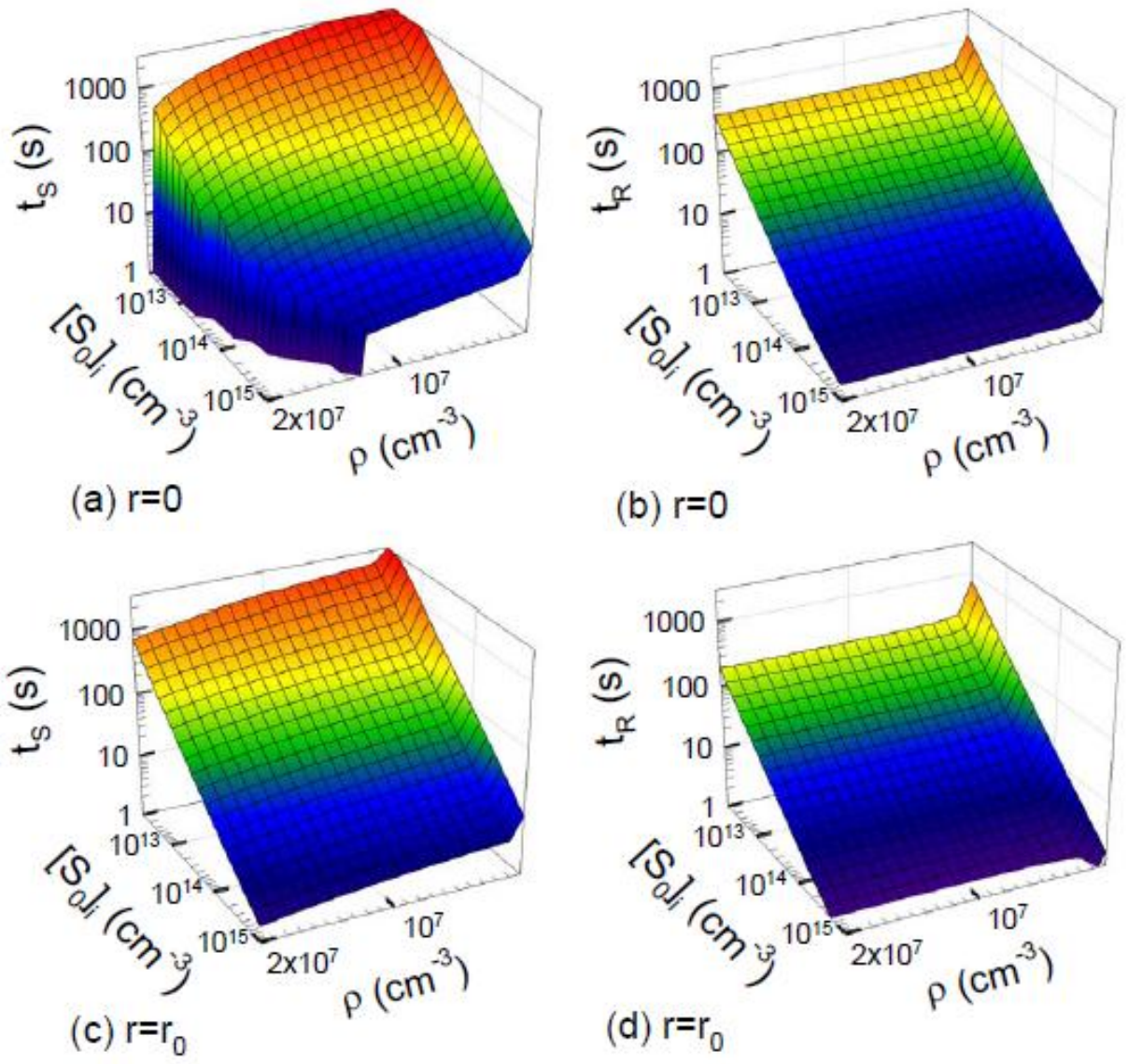

Figure 3.8.5. The decay constants of t_S and t_R versus the initial photosensitizer concentration $[S_0]_i$ and photon density ρ at the cell center $(r = 0)$ for (a) and (b); at the cell boundary $(r = r_0)$ for (c) and (d). The values of other parameters and coefficients are the same as those in Fig. 3.8.4 except the following: $D = 8.00 \times 10^{-7} (cm^2 / s)$, $D' = 2.0 \times 10^{-6} (cm^2 / s)$.

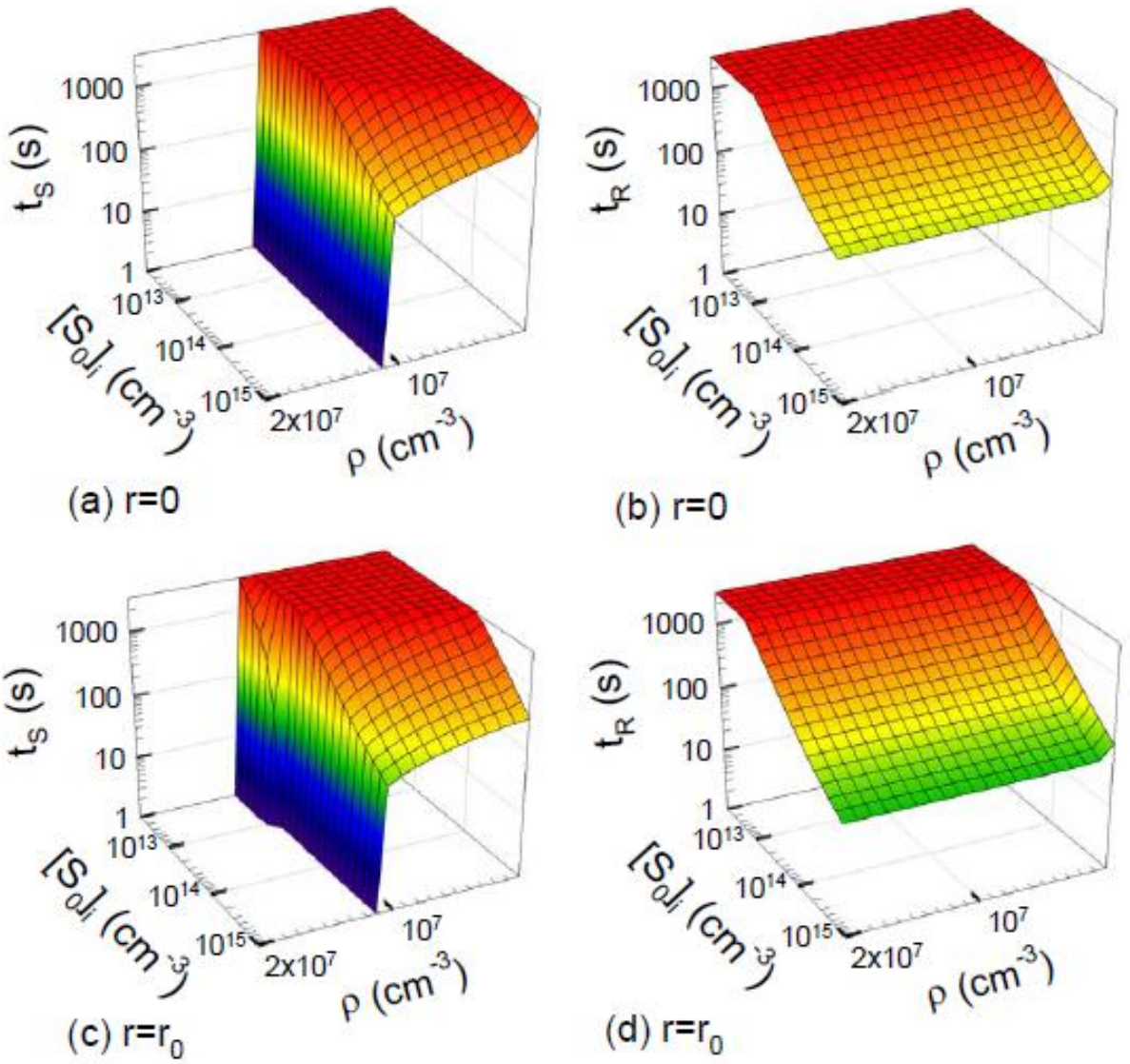

Figure 3.8.6. The decay constants of t_S and t_R versus the initial photosensitizer concentration $[S_0]_i$ and photon density ρ at the cell center $(r = 0)$ for (a) and (b); at the cell boundary $(r = r_0)$ for (c) and (d). The values of other parameters and coefficients are the same as those in Fig. 3.8.5 except the following: $M = 2.00 \times 10^{-5} (cm/s)$.

The results presented in Figs. 3.8.4 to 3.8.6 demonstrate the utility of the modeling tool developed here, which makes it possible to quantitatively investigate and compare the different effects on the molecular aspects of PDT by variation of parameters related to the supply and consumption of oxygen. We examine the mapping results without the presence of additional oxygen consumption described by the Michaelis-Menten term by setting V_m =0 and find no significant changes from the results in Fig. 3.8.6. It appears that the oxygen consumption via metabolism has limited effect on the decay of $[S_0]$ and $[R]$ in PDT for the V_m used and causes no significant differences among the decay constants calculated at different cellular locations. We also observe that for the ranges of $[S_0]_i$ and ρ chosen, the decay constants are of much higher sensitivity to $[S_0]_i$ than that to ρ, which indicates sufficient supplies of photons and oxygen. With the Michaelis-Menten term, we further examine the effect of oxygen diffusion by reduction of the diffusion constants by 10-fold and the permeability by 1000-fold. These variations lead to observable changes of the decay constants at different cell locations as shown in Figs. 3.8.5 and 3.8.6. It is interesting to note that the weakened oxygen transport can cause faster photo bleaching but slower oxidization of the receptors R at the cell center than those at the boundary as the photon density or incident light irradiance is increased.

***The cell survival curves*:** Accurate modeling of cell killing by PDT remains a challenging task because of the complexity of the process. As our first effort towards an eventual solution, the group of Eq. (3.3.1) to (3.3.6) and (3.6.1) are solved under the boundary conditions described by Eq. (3.4.4) to obtain the cell survival ratio or probability N as a function of illuminating time t. The solution is then converted into a function of incident light fluence, $N(F)$, by converting t into light fluence as F = $4\text{x}10^{-9}\ \rho t$ in the unit of (J/cm^2) with ρ and t taking the unit of (cm^{-3}) and (s), respectively[7]. After detailed analysis of the results calculated with different coefficients used in Eq. (3.6.1), we chose the

values of β_0, V_c, and K_c as given in the Table 1 to obtain numerical results that are comparable to the measured data published by other researchers [105, 136, 137]. Fig. 3.8.7 presents typical results of cell survival curves obtained with $\beta_0 = 1.0 \times 10^{-2} (s^{-1})$ and different values of ρ, $[S_0]_i$, $[^3O_2]_i$, D, D' and M. Each set of curves consists of triplicate lines calculated at three spatial locations of cell center, middle and boundary with each assumed to be the targeted sites of PDT cytotoxicity. The cell survival curves presented in Fig. 3.8.7 can be divided into two parts that relate separately to the two terms on the right-hand side of Eq. (3.6.1). The first term is linearly proportional to $[R]$ and determines the slope of the initial exponential decrease of N for small F. As F rises, the second term related to $[^1O_2]$ concentration or ROS stress starts to contribute to the killing rate and causes an accelerated drop of the survival curve.

From Fig. 3.8.7(a) to 3.8.7(d), we show in each diagram three sets of curves calculated at different photon density values with different parameters of initial oxygen concentration and diffusion constants. It is clear from these results that increasing photon density leads to increasing survival ratio at the same fluence, which is widely known in the cell study of PDT as a result of poor oxygen supply for illumination at high irradiance [105, 136, 137]. The effect of poor oxygen supply or hypoxia can be further seen by comparing Fig. 3.8.7(b) to 3. 8.7(a) where $[^3O_2]_i$ is reduced by a factor of 100 to yield significant enhancement of cell survival. The oxygen diffusion constants and permeability also influence cell survival as demonstrated in Fig. 8(c) and 8(d) in which D, D' and M are reduced. These results show higher cell survival ratios correlates to weakened oxygen diffusion and variation of cell killing among cells with different target site locations due to spatial heterogeneity in oxygen distribution. Finally Fig. 3.8.7(e) and 3.8.7(f) present the modeling results using different initial photosensitizer concentrations and diffusion constants. Fig. 8(a) reveals that increasing $[S_0]_i$ leads to reduced cell survival as expected.

But an 142-fold increase in the supply of $[S_0]_i$ is not accompanied by a similarly enhanced cell killing as demonstrated by the relatively small difference between the two sets of curves labeled with $[S_0]_{i1}$ and $[S_0]_{i2}$ in Fig. 3.8.7(e). The reduced oxygen diffusion in Fig. 3.8.7(f) exhibits marked difference among the triplicate lines obtained at different cell locations, especially for the low value of $[S_0]_i$ at $[S_0]_{i3}$, which indicates a strong competition for oxygen between the cytotoxicity of PDT and unrelated metabolism processes represented by the Michaelis-Menten term in Eq. (3.3.4).

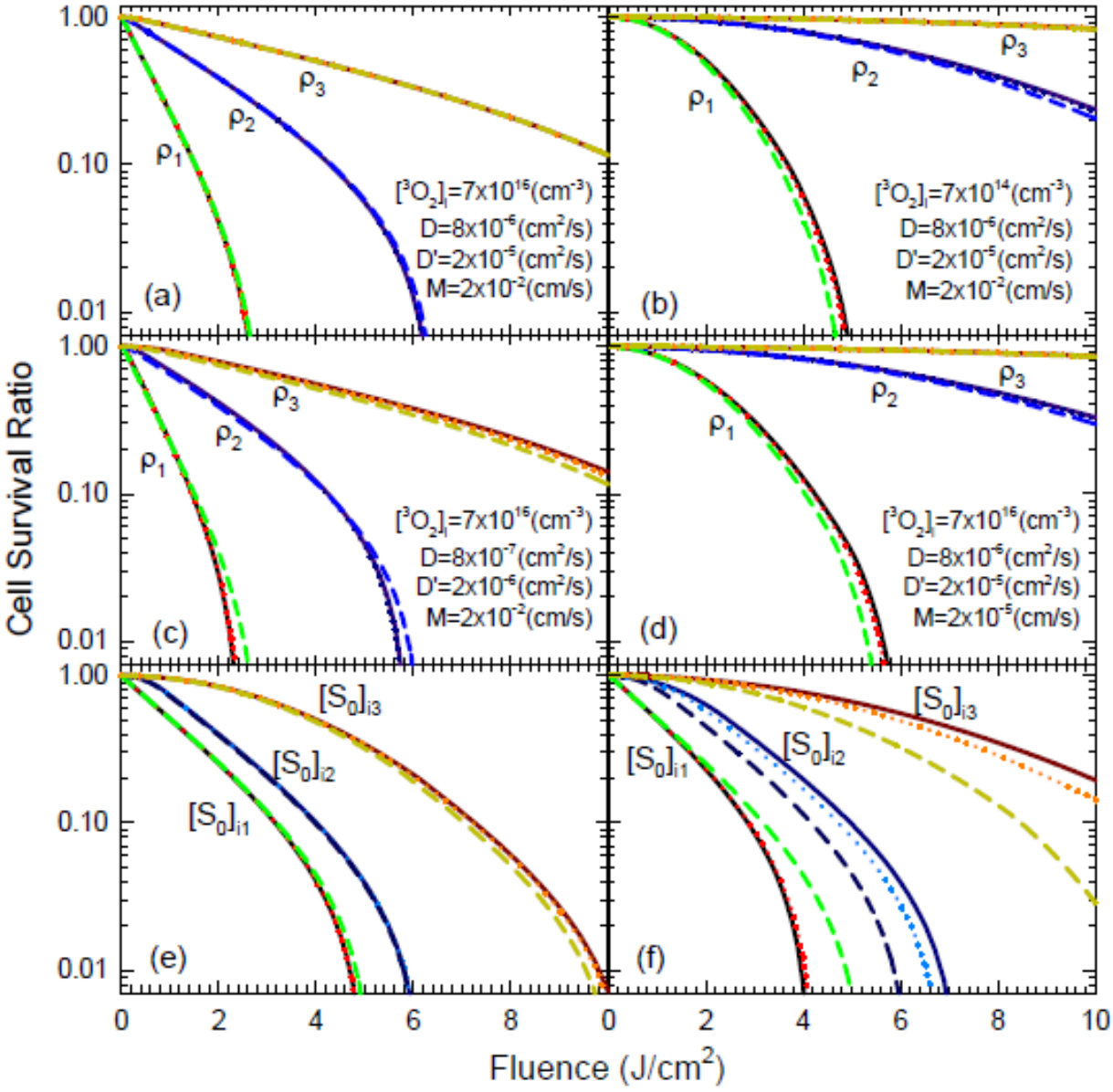

Figure 3.8.7. The cell survival ratio curves calculated with $V_m = 2.9\times10^{18}(cm^{-3}\cdot s^{-1})$ and different photon densities ρ, initial photosensitizer concentrations $[S_0]_i$ and oxygen parameters. From (a) to (d): $\rho_1 = 2.0\times10^{6}(cm^{-3})$, $\rho_2 = 7.0\times10^{6}(cm^{-3})$, $\rho_3 = 2.0\times10^{7}(cm^{-3})$, $[S_0]_i = 7.0\times10^{13}(cm^{-3})$. For (e) and (f): $[S_0]_{i1} = 1.0\times10^{15}(cm^{-3})$, $[S_0]_{i2} = 7.0\times10^{12}(cm^{-3})$, $[S_0]_{i3} = 1.0\times10^{12}(cm^{-3})$, $\rho = 5.0\times10^{6}(cm^{-3})$. Other parameters in (e) and (f) are the same as

those in (a) except the following: (f) $D = 8\times10^{-7}(cm^2/s)$, $D' = 2\times10^{-6}(cm^2/s)$. All other coefficients are given in the Appendix. Each set of curves marked with either ρ or $[S_0]_i$ consists of three lines calculated at different cell locations: solid: $r = 0$; dot: $r = \frac{r_0}{2}$; dash: $r = r_0$.

To further demonstrate the utility of the PDT model presented here, we show in Fig. 3.8.8 a comparison of our numerical results with the experimental data reported by Qin et al. which were obtained with Lymphoma cells treated by Photofrin®-PDT [105]. The laser irradiance at the wavelength of 635nm was varied to adjust fluence with a fixed illumination time of 30 (s). Fig. 3.8.8 re-plot the cell survival data measured by the clonogenic assay method as presented in Fig. 3B of[105]. We carry out time domain calculations with $0 \le t \le 30$ (s) at three cell locations and plot $N(t = 30)$ versus $[S_0]_i$ as two sets of survival curves in Fig. 3.8.8. The two different values of photon density ρ used for the numerical results are based on the fluence values of F =75 and 300 (mJ/cm^2) as reported in[105]. As can be seen from Fig. 3.8.8 that the present PDT model agrees reasonably well with the measured cell survival data for the case of high fluence at F =300 (mJ/cm^2) by adjusting the values of $[{}^3O_2]_i$ and β_0 from those used in Fig. 3.8.7(a). For the lower fluence case the model overestimates the cell killing which could be attributed to the use of homogeneous and spherical cell configuration and/or the lack of sufficient account of cell repair mechanisms. Despite this deficiency, one can still see that the present model provides an efficient and powerful tool to quantify the dependence of cell survival ratios on various parameters of light, photosensitizer and oxygen for *in vitro* cell studies by type II PDT.

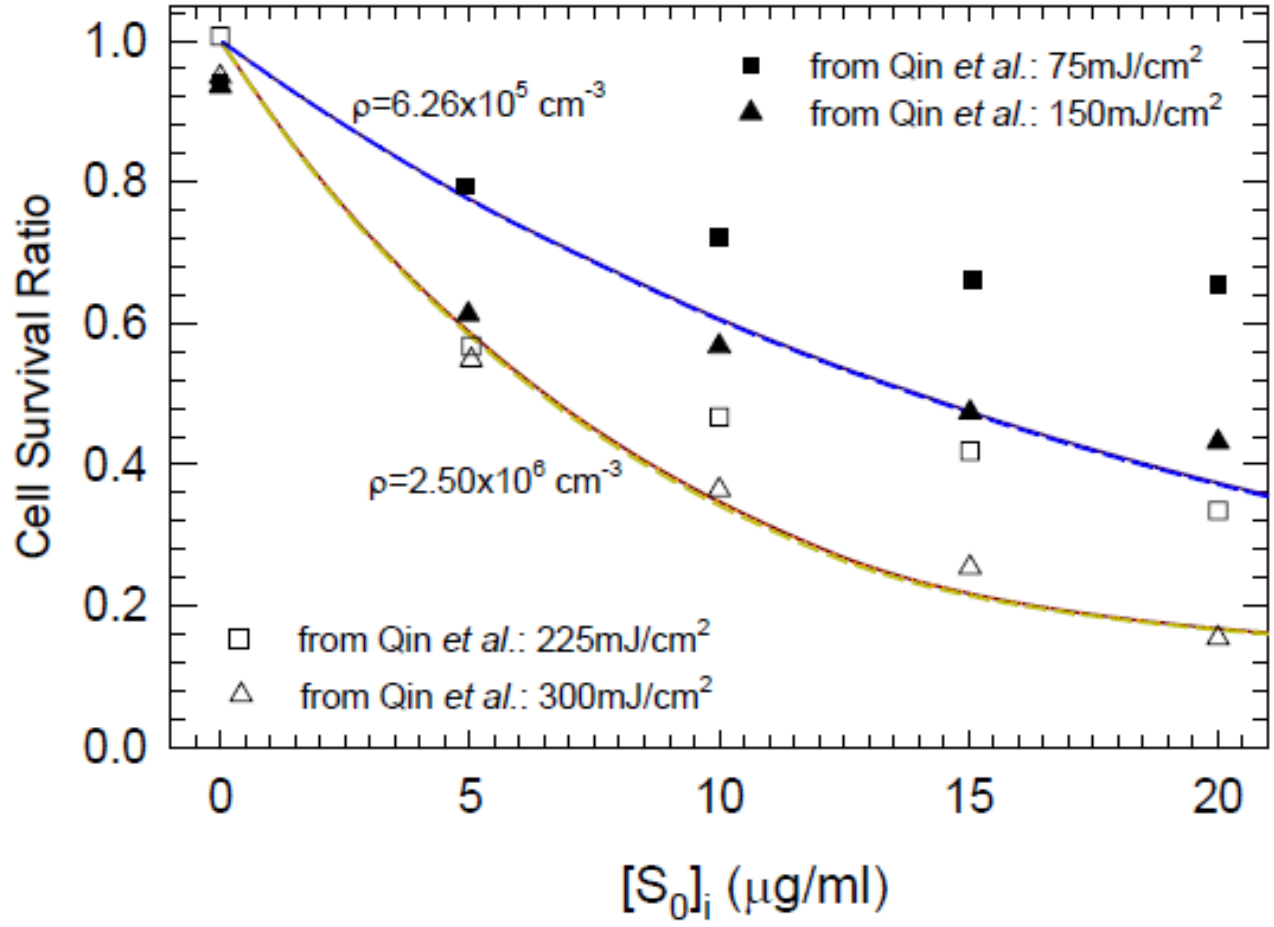

Figure 3.8.8. Comparison of two calculated cell survival curve sets with the measured data represented by the symbols by Qin *et al*. All parameters used in the numerical calculations are the same as those in Fig. 8(a) except the following: $\beta_0 = 8.0\times10^{-2}(s^{-1})$ and $[{}^3O_2]_i = 4.0\times10^{17}(cm^{-3})$. Note that the photon density $\rho = 6.25\times10^5$ and $\rho = 2.50\times10^6(cm^{-3})$ corresponds respectively to fluence F = 75 and 300 (mJ/cm^2) while $[S_0]_i = 4.0\times10^{12}(cm^{-3})$ corresponds to 20 (μg/ml) using the molecular mass of Photofrin as 3000 (g/mol). Each set of curves marked with ρ consists of three lines calculated at different cell locations: solid: $r = 0$; dot: $r = \frac{r_0}{2}$; dash: $r = r_0$.

3.9 Conclusion

Strictly speaking, the claim that the action mechanism of PDT at the tissue level is via the $^1O_2$ pathway in vivo has never been proven since nobody has been able to detect $^1O_2$ in vivo since it is difficult to apply $^1O_2$ scavengers in sufficient concentrations in vivo[48]. However, the oxygen dependency of the PDT effect is the same in vivo as in vitro as it has been demonstrated [138, 139]. In this chapter we present a significantly improved model of type II PDT by including oxygen transport and a quantitative description of cell killing using a spherical cell configuration over the previous efforts by other researchers and us [7, 73, 140]. A group of differential equations with appropriate boundary conditions is developed to simulate the time evolution of key molecule concentrations and oxygen transport as a coupled system. This allows us to extract the decay constants of photosensitizer S_0 and oxidized receptors R to quantify the photo bleaching and cytotoxicity related PDT within the ranges of experimentally controllable parameters of $[S_0]_i$ and ρ with different oxygen and transport parameters. The consistency of the equation group is examined by determination of the conditions for obtaining nonnegative concentrations. In addition, the present model includes a cell killing equation in which the excited singlet oxygen is used as the representative molecules of ROS and linked to the cell killing rates through two different pathways. Using this model one can calculate the cell survival curves from the concentrations of unoxidized receptors $[R]$ and the singlet oxygen molecules $[^1O_2]$ representing the ROS stress. More importantly, the modeling results can be compared directly to the experimental results based on the measurement of oxygen or singlet oxygen concentrations and cell survival ratios or used for design of different *in vitro* studies of PDT. Thus the new model has the capacity to be used as a platform to study *in vitro* the complex molecular interactions leading to cell killing by type II PDT in the presentation of oxygen transport. Further improvement of this model for

detailed analysis of cell killing through PDT can be achieved by considering the molecular pathways underlying cell death and repair and heterogeneous distribution of the target sites in the cell.

CHAPTER 4: CELLULAR DECISION MAKING AND MODELING CELL DEATH

4.1 Rate Distortion Theory

Information can be defined in terms of its ability to increase the probability of something being true[141] and it is carried on a channel which is a physical mechanism for communication. A channel is distinguished by having a limit on its ability to carry information and by the fact that it is susceptible to random interference, called noise[141]. Whenever energy is transferred (produced or consumed) information is transferred. In PDT, light absorption energy is transferred from the photosensitizer to oxygen and other molecules, through a cascade of reactions in the environment of a cell. The “source” treatment parameters generate information that the system of molecular network and interactions must communicate to the “receiver” which is the cell or human tissue. The information encoded in the light and the photosensitizer as the source “word” or “code” (death signal) is transformed into a form (activated photosensitizer) that can be transmitted through the “channel” of molecular interactions and concentrations, and when decoded by molecular “thresholds”, it can be converted to a channel output that has the form of a cell state (necrosis, apoptosis, autophagy, survival) in relation to the tissue environment or human body. In order to determine quantitatively whether or not the performance-efficiency of this bio-communication system is satisfactory, it is necessary to assign numerical values to the various statistical variations and errors that the system may make. In rate distortion theory, it is expected that a distortion measure is applicable to a particular source-channel -receiver combination , which in this case, it has to account for system structure, geometry, forcing functions, initial, boundary and environmental conditions [87],etc. The statistical mechanism that governs the generation of the source outputs (mean and variance of the treatment parameter),and the distortion measure that penalizes the bio-coding errors and determines the fidelity of the reproduction of the cell killing signal

need to be quantified specifically in order to have a complete description. The source produces the stimulus or stimuli that although they are continuous random variables (e.g. levels molecular concentrations) they can be discretized by taking measurements at different times during treatment. Eventually, we want to design an optimal treatment strategy that leads, through intracellular biochemical reactions, to reproduction of the PDT death signal output by the cell, with an average distortion that does not exceed a specified upper level D, for a single tumor cell model or a tumor cell population. To quantitatively answer this question, usually it is the rate distortion function $R(D)$ which is of fundamental importance in information theory. $R(D)$ is the effective rate at which the source produces information and passes it to the user, subject to the constraint that the user can tolerate an average distortion D [95]. In this frame, it will be the effective rate at which the molecular concentrations do signal apoptosis/necrosis/autophagy when the cell can faithfully reproduce this signal only if the distortion does not exceed D. The rate distortion function is related to entropy. Entropy H is the rate at which the source produces information subject to a requirement of perfect reproduction of the initial signal (therefore $D = 0$ and $R(0) = H$)[95]. The treatment pattern of the a priori setting parameters (photo-density, photosensitizer concentration, etc.), is related to the data bio-compression of the death signal through molecular interactions, and the classification of the signal as to cell death or cell survival is done with a possible statistical error that is assigned a numerical penalty (distortion function d) and within bounds for the rate at which this treatment information can be sent ,compressed-decompressed (rate distortion function $R(D)$) given the tolerance of the cell (distortion D).

4.2 Cells as Biochemical Info systems

Besides the therapeutic parameters and the environment of the cell, it is also the inherent nature of a cell as a physical system, such as the genetic pattern, that carry information which the cell has the ability to gather, store and utilize [87]. The cell has stochastic and deterministic dynamical features, such as intracellular molecular, reactions, forces, boundary conditions. Modeling of decision mechanism concerning the state of a cell (apoptosis, necrosis, living cell, etc.) can only be made with less than adequate knowledge of parameters that have a stochastic nature [87]. This knowledge is information which is measured by entropy. The entropy of all biochemical processes in the cell is always positive and information fluxes are formally equivalent to negative entropy [142]. In the case of PDT, the photo-chemically induced molecular signaling distorts the entropic steady state of the cellular system in the unfavorable direction. This entropy "penalty" must be compensated either by net entropy flowing into the system (through exchanges of energy and materials with the environment) or by cell de-organization [142], depending on the thermo dynamical feasibility of these options. The entropically regulated cell-de-organization occurs along the thermodynamic path of least resistance [142].

In the case of a communication channel between a source from which the information takes its origin (drug administration and photo-irradiation resulting in a vector stimulus of molecular concentrations) and a receiver to which the information is delivered (cell and cell survival/death decision probability), according to Zipf's law, the distribution of "words" (molecular interactions and levels of concentrations) is due to the tendency to convey information with least communication effort[143]. We represent this communication effort by the mean amount of information that knowledge of the value assumed by the random variable Y = cell decision, supplies about the value assumed by the random variable X = vector of stimuli, which is the quantity of mutual information $I(X,Y)$ that has to be minimal. Therefore it is the mutual information between stimuli and cell

decision that is minimized and drives the cellular system as a communication channel , rather than fixed predefined molecular pathways which rather encode and decode these dynamics [87]. This cell sensitivity and response to photo-pharmacological insult and its biochemical cascades, can be perceived as a cell decision mechanism for death/survival decision, that requires for its activation, minimal mutual information $I(X,Y)$ between the stimulus of the death inducers X and the cell decision Y .(In the case of cancer cells, a resistance mechanism exist that will be discussed later). The minimization of the mutual information as an application of rate distortion theory to decision making mechanisms in biology has been adapted for testing a framework for designing and analyzing binary decision-making strategies in cellular systems [87], for the information-theoretic characterization of the optimal gradient sensing response of cells [92] and for the rate distortion approach to protein symmetry [144] , [145] among other applications . The mutual information of two random variables in general, measures the information that X and Y share: it measures how much knowing one of these variables reduces the entropy of the other. This reduction of the entropy will be compensated by the cell either by interaction with the environment, while it is in a vulnerable state and its survival probability decreases, or by cell death. The rate distortion function $R(D)$ is the effective rate at which the source generated stimuli carry information subject to the requirement that its output must be reproduced with fidelity D .

4.3 A Brief Summary of Major Molecular Pathways and Biochemical Events induced by PDT

The underlying mechanisms behind the cytotoxic effects displayed during photodynamic therapy on the cellular level are described schematically as Sen(sensitizer) → Sen* (activated photosensitizer) → Cytotoxic Agents → Biological Damage → Cell Death [98]. This sequence of events involves several intracellular factors and molecular interactions.

Singlet Oxygen. A major cytotoxic agent generated during PDT is the singlet oxygen. Singlet oxygen is produced during PDT via a triplet-triplet annihilation reaction between ground state molecular oxygen

(which is in a triplet state) and the excited triplet state of the photosensitizer. DNA damage has been reported several many authors for different photosensitizers [146, 147] [148] [149] [150] and the time course of formation by singlet oxygen of single strand breaks has been recorded from 0 to 120 minutes [151].

***Apoptosis Extrinsic and Intrinsic Pathways*.** Caspases are the main effectors of apoptosis. Caspases can be activated by external stimulus through two major pathways: (1) extrinsic pathway: ligand-dependent or receptor-induced activation through receptors, (2) intrinsic pathway: mitochondria-dependent activation through cytochrome c (cyt c) release due to stress/irradiation/inflammation. Proteins of p53 suppress Bcl-2 and activate Bax, or in other words, p53 upregulate Bax and downregulate Bcl-2 to promote apoptosis. [152] [153]

The extrinsic pathway is initiated through ligation of the death receptor family receptors by their respective ligands. Amongst others this family includes the tumour necrosis factor receptors, CD95/Fas/APO-l and the TRAIL receptors. Receptor ligation is followed by the formation of the death inducing signalling complex (DISC), which is composed of the adapter molecule FADD and caspase 8. Recruitment to DISC activates caspase 8, which in turn either directly cleaves and activates the effector caspases, or indirectly activates the downstream caspases through cleavage of the BH3 protein Bid, leading to engagement of the intrinsic pathway of apoptosis. This intrinsic pathway of caspase activation is regulated by the pro- and anti-apoptotic Bcl-2 family proteins. These proteins induce or prevent the release of apoptogenic factors, such as cytochrome c or Smac/DIABLO, from the mitochondrial intermembrane space into the cytosol. The intrinsic pathway is triggered by stress stimuli, including growth factor deprivation and DNA damage. The release of mitochondrial cytochrome c facilitates the formation of the apoptosome complex (composed of the adapter molecule Apaf-1 and caspase 9), which then cleaves and activates the effector caspases. PDT has been shown to directly damage mitochondria-

associated anti-apoptotic Bcl-2 proteins, thus facilitating Bax/Bak-mediated MMP (mitochondria membrane permeabilization) and the subsequent release of caspase activators, such as cytochrome c and Smac/DIABLO or other pro-apoptotic molecules, including apoptosis-inducing factor (AIF). On the other hand, when primary photodamage involves predominantly other organelles, such as the ER or the lysosomes, different pathways involving the activation of upstream pro-apoptotic BH3-only proteins is required for MMP and apoptotic photokilling. Photosensitizers that target Lysosomes may activate intrinsic apoptosis following the release of cathepsins from photo damaged lysosomes resulting in the cleavage of the BH3-only Bid and consequent MMP.[154] [155]

***Necrosis*.** Necrosis owing to ATP depletion is considered to be the result of severe oxidative cell damage triggered by the mitochondria permeability transition. Massive accumulation of ROS in the mitochondria can trigger the release of additional ROS from the mitochondria, which further increases the oxidative stress in the cell [156]. Low energy level PDT can induce apoptosis while high level PDT induce necrosis. Necrosis results from high levels of cell damage, in which plasma membrane integrity is lost, cells lyse, and tissue inflammation is triggered [157, 158] [159] [160]. In necrotic death upon DNA damage, Calpain proteases play a central role in sensing excessive calcium levels and in turn initiating the death response by activating several classes of effector proteases such as cathepsins. In addition, calpains contribute directly to cell destruction by degrading essential structural components of the cell. (ROS surpresses Bcl-2 , suppression of Bcl-2 leads to increase of IP3R which leads to Calcium increase, which leads to necrosis) [161]. The chronological and molecular order of the events accompanying necrosis remains elusive. For example, the relationships among Ca_2^+, ATP and ROS can be complex, presumably because of the existence of self-destructive feed-forward loops. Although taken alone each of these events is not specific to necrosis (and indeed some might be shared with apoptosis), it is the possible accumulation of these events in an organized, programmed cascade of self-destruction that might define cell death [162] . Bax activation or apoptosome formation (or both of those) in apoptosis signaling have been

considered to operate in a slow time scale. This time scale varies from cell to cell and from stimulus to stimulus. The tBid-Bcl-2-Bax interaction along with the Bcl-2 level determines the time course of Bax2 activation and thus apoptotic activation through the mitochondrial pathway of apoptosis. Bax inhibition by Bcl-2 molecules reduces the effective rate for Bax conversion to activated Bax and subsequent Bax_2 complex formation. [163-165].

***Cleaved PARP as marker of apoptotic death*.** A very early step upon illumination is cytochrome c release from the mitochondria into the cytosol of treated cells. The cytochrome c release might be correlated to the loss of the mitochondrial membrane potential that has been observed in experiments, and might be related to MOMP (mitochondrial permeability transition pore). Ca^{2+} release through MOMP is correlated to cytochrome c loss, although PDT has been show to degrade critical hsitidines of the pore. PDT has a very subtle effect on mitochondrial membrane. Cells could die from ATP depletion (necrosis) or indeed follow the apoptosis activation of the caspase-pathway. Caspase 3 is the caspase that cleaves a large number of proteins that are involved in cell structure and maintenance, such as DFF (DNA Fragmentation Factor) and PARP (PolyADP-Ribose Polymerase). PARP has been used as the marker of the apoptotic extense. PDT treatment with with Pc 4, BPD, or aluminum phthalocyanine (AlPc) has been shown to lead to cleavage of PARP in different cell lines[166-170]. It has been also demonstrated that the damage of plasma membranes was related to the intracellular ROS formation triggered by PDT. Among the several downstream signaling events following the generation of ROS in the vicinity of the plasma membranes, the activation of JNK and caspase 3, cleavage of PARP have been repeatedly reported . [171] [172] [100]. It is reported that cleaved PARP shows a jump increase at about 4-5 hours.

PDT can induce necrosis at several levels. While mediators of necrosis such as calcium and reactive oxygen species (ROS) have been reported to contribute to apoptosis, recent studies have begun to demonstrate that the ability of such mediators to initiate necrotic cell death depends on active

participation by the dying cell. Mitochondria are a major source of ROS that can initiate necrosis. Excess mitochondrial ROS can damage DNA by causing cleavage of DNA strands, DNA–protein cross-linking, and oxidation of purines [173]. This may lead to DNA-damage response, including activation of p53 and PARP. While activation of p53 may cause apoptosis and cell cycle arrest, hyper activation of PARP leads to necrosis [174] [175, 176] [177, 178].

***TNF following PDT treatment*.** In [179] macrophages have been shown to produce TNF and to become cytotoxic under the influence of porphyrin and light. It is therefore likely that the photodynamic activation of macrophages may play a major role in the therapeutic effect[180] [179]. The initiators of apoptosis program are tumor necrosis factor-alpha (TNF-α) that binds to the TNF receptor; Lymphotoxin (also known as TNF-β) that also binds to the TNF receptor; Fas ligand (FasL), a molecule that binds to a cell-surface receptor named Fas. TNF is the initiating molecule of the extracellular trigger (external pathway) for the intracellular composition of Death Induced Signaling Complex (DISC) (common to external and internal pathways). In [181] , an energy-dependent production of TNF by macrophage treated with PDT, stimulated or unstimulated with endotoxin, was demonstrated, and TNF production was inhibited at the highest treatment energy levels. These data represent the first description of cytokine production by PDT-treated macrophages, and may serve as another mechanism of PDT cytotoxicity in vivo, either directly by TNF-mediated tumor necrosis, or indirectly by vascular effects on tumor vessels. [181] [182] [183] [184] [185]. Macrophages were reported to release TNF-a following PDT treatment and to preferentially recognize PDT treated cancer cells as their targets. [184] presents Macrophage activation and TNFa cytotoxicity and combinations of PDT with other treatments , such as immuno-stimulants including TNFa There is indeed evidence of synergy between immuno-modulators and PDT in the destruction of experimental tumors [181] [179, 185].

Autophagy: Beclin 1 has a key role in the initiation of autophagy, a process of self-cannibalism in which cytoplasmic constituents are sequestered and targeted for lysosomal degradation. Autophagy is controlled in large part by beclin 1 (BECN1), a myosin-like, BCL-2-interacting protein. When not bound to BCL-2, BECN1 participates in a multiprotein complex that initiates the earliest stages of autophagosome assembly. In response to stress, both beclin 1 (BECN1) and BCL.2 are phosphorylated, causing the BCL-2/BECN1 complex to dissociate.BECN1 is phosphorylated by death associated protein kinase (DAPK), and BCL.2 is phosphorylated by JUN terminal kinase (JNK), a downstream target of the inositol-requiring protein 1 (IRE1; also known as ERN1) arm of the unfolded protein response [101] . Autophagy can suppress the stress signal by providing the cell with ATP and raw materials for new protein synthesis. Under low stress conditions, autophagy promotes cell survival; at moderate stress, it may lead to autophagic cell death; and under conditions of high cellular stress, calcium release may stimulate apoptosis by the intrinsic (mitochondrial) pathway [186] [101]. Massive oxidative stress leads to autophagy through different pathways and massive accumulation of ROS in the mitochondria can trigger the release of additional ROS from the mitochondria, which further increases the oxidative stress in the cell [157, 158] [159] [156]. Autophagy is stimulated by various cellular stresses including oxidative stress. Given the functional duality, activation of autophagy may either impede or facilitate PDT-mediated cell killing. Although it has been postulated based on experiments that autophagy is a mechanism to preserve cell viability following photodynamic injury (knock down of autophagy genes, lowers the threshold for apoptotic cell killing), tumor necrosis factor (TNF)-a has been shown to induce autophagic cell death through a ROS-dependent mechanism [186] [187, 188] [189].

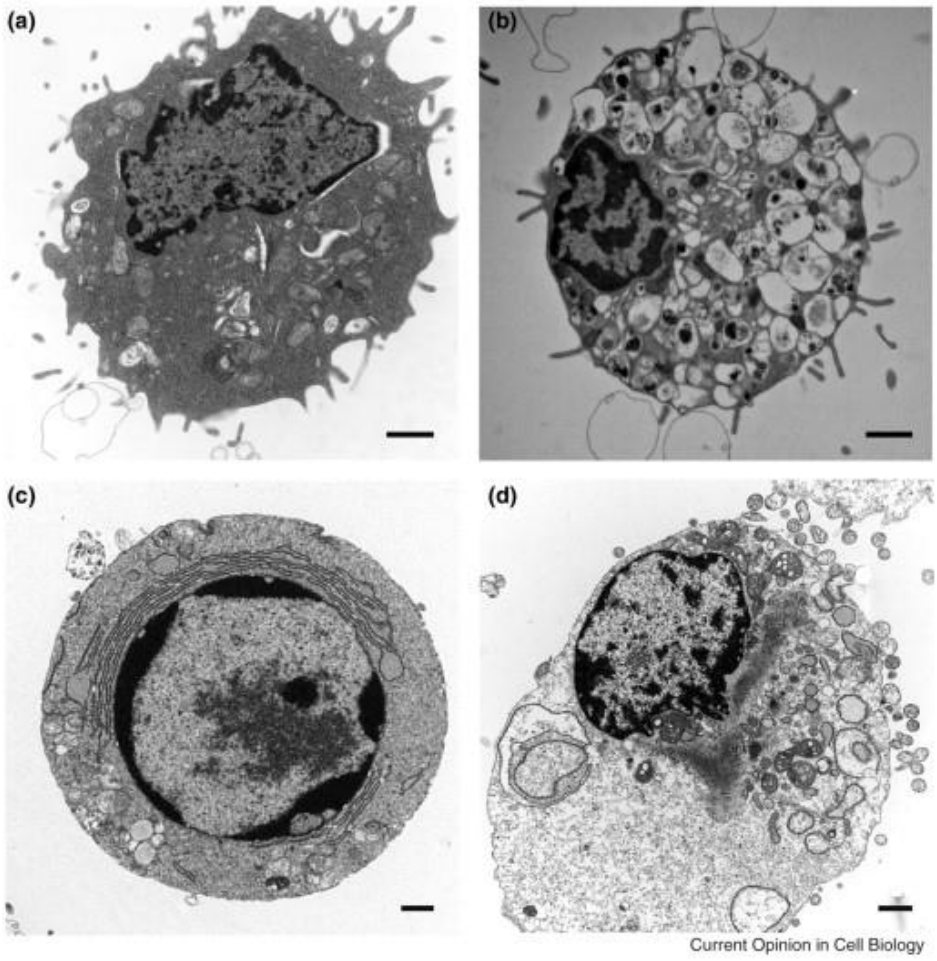

Figure 4.2.1. Morphological features of autophagic, apoptotic and necrotic cells. (a) Normal, (b) autophagic, (c) apoptotic (d) and necrotic cells. Whereas the morphologic features of apoptosis are well defined, the distinction between necrotic and autophagic death is less clear. The scale bar represents 1 μm[190].

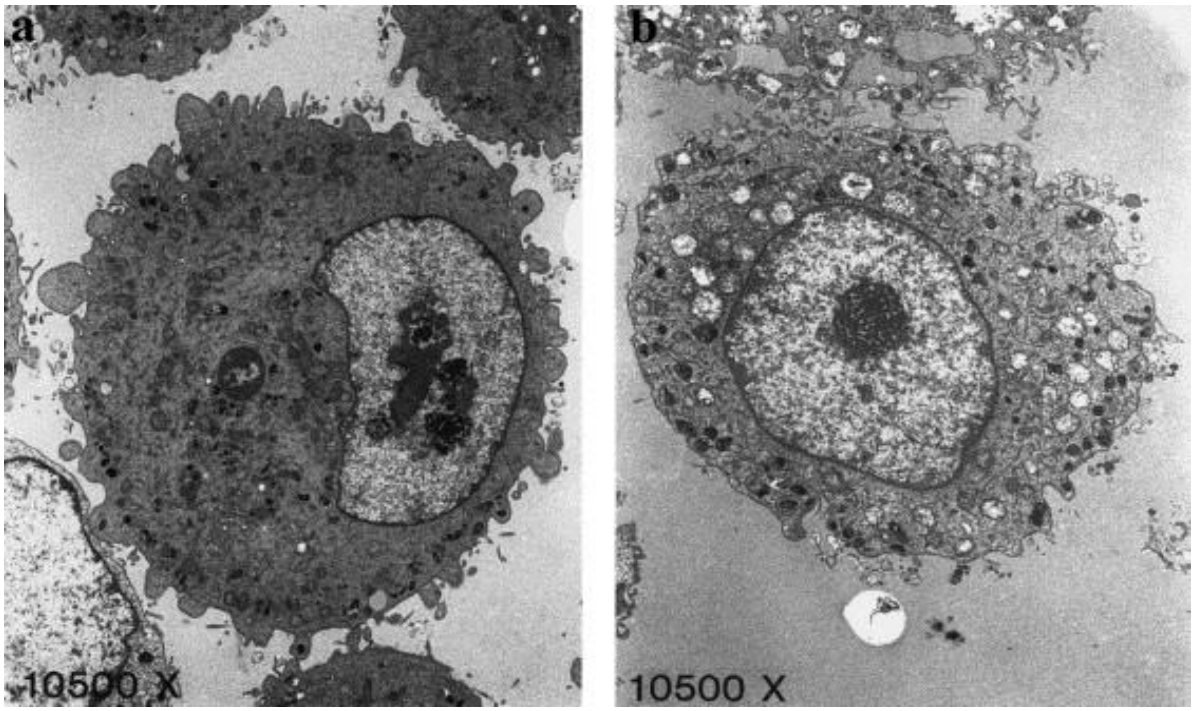

Figure 4.2.2. Transmission electron micrographs of monolayer R3327-AT cells treated by *in vitro* PDT [191]. (a) Non-treated cell with normal appearing mitochondria, and (b) PDT-treated cell with matrix swelling of mitochondria.

A schematic representation of the known molecular pathways and biochemical events induced by PDT treatment leading to cell death is given in figure 4.3.1. A molecular interaction graph with information about the potential dynamic behavior of a cellular system that can be translated into reasonable mathematical terms that are suitable for computer simulation. ***Blue color*****:** Reactions that lead to the activation of the photosensitizer(Photofrin in our case) and the generation of reactive oxygen species (ROS). The kinetic mathematical model of [102] is used to describe the molecular pathways. ***Red color*****:** Exposition to tumor necrosis factor (TNF) or TNF-related apoptosis-inducing ligand (TRAIL) as a result PDT treatment activate effector caspases that dismantle the cell. The kinetic mathematical model of [100] is used to describe the molecular dynamics. ***Light blue:*** The interplay between autophagy and apoptosis in response to oxidative stress. A signaling mathematical model introduced in [101] is used to describe the dynamics. ***Yellow color:*** Components and interactions that have either been observed or conjectured in the literature but no equation has been identified(thin lines) or they have been observed and we have a mathematical equation to describe them (thick lines) . An arrow signifies the upregulation process of a cellular molecular component as a signaling response to another molecular component, and and a line with a vertical line segment signifies the downregulation process of a cellular molecular component as a signaling response to another molecular component. A coherent PDT mathematical model has been synthesized from the three kinetic models, with the necessary modifications to account for biochemical events, such as the initiation of the degradation process of Bcl-2 by ROS, that could bind to Bax to prevent its activation [192]. All rate equations, initial molecular concentrations, coefficients and constants can be found in the supplementary information tables.

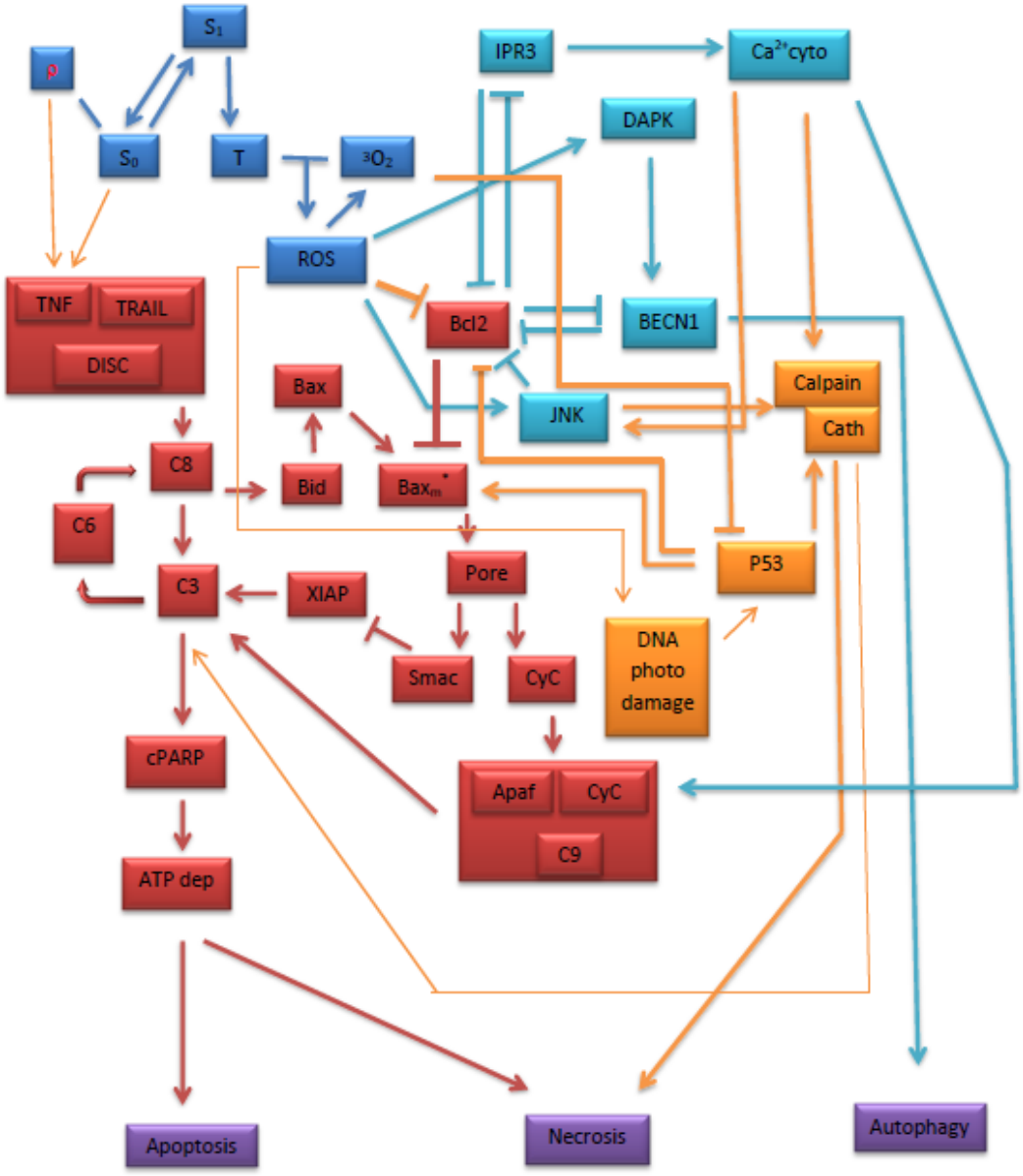

Figure 4.3.1. A schematic representation of the known molecular pathways and biochemical events induced by PDT treatment leading to cell death

4.4 Mathematical Modeling Scheme

Following[100], biochemical reaction equations were derived from the following scheme, for the apoptosis/necrosis pathways. For a given binary reaction i the biochemical equation is represented by one of following general mass-action paradigms:

$$E + S \leftrightarrow E:S \rightarrow E + P \Leftrightarrow \begin{cases} \dfrac{d[E]}{dt} = -k_i[E][S] + k_{-i}[E:S] + \kappa_i[E:S] \\ \dfrac{d[S]}{dt} = -k_i[E][S] + k_{-i}[E:S] \\ \dfrac{d[E:S]}{dt} = k_i[E][S] - k_{-i}[E:S] \\ \dfrac{d[P]}{dt} = k_i[E:S] \end{cases} \tag{4.4.1}$$

For the autophagy pathway, we follow [101] and the neural network modeling method as it is described in [101] and has been used in[193-195]. We use an intermediate modeling strategy that employs nonlinear ODE to describe protein regulatory networks but is not tied to specific reaction mechanisms and rate constants. More precisely, we use ODEs of the form:

$$\frac{dX_i}{dt} = \gamma_i \cdot [F(\sigma W_i) - X_i] \tag{4.4.2}$$

$$W_i = \omega_{i0} + \sum_{j=1}^{N} \omega_{ij} X_j \tag{4.4.3}$$

where X_i is the expression level of a molecular concentration $0 \le X_i \le 1$ and $F(\sigma W_i) = \dfrac{1}{1+e^{-\sigma W}}$ is a sigmoidal function that varies from 0 (when $W << -\dfrac{1}{\sigma}$) to 1 (when $W >> -\dfrac{1}{\sigma}$). The parameter σ controls the steepness of the sigmoidal function at its inflection point. W_i is the net effect on molecule

i of all molecules in the network. The coefficient ω_{ij} is less than 0 if molecule j inhibits the expression of molecule i, more than 0 if molecule j activates molecule i, or equal to 0 if there is no effect of molecule j on molecule i. This equation has the great advantage that it is subject to all the powerful analytical and simulation tools of nonlinear ODEs, yet, in the limit of large σ, it behaves like a discrete Boolean network[196]. When $\sigma >> 1$, X_i tends to flip (on a timescale $\approx \gamma^{-1}$) between 0 and 1, and the dynamical system approximates a Boolean network[196].

4.5 Background of the logical design for cell decision making

Cells, as physical systems, possess the ability to gather, store and utilize information. This information may pertain either to state of the system's immediate environment or to the inherent nature of the system itself, as in the case of genetic information. To collect and process information is a feature of living systems; therefore we consider cells as info systems [87]. Cells as biochemical info systems have features that are either fully stochastic, or part stochastic and part-deterministic. Their stochastic nature can be attributed to randomness in one or more of the following components: system structure (geometry); system dynamics (biochemical reactions, constants and concentrations); forcing functions; and initial, boundary and environmental conditions [87]. A stochastic description of these cellular systems is needed, and mathematical modeling of decision mechanisms concerning their states (apoptosis, senescence, etc.) will be made with less than adequate information. Communication theory enables development of such an explicit and quantitative description that accounts for uncertainty in the presence of limited data. Our aim will be to understand the reliability of a molecular cell death stimulus controlling the survival of a cell. A decision strategy will be parameterized by input/output kernel probability distributions of the form stimulus/decision, instead of a deterministic function that

represents a “noiseless system”. The input kernels are determined by the biophysics of this mechanism. The mutual information describes the reliability between input/output. Although the input can be a continuous quantity, such as a molecular concentration, the noise present in the regulatory elements corrupts the computation and does not allow the arbitrary resolution of a real-valued input to propagate to the output; instead, the mutual information tells us how precisely different inputs are distinguishable to the organism [87] [95].

While existing techniques used by other authors have been tailored to describe and understand binary decision-making based on a single stimulus, our framework extends to handle multiple stimuli by replacing the random variable X with a random vector $X = (X_1, X_2, X_3)$ and modifying the mathematics accordingly. Moreover, rate distortion theory can be recast to consider more complex cellular processes as we will discuss later. For a probability mass function $p_X(x_1, x_2, x_3)$ of a random variable $X = (X_1, X_2, X_3)$ the amount of information of an event (x_1, x_2, x_3) is the amount of information one receives upon being told that the random variable has assumed this value and it is defined by the equation:

$$i(x_1, x_2, x_3) = -\log_2 p_X(x_1, x_2, x_3) \qquad (4..5.1)$$

For the case of two random variables, a vector X and a scalar Y , with probabilities p_X and $p_Y = q$, and joint distribution p_{XY} the “conditional distribution” and “conditional information”(this is the measure of the information one receives upon being told that the event $Y = y$ has occurred if one already knows the occurrence of the event $X = (x_1, x_2, x_3)$) are defined by the functions $Q_{Y|X}(y|x_1, x_2, x_3)$ and $i(y|x_1, x_2, x_3)$ where

$$i(y|x_1, x_2, x_3) = -\log_2 Q_{Y|X}\left(y|x_1, x_2, x_3\right) \tag{4.5.2}$$

The "mutual information" is defined by the following relation (this is the difference between the amount of information that the event $Y = y$ has occurred conveys to someone ignorant of what value X has assumed, and that which it conveys to someone who already knows that the event $X = (x_1, x_2, x_3)$ has occurred[95]):

$$i(y, x_1, x_2, x_3) = i(y) - i(y|x_1, x_2, x_3) = \log \frac{Q_{Y|X}(y|x_1, x_2, x_3)}{q(y)} \tag{4.5.3}$$

The average mutual information represents the mean amount of information that knowledge of the value assumed X supplies about the value assumed by Y and is defined as:

$$I(X,Y) = \sum_{x_1, x_2, x_3, y} p_X(x_1, x_2, x_3) \cdot Q_{Y|X}(y|x_1, x_2, x_3) \cdot \log \frac{Q_{Y|X}(y|x_1, x_2, x_3)}{q(y)} \tag{4.5.4}$$

An alternative equivalent definition follows from entropy considerations. The mutual information can be understood as a measure for *prior* uncertainty the receiver has about the sender's signal $H(Y)$, diminished by the uncertainty that is left after receiving information about the sender's signal $H(Y|X)$. Of course the decrease in uncertainty is due to the communicated amount of information, which is $I(Y, X)$: [87, 95]

$$H(Y) = -\sum_y q(y) \cdot \log q(y) = -\sum_{x_1, x_2, x_3, y} p_X(x_1, x_2, x_3) \cdot Q_{Y|X}(y|x_1, x_2, x_3) \cdot \log q(y) \tag{4.5.5}$$

$$H(Y|X) = -\sum_{x_1, x_2, x_3, y} p_X(x_1, x_2, x_3) \cdot Q_{Y|X}(y|x_1, x_2, x_3) \cdot \log Q_{Y|X}(y|x_1, x_2, x_3) \tag{4.5.6}$$

$$I(Y,X) = H(Y) - H(Y|X) = \sum_{x_{,1},x_2,x_3,y} p_X(x_1,x_2,x_3) \cdot Q_{Y|X}(y|x_1,x_2,x_3) \cdot \log \frac{Q_{Y|X}(y|x_1,x_2,x_3)}{q(y)} \quad (4.5.7)$$

where we have used the fact that

$$q(y) = \sum_{x_1,x_2,x_3} p_X(x_1,x_2,x_3) \cdot Q_{Y|X}(y|x_1,x_2,x_3) \quad (4.5.8)$$

In lossy data compression, the decompressed data may be different from the original data. Typically, there is some distortion between the original and reproduced signal [95]. A distortion measure d is a mathematical entity which specifies exactly how close the approximation is. Generally, it is a function which assigns to any event $(X,Y) = (x,y)$ (often called letters) in the product sample space $X \times Y$ (often called the "alphabet") a non-negative number denoted $d(x,y)$. The distortion function defines accurate sensing, penalizing mistakes and quantifying the disadvantages of alternative decisions [87]. With each conditional probability assignment ("strategy") $Q_{Y|X}(y|x_1,x_2,x_3)$ and for the associated joint distribution given by $p_{YX}(y,x_1,x_2,x_3) = p_Y(y) \cdot Q_{Y|X}\left(y|x_1,x_2,x_3\right)$, the "expected" distortion depends on the conditional probability (This is the "average" distortion associated with this conditional probability) [95]:

$$d\left(Q_{Y|X}\right) = \sum_{x_1,x_2,x_3,y} p_X(x_1,x_2,x_3) \cdot Q_{Y|X}\left(y|x_1,x_2,x_3\right) \cdot d(x_1,x_2,x_3|y) \quad (4.5.9)$$

A conditional probability assignment is said to be D admissible if and only if

$$d\left(Q_{Y|X}\right) \leq D \quad (4.5.10)$$

The set of all D admissible assignments (set of all D admissible strategies) is denoted Q_D. Each conditional probability gives rise not only to an average distortion, but also to an average mutual

information $I(X;Y) = I\left(Q_{Y|X}\right)$. The minimum mutual information over all D admissible "strategies" (conditional probabilities) is given by the rate distortion function:

$$R(D) = \min_{p_{Y/X}(x/y) \in Q_D} I(p_{Y/X}) \tag{4.5.11}$$

The meaning of the rate distortion function is the following[95]: suppose we are interested in whether or not it is possible to reproduce the source (death stimuli) at the channel output (cell decision) with fidelity D. An average of at least $R(D)$ bits per letter (letter here is a concentration level) of information from the total of H bits per letter produced by the source must reach the output in order for this to be possible. That is, at most $H - R(D)$ bits may be lost. We may express the variation problem defining $R(D)$ as follows: First, a stimulus probability p_X is given and a distortion function is assigned d. A maximum permissible value of average distortion is set as D, and the problem is to minimize the average mutual information $I(Q_{Y|X})$ subject to the constraints

$$Q_{Y|X}(y|x_1, x_2, x_3) \geq 0$$

(4.5.12)

$$\sum_y Q_{Y|X}(y|x_1, x_2, x_3) = 1$$

(4.5.13)

$$\sum_{x,y} p_X(x_1, x_2, x_3) Q_{Y|X}(y|x) d(x, y) = D \tag{4.5.14}$$

The problem is solved with the methods of the Lagrange multipliers[95] by forming an augmented functional (in the following equations, (x_1, x_2, x_3) is denoted by the vector x) :

$$J(Q_{Y|X}) = I(p_X, Q_{Y|X}) - \sum_x \mu_x \sum_y Q_{Y|X}(y|x) - s \cdot \sum_{x,y} p_X(x) Q_{Y|X}(y|x) \cdot d(x,y) \quad (4.5.15)$$

Where the parameters μ_X, s are Lagrange multipliers. The solution is known to be:

$$Q_{Y|X}(y|x) = \frac{q(y) e^{s \cdot d(x,y)}}{\sum_{y'} q(y') e^{s \cdot d(x,y')}} \quad (4.5.16)$$

For a given s, we can derive q from implicit equations of the form:

$$1 = \sum_x \left(\frac{p_X(x) \cdot e^{s \cdot d(x,y)}}{\sum_{y'} q(y') \cdot e^{s \cdot d(x,y')}} \right) \quad (4.5.17)$$

We can generate a point on $R(D)$ parametrically in terms of q and s :

$$D = \sum_{x,y} \left(\frac{p_X(x) \cdot q(y) \cdot e^{s \cdot d(x,y)} \cdot d(x,y)}{\sum_{y'} q(y') e^{s \cdot d(x,y')}} \right) \quad (4.5.18)$$

$$R = s \cdot D + \sum_x \left(p_X(x) \cdot \frac{1}{\sum_{y'} q(y') e^{s \cdot d(x,y')}} \right) \quad (4.5.19)$$

4.6 Logical design and general discrete form of the Blahut Arimoto algorithm

The search for extremizing probability distributions is a problem in the calculus of variations with constraints. The Blahut–Arimoto algorithm, is an iterative technique (that works with probability density estimates) for numerically solving the minimization of the mutual information functional and obtaining the probabilities of arbitrary finite input/output alphabet sources. The main idea consists of a mapping from the set of channel input probability vectors into itself such that the sequence of

probability vectors, generated by successive applications of the mapping, converges to the vector that minimizes the mutual information[197]. The basic steps are as follows[87]:

1. Initialize the probability distribution of the decision Y, namely q.
2. Given q compute the conditional probability distribution $Q_{Y|X}$ that minimizes the mutual information $I(X,Y)$ while satisfying the distortion constraint

$$Q_{Y|X}(y|x) = \frac{q(y)e^{s\cdot d(x,y)}}{\sum_{y'} q(y')e^{s\cdot d(x,y')}} \tag{4.6.1}$$

3. Given $Q_{Y|X}$ compute the probability distribution q that minimizes the mutual information $I(X,Y)$
4. Repeat steps 2 and 3 until $Q_{Y|X}$ and q converge.

As these steps are carried out, the mutual information has been shown to be $R(D)$, where D is determined by the lagrange multiplier chosen in the minimization. Repeating this process with different values of the Lagrange multiplier, generates a collection of optimal strategies $Q_{Y|X}$ and probabilities q.

In particular and with respect to the photodynamic stimulation, the formulation goes as follows (Fig. 4.6.2):

a. First, solve the ODE group in time domain and obtain the normalized concentrations of three marker molecules, indicators of apoptosis, necrosis and autophagy, at a time t.

$$x_1(t) = \frac{[^1O_2](t)}{[^1O_2]_{\max}}, \quad x_1(t) = \frac{[cPARP](t)}{[cPARP]_{\max}}, \quad x_1(t) = \frac{[BECN](t)}{[BECN]_{\max}} \tag{4.6.2}$$

For our simulations, PDT treatment starts at $t = 0$ (s) and treatment ends at $t = t_d$ (this can be 10 to 30 minutes and determines the fluence or optical dose for a given photon density) and observation ends at $t = t_{\max} = 7.5$ hours.

b. Define the stimulus probability distribution $p_X(x) = p_X(x_1, x_2, x_3)$ (probability of the molecular concentrations occupying specific coordinates in the concentarion space at time t). Define the smooth and compactly supported "bump function" approximation to the delta function [198], in the "phase space" of the normalized concentrations which is:

$$\eta(x_1, x_2, x_3) = \begin{cases} \exp\left(-\frac{1}{1-\left(x_1^2 + x_2^2 + x_2^3\right)}\right) & if \quad x_1^2 + x_2^2 + x_2^3 \le 1 \\ 0 & if \quad x_1^2 + x_2^2 + x_2^3 > 1 \end{cases} \tag{4.6.3}$$

and can be interpreted as the Gaussian function scaled to fit into the unit disc.

c. Rescale the bump function, and subtract $X(t) = (x_1(t), x_2(t), x_3(t))$ from the vector $X = (x_1, x_2, x_3)$ to shift the center of this delta function to the point $X(t)$ since most of the probability is condensed at this point. This defines the probability distribution vector given by :

$$p_X = \eta_\varepsilon(x_1, x_2, x_3) = \frac{1}{\varepsilon^3} \cdot \eta\left(\frac{x_1 - x_1(t), x_2 - x_2(t), x_3 - x_3(t)}{\varepsilon}\right) \tag{4.6.3}$$

and the domain of nonzero values is now $x_1^2 + x_2^2 + x_2^3 \le \varepsilon$. We notice that this is a molifier of the Dirac delta function (η_ε converges to δ in the sense of measures , $\eta_\varepsilon \xrightarrow{L_1} \delta$), and for values of ε small enough, the radius of the compact support is shorter than the stepz size of the spatial grid of the simulations(Fig. 4.6.1). Since we are interested in the probability of the

event, which is the integral of the distribution, we may replace it by a delta function centered at $X(t)$.

d. Initialize the probability distribution q of the cell decision with binary values of cell fate y :

$$q(y) = \begin{cases} 1-q_0 & for \quad y = 0 \quad (death) \\ q_0 & for \quad y = 1 \quad (survival) \end{cases} \tag{4.6.4}$$

e. Define the distortion measure vector $d(x_1, x_2, x_3, y)$. The decompressed data need not be exactly the same as the original data[199]. The most common distortion measures the Hamming distortion measures of the form:

$$d(x_1, x_2, x_3 | y) = \begin{cases} & x_i \geq x_i^{th} & x_1 < x_1^{th}, x_2 < x_2^{th}, x_3 < x_3^{th} \\ y = death & 0 & d_1 \\ y = survival & d_2 & 0 \end{cases} \tag{4.6.5}$$

Where the first inequality hold for at least one x_i and d_1, d_2 are real positive numbers. The distortion function describes the goals of a decision-making pathway by quantifying how disadvantageous, or ‘‘distorted,’’ a decision y is in response to a stimulus $x = (x_1, x_2, x_3)$. In our case, suppose that when all molecular concentration are below a threshold x_i^{th}, the cell should not die ($y = survival$) ; for at least one concentration greater than its fixed threshold x_i^{th} , the cell should die $(y = death)$. In practice, the thresholds may not be clear and a cell can be forgiven for make either decsion in response to a stimulus close to the threshold. To represent this situation, a graded distortion function needs to be used [87], so that stimuli demonstrably above or below a threshold x_i^{th} elicit a nearly determinsitc opyimal response (probability of cell death is close to zero or one, and for stimuli around the thershold, the optimal response is such that survival/death decisions are both expected to occur, with significant probability. Stimulus levels near a threshold should lead to bimodal probability distributions with survival and death observed in a cell

population, as it has been seen experimentally in several cell fate decision processes in [87], [200, 201]. In other words, the distortion measure is the penalty for an incorrect classification of the level of a molecular concentration, which leads to errors in the stimulus pattern recognition, which in this frame is the assignment of a cell fate probability to the given input by the biomolecular reactions.

f. Assign the Lagrange multiplier constant S. We choose a negative number for the slope (the S increases from $-\infty$ to 0 and D increases from 0 to $D_{\max}$, therefore the least distortion correspond to very large negative S.

g. Calculate the strategy $Q_{Y|X}$ as defined by $Q_{Y|X}(y;x_1,x_2,x_3)=\dfrac{p_Y(y)e^{s\cdot d(x_1,x_2,x_3,y)}}{\sum_{y'}p_Y(y')e^{s\cdot d(x_1,x_2,x_3,y')}}$ that minimizes the mutual information between the input (death stimuli, normalized concentrations) and the output (cell decision). This strategy will be calculated following the Blahut-Arimoto algorithm [197]. This can be done in following steps:

I. Assign σ that determines the accuracy of the algorithm. Define $x=(x_1,x_2,x_3)$

II. Initialize with the exponential

$$A(x_1,x_2,x_3,y)=e^{s\cdot d(x_1,x_2,x_3,y)} \tag{4.6.6}$$

then calculate in the following order:

α. The denominator $a(x_1,x_2,x_3)=\sum_y q(y)A(x_1,x_2,x\ ,y)$. (4.6.7)

β. Calculate $c(y)=\sum_{x_1,x_2,x_3}\dfrac{p_X(x_1,x_2,x_3)\cdot A(x_1,x_2,x_3,y)}{a(x_1,x_2,x_3)}$. (4.6.8)

γ. Update $q(y)=q(y)c(y)$ for binary y.

δ. Calculate the upper bound and the lower bound:

$$T_U=-\sum_y q(y)\log_2(c(y)),\qquad T_L=-\max_{1\le j\le 2}\log_2(c(y)) \tag{4.6.9}$$

If $T_U - T_L \geq \sigma$ go back to step α. Otherwise go to step ε.

ε. Update $a(x_1, x_2, x_3) = \sum_y q(y) A(x_1, x_2, x_3, y)$.

στ. Calculate the "strategy" $Q_{Y|X}(y|x_1, x_2, x_3) = \dfrac{A(x_1, x_2, x_3, y) \cdot q(y)}{a(x_1, x_2, x_3)}$ (4.6.10)

ζ. Calculate the survival probability $q(y) = \sum_x p_X(x_1, x_2, x_3) \cdot Q_{Y/X}(y|x_1, x_2, x_3)$ (4.6.11)

η. Calculate the expected distortion

$$D = \sum_x p_X(x_1, x_2, x_3) \cdot (\sum_y Q_{Y|X}(y|x_1, x_2, x_3) \cdot d(x_1, x_2, x\ , y)) \quad (4.6.12)$$

θ. Calculate the rate distortion function approximation for this strategy

$$R(D) = s \cdot D - \sum_x p_X(x_1, x_2, x_3) \cdot \log_2\left(a(x_1, x_2, x_3)\right) + \frac{T_U + T_L}{2} \quad (4.6.13)$$

The method of the Lagrange multipliers in this code is not only a mathematical formalism. Finding extrema of a function is a most common problem, but difficulties often arise when one wishes to maximize or minimize a function subject to fixed outside conditions or constraints. The method of Lagrange multipliers is a powerful tool for solving this class of problems without the need to explicitly solve the conditions and use them to eliminate extra variables. In cases where the function and the constraint have specific meaning, the Lagrange multiplier has an identified significance as well. For example in mechanics and in the definition of the Lagrange function, the multipliers describes the force of the constraint

$$L[x_i, \dot{x}_i, \lambda, t] = L[x_i, \dot{x}_i, t] + \lambda \cdot g(x_i, t) \quad (4.6.14)$$

$$F = -\nabla V_{potential} = \lambda \cdot \nabla g \quad (4.6.15)$$

In economics, in the study of shadow prices, co-state values, the multipliers is the most the firm would pay for another unit of capital. In information theory and specifically the minimization of the functional of the multual information, the Lagrange multiplier s represents the rate of change of the rate distortion function [95]:

$$R'(D_s) = s \tag{4.6.16}$$

4.7 Simulation and visualization

A group of rate equations are used to quantitate the time evolution of the following molecule species in a Type II PDT process: photosensitizers (Photofrin) in ground state S_0, single and triple excited states S_1 and T; oxygen molecules in triplet grounded and single excited states $^3O_2$ and $^1O_2$; Death ligand such as *TRAIL* and *TNF*; inactive receptor complex *R**;FLICE-like inhibitory protein *flip*; procaspase-8 and procaspase-10,inactive,both as *C8*, bi-functional apoptosis regulator *Bar*; (cleaved) active caspase-8 and caspase-10 *C8** ; procaspase-3 and procaspase-7 ,inactive, both as *C3* ; procaspase-6,inactive capsase-6 *C6*; (cleaved) active caspase-3 and caspase-7 *C3**and active caspase-6 *C6**; X linked inhibitor of Apoptosis in the cell *XIAP*; Poly (ADP-ribose) polymerase *PARP*, as DNA damage repair enzyme , here all substrate of active caspase-3 *C3**;The BH3 interacting-domain death agonist *Bid* as a substrate of cleaved caspase-8 in its inactive form; the anti-apoptotic protein *Bcl-2*; the Bcl-2–associated X protein in its inactive form *Bax* and its active form *Bax** ; *Bax* in the mitochondrial compartment as Bax_m; cytochrome c inside the mitochondria in the mitochondrial compartment CyC_m and cytochrome c release from the mitochondria but remaining in mitochondrial compartment CyC_r; cytochrome c in cellular compartment *CyC* ; second mitochondria-derived activator of caspases. Sma_c and *Smac/Diablo* released from the mitochondria but remaining in mitochondrial compartment, $Smac_r$; Apoptosis activating factor *Apaf-1*, substrate of *CyC*, in its inactive form Apaf1; active form of Apaf-1, *Apaf**; inactive form of procaspase- 9 *C9*; the apoptosome *Apop* which is the complex Apaf*:C9; inositol-requiring protein 1

IRE1; JUN N-terminal kinase, *JNK*; death associated protein kinase *DAPK*; Beclin mediator of autophagy phosphorylated by death associated protein kinase *DAPK*, *BECN1*;the tumor suppressor protein *p53*; the intracellular concentration of calcium *Ca2+*; the protease Cathepsin *Cath* and the protease *Calpain*; the inositol 1,4,5-trisphosphate receptor *IP3R* or *IPR3*; Even though the singlet excited oxygen molecules $^1O_2$ may play a critical role by themselves, it is well known that other *ROS* species are also involved in the cytotoxicity of PDT with mitochondria as the possible source and target sites. The $^1O_2$ should be interpreted as the representatives of *ROS* [35] . The molecular equations, together with the definitions of coefficients and their values that were used to mathematically model the molecular network described above have been detailed in [102], [100], [101]. A 70 rate equation group can be solved to characterize the main molecular interaction involved in Type-II PDT. We use the ordinary differential equation (ODE) stiff solver (ode15s) by MATLAB (The MathWorks, Natick, MA) to obtain the solution vector as a function of illumination time t from the start of illumination at t = 0 to 1800 (s). Experimental verification of these quantities that describe the levels of all these molecular concentrations can be very difficult if not impossible and they relate indirectly to the ultimate consequence of PDT for cell killing. In [102] we introduced a cell killing model that related the molecular concentrations of the singlet oxygen and the unoxidized receptors to the cell survival ratio, which can be measured with an in vitro cell model. The output of this equation group is the time dependent levels of molecular concentrations for the stimulus vector of $x(t) = (x_1(t), x_2(t), x_3(t))$ corresponding to singlet oxygen $^1O_2$, *cPARP* and *Caspase 3*. The concentrations were normalized with respect to their maximum values and their range is [0, 1]. The total time for the simulations was up to 30,000 sec to monitor post- treatment cell killing. We used the stiff solver (ode15s) by MATLAB (The Math Works, Natick, MA) to obtain the solution vector as a function of illumination and observation times, from the start of illumination at t = 0 to 1800 (s) (end of illumination time) and from 1800 to 30,000 (s). Experimental verification of these quantities that describe the levels of all these molecular concentrations can be very difficult if not impossible and they relate

indirectly to the ultimate consequence of PDT for cell killing. In [102] we introduced a cell killing model that related the molecular concentrations of the singlet oxygen and the unoxidized receptors to the cell survival ratio, which can be measured with an in vitro cell model. The same software (MATLAB) is used for producing the simulations for the decision mechanism of a single cell model design. The output of the time dependent Blahut Arimoto algorithm is the cell survival probability. The distortion measure *d* that quantifies how disadvantageous a decision y is, in response to the stimulus vector $x = (x_1, x_2, x_3)$ is defined by the equation $d\big((x_1, x_2, x_3|y = survival)\big) = 10$ if $x_i \geq x_i^{th}$ for some i, and $d\big((x_1, x_2, x_3|y = death)\big) = 10^{-1}$ if $x_i \leq x_i^{th}$ for some i, and a small number otherwise. The thresholds x_i^{th} for the normalized concentrations were all set to 0.5. This distortion measure penalizes a cell survival error more than cell death error for given stimuli, by one order of magnitude. For the range of the Lagrange multipliers the equation $s = -e^{-n}$ was used and in the simulations n varied over a finite set of integers (a sample of n values from 1 to 20 was taken for the simulations below). The initial survival probability $q^0(y = surv) = 1 - q_0$ was set equal to 0.9. The treatment parameters for the PDT model that was introduced in our previous work [102], was linked to the input of this algorithm (Fig.1:"PDT Biomolecular equations"). Tables containing the molecular components involved in the PDT model, molecular interaction network, interaction constants and initial conditions of all concentrations are available at the supplementary information section.

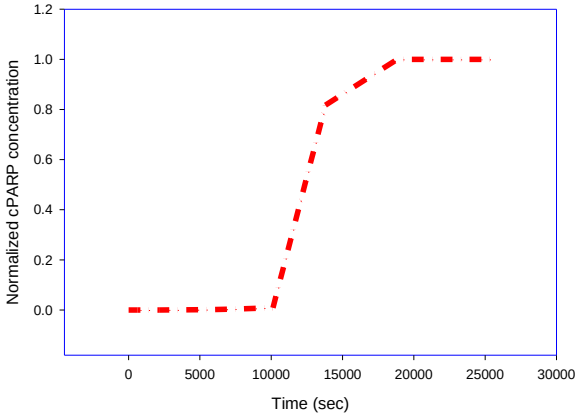

Figure 4.7.1. PARP activation is an immediate cellular response to metabolic, chemical, or radiation-induced DNA SSB damage. Upon DNA cleavage by enzymes involved in cell death (such as caspases), PARP can deplete the ATP of a cell in an attempt to repair the damaged DNA. ATP depletion in a cell leads to lysis and cell death. PARP also has the ability to directly induce apoptosis, via the production of PAR, which stimulates mitochondria to release AIF. This mechanism appears to be caspase-independent.

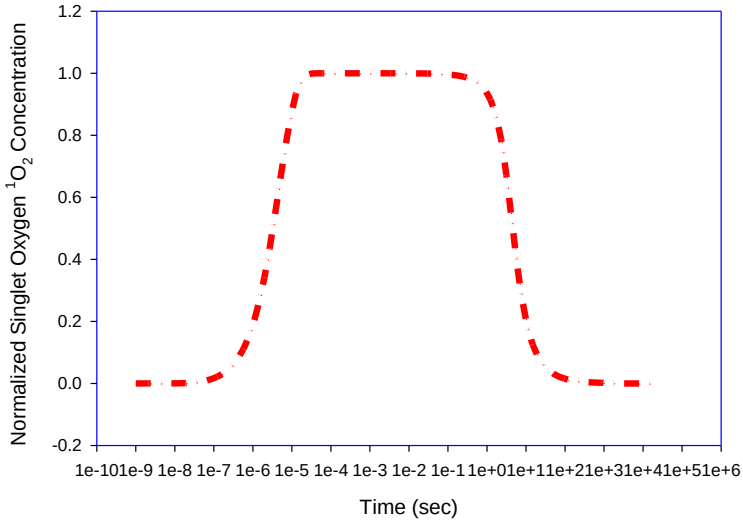

Figure 4.7.2. Singlet Oxygen is the most important cytotoxic agent generated during PDT(it decays after photo irradiation time). Singlet oxygen is produced during PDT via a triplet-triplet annihilation reaction between ground state molecular oxygen (which is in a triplet state) and the excited triplet state of the photosensitizer.

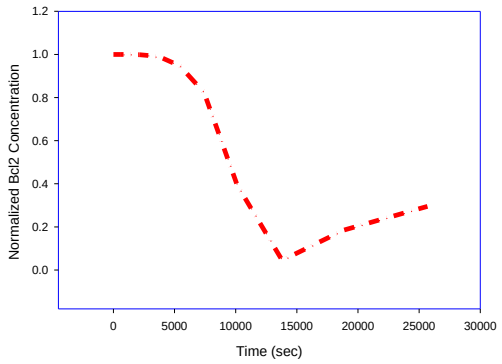

Figure 4.7.3. ROS initiates the degradation process of Bcl-2 that could bind to Bax to prevent its activation. At a later time after the photo-irradiation a post-treatment increase of Bax is observed.

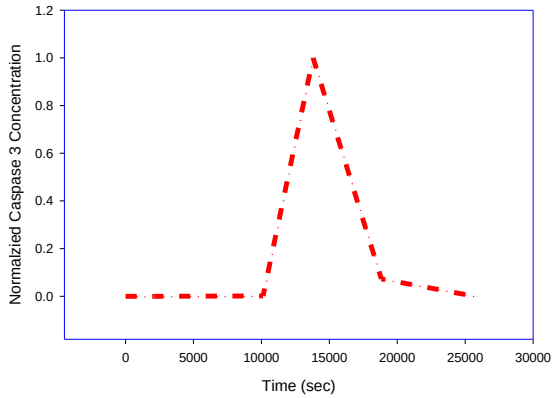

Figure 4.7.4. Actived Caspase 3 is potent effector of post-treatment cell apoptosis: For the intrinsic cell death pathway, apoptosis is triggered by intracellular events such as DNA damage and oxidative stress. For the extrinsic cell death pathway, apoptosis is triggered by extracellular stimuli such as TNF and TRAIL. A sharp increase in the levels of Caspase 3 indicates the beginning of apoptosis.

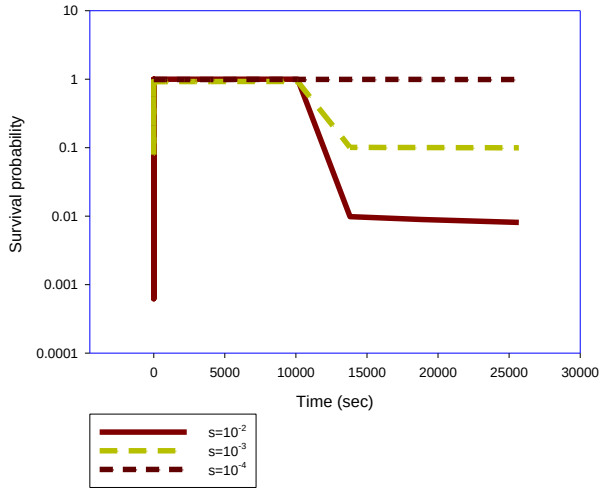

Figure 4.7.5. A sample of a survival probability curves as predicted by the Blahut Arimoto algorithm for the cell model. Value of the parameter $s = -10^{-2}, -10^{-3}, -10^{-4}$ Photon density $\rho = 10^{6} cm^{-3}$. Photo sensitizer (Photofrin) concentration in a cell $[S_0] = 5 \times 10^{13} cm^{-3}$. Single cell oxygen concentration $[^3O_2] = 6.06 \times 10^{17} cm^{-3}$.

4.8 Results and discussion

The effort to link biochemical pathways and collective interactions to the behavior of whole cells and to infer causality from statistical correlation in large data sets is not a simple task in the case of photo-chemotherapy, and to account for all biological variation is a very challenging goal. The existence of more than one PDT tissue destruction mechanism in vivo for the treatment of intraocular retinoblastoma like tumor, has been suggested and demonstrated in [202] where an early direct cell damage was followed by a subsequent late damage occurring in the tumor tissue left in situ after treatment, resulting in a biphasic pattern in the cell survival curve as a function of time. In[203], experiments on Chinese hamster cells with phthalocyanine dyes and split light fluence indicated that cells can repair sublethal photo cytotoxic damage during the course of several hours. Although direct

cytotoxicity to the tumor cells has been shown to be relatively small after PDT and to increase with time after treatment[204], examples of in vitro mammalian cell curves as functions of exposure time for different photosensitizer concentrations show that for an acute high dose treatment (vast majority of PDT treatments) the cell survival ratio decreases to less than 1% in the course of a few minutes. In [205], the effects of low dose gamma irradiation on promyelocytic leukemia Hl 60 cells were investigated and it was recorded that after radiation exposure, the survival cells continue to divide so both the numbers of control (untreated) and treated cells with all-trans-retinoic acid can increase with increasing time.

Discrepancies may be due to many factors such as light attenuation passing through the skin resulting in a relatively lower energy dose to some cells than others or the fact that the tumor vasculature is a primary target of PDT, indicating that endothelial cells are the clinically relevant cell population that might have a significant effect on the cell survival curves. Therefore, the local micro-environment might have significant impact on PDT response. If the photosensitizer is present in the endothelial cells lining the blood cells, then these cells can be killed resulting in vascular occlusion, cessation of blood flow, thrombus formation and oxygen/nutrient deprivation leading to tissue destruction[206]. Vascular effects can be secondary to cell death or conversely, cell death can be secondary to vascular shutdown. Another factor that might affect the final outcome is the triggering of the immune responses, local or systemic[206]. A conceptual and mechanistic system biology mathematical model can yield valuable insights since cellular behavior cannot be summarized in population averages[207]. The Blahut Arimoto model has several features that are consistent with the experimental results. For the parameter s, estimation can be performed using experimental data, and a range of values can be recovered. The shapes of the survival curves and the extents of their correlation with the parameter s will depend on the structure of the rate equations the type of cell decision algorithm adopted and the accuracy of the experimental data. Different values of the parameters will be predictive of different model curve topologies[208]. The cell s parameter distribution in a cell population

for this biochemical models is remains non-identifiable, high-likelihood predictions can still be made by appropriate calibration of the parameters.

Cells have special machinery that rapidly recognizes damage and repairs it, therefore allowing the cell to retain its structure. [209], [210] [211] . The cell repair mechanisms that are related to the development of drug resistance in cancer cells are complex and of various kinds and are associated with many factors, such as cell type and intracellular and extracellular environment. For example, superoxide dismutase, which is present in both the mitochondria and cytoplasm of eukaryotic cells, is an enzyme that restrains the toxicity of reactive oxygen species such as $^1O_2$, one of the PDT agents. Cell killing through PDT is a unique case study of system biology in which cell repair and death in response to combined stimulations of photosensitizer and light can be quantitatively investigated and modeled[102].

The survival probability predicted by the rate distortion function and calculated by the Blahut Arimoto algorithm , and the variability in the graphs resulting from different values of the parameters provide a framework for the interpretation of self-renewal capabilities of the cell and its ability to generate drug resistance [212]. There is significant difference between the survival probabilities as function of time and an example is shown in the figures below. It is documented by several experimental studies that tumor cell killing and tumor destruction are not always evident during PDT treatment, but due to the involvement of host related factors, the effect of PDT cell killing might become evident post-treatment and over a longer period of time [77] .

4.9 Conclusions

In this study a model of a cell decision mechanism is proposed, which captures certain observed characteristics of a cell behavior during photo-irradiation and pharmacological treatment (Type II PDT) using rate distortion theory to quantify the goals of a binary decision process (cell survival - cell death). The main components of the model are, the time dependent distribution of molecular stimuli, the

distortion function (or measure), the conditional probability of the cell decision strategy, the cell survival probability, the expected distortion and the rate distortion function which quantifies a limit on how well the goals can be achieved given the stimulation. The results are independent of the biological mechanism by which the cell strategy is implemented and the Blahut Arimoto algorithm is used to derive optimal pathways. The model requires knowing the probability distribution of the stimuli as its input. For a variety of Lagrange multipliers, there is a corresponding variety of optimal pathways, but an approximation of the distortion function around which the pathway is optimized, is possible, based on algebraic properties of the algorithm (the distortion constraint) and numerical and experimental data[87]. According to [88] cellular decision-making has the following main features: a cell must (1) estimate the state of its environment by sensing stimuli; (2) make a decision informed by the consequences of the alternatives; and (3) perform these functions in a way that maximizes the fitness of the population. These characteristics are described in a single process using rate distortion theory. The rate distortion framework enables design and evaluation of that process with a fundamental optimality criterion [87]. A diverse range of cellular responses to treatment and biological variation is the result of little information and distortion is associated with the decision mechanism of the cell, a decision mechanism that allows for intrinsic molecular noise, cell structure, possible PDT bystander effects, treatment parameter variations and other properties of a single cell and this therapeutic modality.

Intracellular molecular interactions can be studied with the purpose of extracting useful conclusions, by using computational methods. In this chapter we present the development of a systems biology model that includes detailed molecular pathways induced by PDT treatment leading to cell death, coupled to a cell decision making algorithm that is based on the mutual information between cell death stimulation and cell response as the output of a bio molecular communication channel. This line of research can be relevant to future improvement and management of cancer treatment methodologies. The cell survival

probability is modeled as the output of an optimization process of transmitting the death signal through a communication channel with a possible environmental and/or inherent distortion. Modeling results can be compared directly to experimental results that are based on the levels of measurable molecular concentrations and cell survival ratios, for optimization of the unknown parameters, or/and used for design of different in vitro studies of PDT. This modeling establishes a framework to address questions such as why do cell types, despite sharing the same genome, in general represent stable entities and do not gradually "drift away" and "morph" into one another, but instead, get "stuck" in precisely those expression profiles that represent the observable cell fates and what is the molecular basis of the rules that govern such cell fate dynamics [213].

As a final consideration we need to note that while the predictions of the calculations of a system of 70 molecular rate equations coupled to the a time dependent Blahut-Arimoto algorithm for cell decision making are necessarily limited by uncertainties in the choice of the various model parameters as well as by the simplifying assumptions of the model itself, they nevertheless provide an approximate theoretical framework within which the interaction between the PDT parameters and the biomolecular concentrations are linked to the quantized cell fate states through the mechanism of mutual information.

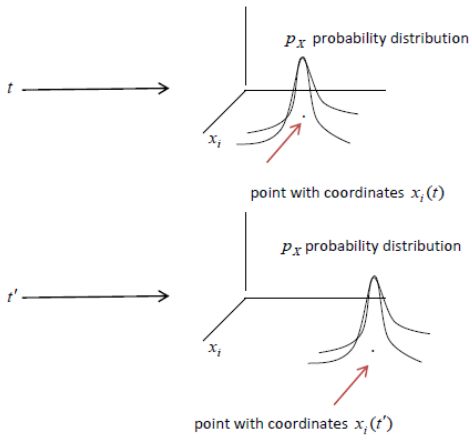

Figure 4.6.1. The dynamic evolution of the stimulus probability vector in the concentration space.

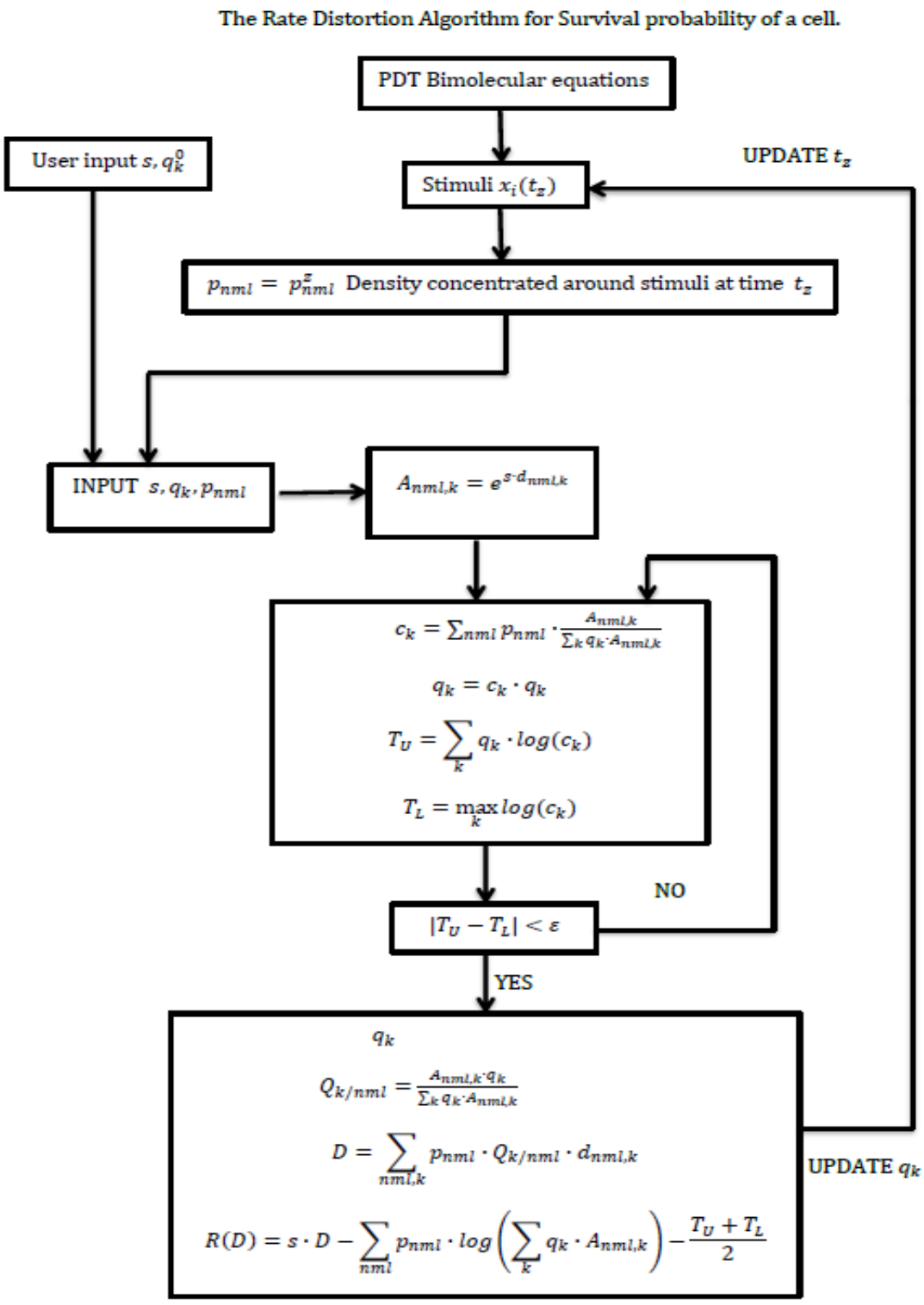

Figure 4.6.2. The time dependent Blahut Arimoto Algorithm

4.10 Interaction information and the Bystander Effect

In the previous sections it was presented a communication theory model for the study of inactivation of cells by direct damage (necrosis/apoptosis). In addition to this, photosensitized induction of apoptosis has been observed as a result of communication between cells in a colony[214], a phenomenon called "bystander effect". In recent studies, comparisons between theoretical considerations(use of binomial distributions for prediction of independent inactivation of cells in microcolonies) and experimental data[214] have been incompatible, indicating that a bystander effect is involved in cell death in these colonies. Although it has been proposed that intercellular signaling takes place through molecules that are produced during the apoptotic process (such as interleukin 1β), the observation that unirradiated cells exhibit irradiated effects as a result of signals received from nearby irradiated cells, has not been fully understood. Further results suggest that a bystander effect is involved in ultraviolet-radiation-induced genomic instability and that it may be mediated in part by gap junctional intercellular communication[215]. Bystander effects contradict the generally accepted assumption that biological damage caused by ionizing and nonionizing radiation is limited to the cell in which the primary energy deposition takes place, but rather suggest that cells should be inactivated randomly with regard to position and experiments have shown that the cells are not inactivated independently of each other[216]. Going beyond the framework of PDT, it is believed that Radiation induced Bystander effect and it is now a well-established consequence of exposure of living cells to radiation [217-219].

Cell to cell communications in normal and carcinogenic cells have been discussed extensively[220, 221]. It is believed that in general cell to cell regulatory signals are conducted by chemical and electrical signals [219] where the chemical signals are transmitted via Gap Junctional Intercellular Communication (GJIC) or by Distant Signaling Intercellular Communication (DSIC). The assumption is that these signals are propagated by a Brownian diffusive motion, because this yields

satisfactory results in simulations of bystander effects [222]. However, a quantitative biophysical model of the radiation-induced bystander effect needs to account for processing of information by the cellular environment through biochemical siganling, in order to determine more accurately how and when the bystander signals switch a cell into a state of cell death.

The "interaction information" [223] is a generalizations of the mutual information, and expresses the amount information (redundancy or synergy) bound up in a set of variables, beyond that which is present in any subset of those variables:

$$Q(X,Y,Z) = I(X,Y|Z) - I(X,Y)$$

Q measures associations between variables, and not the direction of the transmission: This means that nothing is gained formally by distinguishing transmitters from receivers, therefore it goes beyond the Shannon framework of linear transmissions[224]. An interaction is a regularity, a pattern, a dependence present only in the whole set of events, but not in any subset. It is symmetric and undirected, so directionality no longer needs to be explained by, e.g. causality[225]. Positive interaction implies synergy. Q measures the amount of influence on the relationship between X and Y , resulting from the introduction of Z[225]. It is the amount of information that is common to all variables but not present in any subset. Positive interaction information of three variables has been associated with the non-separability of a system in quantum physics[226], with the origin of synergy in relationships between neurons [227], with cooperative game theory with applications in economics and law [228]. To understand the bystander synergistic effect in the case of radiation, we observe that a low dose irradiation (X) to a cell (Y) is more unlikely to correlate to a nearby unirradiated cell (Z) exhibiting irradiated effects. But if a low dose irradiation induces cell death to an irradiated cell, it would provide much more information about the possibility of a nearby unirradiated cell exhibiting irradiated effects, than if a high dose radiation would induce cell death to the irradiated cell. The corresponding reduction

in the possibility of a bystander effect is the sum of all three interactions connected to it, on the basis of state of the irradiated cell, the radiation dose, and on the basis of cell state and radiation dose simultaneously. Suicide gene therapy[229] and gene transfer technology use the bystander effect ability of the transfected cells to transfer death signals to neighboring tumor cells [230]. Specific applications also extend in the practice of hematopoietic stem cell transplantation. It is expected that the interaction information can be used to provide quantifying tools, for the mathematical modeling of these clinical applications. The establishment of such a foundation, based on the mathematical properties of interaction information is currently under investigation.

CHAPTER 5: ANALYTICAL CONSIDERATIONS AND CONCLUSIONS OF THE STUDY ON THE PROBABILITY OF SURVIVAL AND MODELING OF CELL KILLING BY PDT

5.1 Predator Prey Models

Survival functions can be derived using predator-prey model. The predator-prey model has been used for the description of the survival probability in dynamic energy budget models [231] under the assumption that that the per capita death rate has two contributions, a constant loss b due to random misfortunes, and a density-dependent loss due to predation, with a Holling Type II functional form [231].

$$\frac{dp}{dt} = -bp - \phi(x(t))\frac{vp}{v+p} \tag{5.1.1}$$

$$p(0) = 1 \tag{5.1.2}$$

$$\phi(x) = \frac{rH}{r+H} \tag{5.1.3}$$

p is the survival probability , v is a constant that measures the deviation of the functional response from linear, x is the length dimension of a prey and r is the predation rate, H is the prey size for which the predation rate is half-maximum. This model was designed to predict the growth and reproduction patterns of a species based on the characteristics of individual organisms, particularly the strategy used to allocate resources. The size of an individual is given by the length x , surface area S , and volume V and the maintenance and assimilation rates are assumed to be related to these measures of size. This model takes an individual-based approach where all members of the prey population are “copies” of this one individual, and each “copy”, could be the “model individual” itself

The use of a predator-prey model (a continuous model used for the simulation of discrete population dynamics) for the modeling of survival probability(a continuous variable) suggests the quantization of survival probability. Indeed, the quantization of probability has been proposed by other authors [277],[232] [233]. The existence of the chance-quantum (c.q.), implies that [Go 43]:

a. if the probability of an event is equal to or greater than one c.q., it may ultimately occur.
b. If an event has a calculated probability of less than one cq. it will not occur.
c. Events may differ in probability only by an integral number of cq.
d. For an event having an appreciable probability (equivalent to many cq.), a change in surrounding conditions leading to a computed change in probability of less than one cq. will in fact cause no change in the probability of the event.
e. The interrelations between the cq. and the "energy" quantum (as well as the elsewhere proposed time quantum) may be close and significant.

The idea of quantization of probability has been used in applications of linear circuits, in particular in the study of circuit analysis and methods needed to adequately predict circuit performance as a function of components tolerances (standard deviations from the mean). To obtain maximum component efficiency the quantized probability design (QPD) was developed in [232] , a statistical method for predicting the tolerance limits for a circuit, where the parameters of are weighted according to their effect on the circuit as follows[232]:

a. First-Order Weighting: Components whose parameter variations affect circuit operation critically are taken at end-of-life tolerance(The end-of-life tolerance includes initial tolerance plus environmental change plus variation due to aging.)
b. Second-Order Weighting: Components whose parameters affect circuit operation to a limited extent are taken at initial (purchase) tolerances.

c. Third-Order Weighting: Components whose parameters have negligible effect on circuit operation are taken at nominal values.

In this work, the authors quantize the tolerances (standard deviations) of the independent variables of a system (which follow normal distributions) $x_1, x_2, x_3, \ldots$ which then imposes quantization restrictions to a circuit response (the expression for the voltage gain of the circuit $y = A(x_1, x_2, x_3, \ldots)$ through the equation for the standard deviation:

$$\sigma_y = \left[\left(\frac{\partial A}{\partial z_1} \sigma_{x_1} \right)^2 + \left(\frac{\partial A}{\partial z_1} \sigma_{x_2} \right)^2 + \ldots \right]^{\frac{1}{2}} \tag{5.1.4}$$

Furthermore, this criteria for quantization impose mathematical constraints to the probability density functions of variables $f(x_i)$ as well as system response $f(y)$:

$$\sigma = \left[\int_X (x_i - \mu)^2 f(x_i) dx \right]^{\frac{1}{2}} \tag{5.1.5}$$

This new probability is a "quantized probability" that might need a new definition of the axioms to accommodate the new mathematical constraints.

Bathtub analog. In [234], the analog of the bathtub that is filling with drops of water, which we perceive as a continuous flow is considered. While the level changes while an observer is out of the bathroom, and the changed level appears as a discrete step, rather than a continuous curve, there is still a continuous flow of discrete drops of water while the observer is gone. The changed level and its stepped appearance does not make it a discrete event system [234]. Adopting this logic, we replace the bathtub by the biochemistry of a cell, the drops of water by discrete quantized units of cell survival probability (biochemical survival units as defined below), the total water level in the bathtub by the continuous cell survival probability(biochemical life of the cell), which now is the sum of discrete quantized cell survival probabilities. This results in a duality in the perception of the nature of probability

of survival of the cell. This allows the interpretation of survival probability as a discrete population, whose dynamics can be modeled using continuous equations, in particular predator-prey equations where the prey is the life of the cell and the predator are the cell death effectors.

Information The Oxford definition of the word information is "knowledge communicated concerning some particular fact, subject or event; that of which one is apprised or told; intelligence, news". This definition assigns to the word a double meaning of both facts and transmission of facts[9]. This definition of information is content neutral and resembles Shannon's approach which interprets information as what reduces uncertainty, and presupposes knowledge of a priori probabilities[10]. These probabilities need to be designed or calculated in a way that they will reflect the varieties of environmental stimuli.

It is important to decipher the meaning of information available to a cell as something that determines its activity. Information has no mass, energy, or spatial extension, it cannot be seen, touched, or smelled. Nevertheless it is a distinct, objective entity[2]. This entity and can be traced through detectable differences. For example, the cell, as an information system has the ability to discriminate and select between cell fates (which is what we call cell decision making). In fact, the manifestation of information can be found in the existence of alphabets (where as alphabet we interpret the set of physical states that can be realized in some system[9]), the combination of codes (where as a code we consider a collection of the letters of alphabets that follow some pattern-words) and the variety of codes that determine the state of the system.

[9] "What is information?" Karl-Erik Sveiby Oct 1994, updated 31 Dec 1998
http://www.sveiby.com/articles/Information.html
[10] "What is information?" Andrzej Chmielecki Philosophy and Cognitive Science
World Congress of Philosophy, in Boston, Massachusetts from August 10-15, 1998

In the case of a biological cell, the genetic code is an example[9]. The alphabet consists of four nucleotides which can be discriminated by some enzyme. Any linear sequence of nucleotides in a DNA or RNA chain is a code, and information enters when the double helix and the enzyme polimeraze detects which one of the four nucleotides occurs at a particular place in the chain, and then adds to it a complementary one (processes of replication and transcription).

In our framework, the situation is different. We consider the cell an entity that processes para-information (I1) that is delivered through transfer information (I2) while the cell possesses structural information (I3) and derives meta-information (MI). Here we use terminology from cognitive science, where "para-information" is the elemental, primordial type of information, the simplest kind of information and a code that can potential associate with "structural information". In our case, information from stimulation (I1) is transferred through (I2), received from molecules-receptors of the cell and then is processed. The system adds information from its own resources ((I3), cell structure as a sort of memory) to the current inflow of receptor based information, and through molecular interactions, the molecular network of the cell produces measurable concentrations that reflect the association of these manifestations of information. This newly formed, resultant information is the "meta-information" that we model as the input of the system, with a probability distribution for the cell stimulation in the cell decision making algorithm.

In the work of James, G. Miller[235] we find a definition of what a goal is for a living system:

"*By the information input of its charter or genetic input, or by changes in behavior brought about by rewards and punishments from its suprasystem,* ***a system develops a preferential hierarchy of values that gives rise to decision rules which determine its preference for one internal steady-state value rather than another. This is its purpose. A system may also have an external goal.*** *It is not difficult to*

distinguish purposes from goals. I use the terms: an amoeba has the purpose of maintaining adequate energy levels, and therefore it has the goal of ingesting (= swallow) a bacterium."

The goal of the system of the cell is determined by a system on a higher level. The tumor or the healthy tissue surrounding the cell can be viewed as the super-system that performs regulatory functions (such as immune dynamics, angiogenesis, etc.). PDT or any other modality basically interferes with the operation of a cell through signals (the signals contain information which has meaning for the purpose of the system). The condition of an "observer" outside the system that determines the goal of the system is a prerequisite for the definition of information by Wiener.

Cybernetics, as conceived by Norbert Weiner in the 1940's, is a master science founded on the issues of control and communication. It is concerned with self-correcting and self-regulating systems, be they mechanical or human[11]; Cybernetics posits that the functioning of the living organism and the operation of the new communication machines exhibit crucial parallels in feedback, control, and the processing of information[236]. In the framework of cybernetics, *"**information must be conceived as discrete bundles, physically decontextualized and fluidly moving.** For ultimately, the control processes of complex systems are a matter of regulated feedback which requires that processes of communication be conceived of as exchanges. Within this cybernetic model, feedback is not free and equal; rather it is governed by the system's constant battle with entropy, chaotic disorganization or noise."*[12]

Finally, we notice that in the neoclassical theory of economics, price becomes equivalent to "the bit," in that information is reduced to a homogeneous form characterized as ***discrete atomic units***. ***At the***

[11] David Sholle, "What is Information? The Flow of Bits and the Control of Chaos" MIT communication forums, http://web.mit.edu/comm-forum/papers/sholle.html

[12] Pfohl, S. (1997). "The cybernetic delirium of Norbert Wiener". In A. Kroker & M. Kroker (Eds.), Digital Delirium (114-131). New York: St. Martin's Press.

same time conceived of as a flow; but here, this is seen within spatial and temporal dimensions defined in terms of the market. *Information is the "energy" in the system that functions within the control processes of cybernetic capitalism.* The enemy of the smoothly functioning market system is disorganization, noise, chaos. Indeed, it is reported in[237] that Hayek in 1945 lauded the informational properties of the price system, viewing prices as 'quantitative indices' (or 'values') :"*Each index or price Hayek contended should be understood as concentrated information reflecting the significance of any particular scarce resource relative to all others. The index of price borne by each commodity, Hayek enthused, permits autonomous economic agents to adjust their strategies 'without having to solve the whole puzzle [input-output matrix] ab intitio* ". At the same time a second economic definition of information is conceptualized as a commodity. Information good in economics is defined as type commodity whose main market value is derived from the information it contains. This definition is related to uncertainty in that before consumption of the good, a consumer may not be able to assess the utility of the goods accurately and reliably, as is the case with a movie or an advertisement. In [238] information is defined as a commodity, and "perfect information" is considered to be the key element to explain efficient market hypothesis. Perfect information is defined in game theory as the information that is free, complete, instantaneous and universally available to a player, during and after the game, such as the information ones receive during a chess game, that he can see all the board and determine all combinations of legal moves.

5.2 Survival (Lifetime or Life) Units Duality

Survival Units Duality refers to the idea that the life a cell can discretized (quantized) in quanta of life which are assumed here as the basic units of life in every cell. New cells are produced by existing cells, and therefore the termination of a cell does not allow to assign any morphological or biochemical characteristics to the life of the cell itself, since these can only be considered as the manifestations of

the monitoring, interaction and response of the cell, as a biochemical unit undividedly united to cellular life ("life units"), to the extracellular environment. Cellular life is a set of life units, where each cellular life unit contains the whole complete life of the cell in itself, therefore allowing the cell to repair itself after any loss of survival units due to the attack of cell death inducers or other factors. In analogy to many-particle physics one replaces the actual cell life by a cellular life density.

Axiomatic interpretations:

a. Each cell's life is made up of finite number of survival units

b. All cells of the same type have the same life or number of life units.

c. Survival units cannot be described biochemically, although they are results of the cellular biochemistry.

d. The activity of an organism depends on the total activity of interdependent life units.

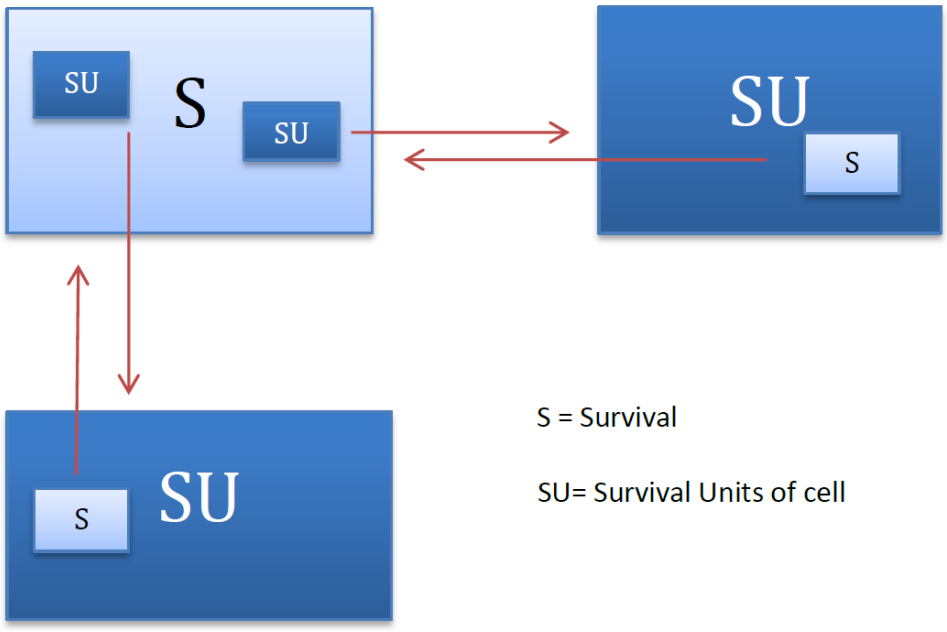

Figure 5.2.1. A schematic representation of the idea of cell survival units modeling. Cell life as a sum of survival units (quantums) , and a life quantum (a "survival probability quantum") contains life in an embryonic form that might or might not develop to a 100% probability of survival depending on the state cell (for example, recovery after photo-chemo therapeutic treatment, stress, hyperthermia, etc.).

Russell's Paradox and information. Mathematics is based on generally accepted axioms of set theory. A set is a collection of objects, or elements. Sets are defined by the unique properties of their elements and sets and elements may not be mentioned simultaneously, since sets are determined by their elements and therefore one notion has no meaning without other. According to Peano's notation A=[239], where A is a set, P is a property, x is an element of the set A. Bertrand Russell, while working on his "*Principia Mathematica"* (Principles of Mathematics) in 1903, he discovered a paradox that arised from Frege's set theory that leads to a contradiction [240]. It says "the sets of all sets which are not members of themselves contains itself." In mathematical terms, let $S = \{x : x \notin x\}$,then $S \in S \Leftrightarrow S \notin S$. Although the precise rules for set formation have been under intense investigations and several different logicl systems have been proposed, sets that contain themselves as elements, like S, are definitely ruled out, as "abnormal". Based on the work Russell and Whitehead, Kurt Gödel was able to show that that a theorem could be stated within the context of Russell and Whitehead's system that was impossible to prove within that system [241]. Gödel created a paradox that showed a theorem could be true within the framework of *Principia Mathematica* but was also not provable by the rules of Russel's *Principia Mathematica* [13]. Gödel's Incompleteness Theorem states that there are mathematical statements that can never be proved, in any consistent system of axioms such as the arithmetic system.

Zermelo–Fraenkel set theory with the axiom of choice is an axiomatic system that was proposed to formulate a theory of sets without Russell's paradox. ZF embodies to a degree a certain conception of

[13] Kelly LaFleur, Russell's Paradox, Department of Mathematics University of Nebraska-Lincoln, July 2011

set which is called “combinatorial” or “iterative conception” [242]. The formation of a set starts with some individuals, collected together to form a set. Suppose we start with individuals at the lowest level. At the next level, we form sets of all possible combinations of these individuals. And then we iterate this procedure: at the next level, we formna ll possible sets of sets and individualsf rom the first two levels. And so on. Given the set of all sets at a particular level, the next level will contain the members of its power set. Every set appears somewhere in the hierarchy [242]. At no level of the hierarchy do we reach the universal set of all sets; in this framework it turns out that no set is a member of itself and therfeore the Russell set, if it existed, would be the universal set. But there is no universal set in the iterative hierarchy. However, several issues have been addressed with respect to the ZF system. For example, issues arise in the ZF quantification over sets, and a domain of quantification is needed, but no set of no set in the hierarchy can serve as this domain [242].

To overcome these issues, two alternatives have been suggested. One is the “new foundations”(NF) system, introduced by Quine [243], and the other is the prospects for a set theory with a universal set, according to program of Cantor and Von Neumann. The NF system is based on two axioms: the axiom of “extensionality” and the axiom of a “comprehension schema” that uses the concepts of “stratified formulas”. A substantial difficulty appeared in the study of NF. The axiom of choice (AC) is an axiom of set theory equivalent to the statement that the product of a collection of non-empty sets is non-empty. Specker has shown that the axiom of choice fails in NF [244]. This evidence indicated that one should probably follow the alternative of admitting a universal set, with subcollections that are not sets [245]. A semiset is a subclass of a set, and a proper semiset is a subclass of a set that is not itself a set. Semisets are given via properties and predication (the attributing of characteristics to a subject to produce a meaningful statement combining verbal and nominal elements, a propositional function, encyclopedia Britannica). [242]

The need for the distinction between two kinds of collection [242] can be found back in the work of Schroder and Cantor:

"If we start from the notion of a definite multiplicity of things, it is necessary, as I discovered, to distinguish two kinds of multiplicities (by this I always mean definite multiplicities). For a multiplicity can be such that the assumption that all of its elements "are together" leads to a contradiction, so that it is impossible to conceive of the multiplicity as a unity, as "one finished thing". Such multiplicites I call absolutely infinite or inconsistent multiplicities.... If on the other hand the totality of the elements of a multiplicity can be thought of without contradiction as "being together", so that they can be gathered together into "one thing",I call it a consistent multiplicity or a "set". [14]

Cantor's conclusions are the ancestors of today's distinction between classes and sets, as they appear in the work of Von Neumann [246]. For von Neumann all sets are classes, but not all classes are sets. And those classes that are not sets - the so-called proper classes -cannot themselves be members [242]. In Von Neumann's axiomatization theory, some major advnatages are [242]: There are extensions for the predicates 'set', 'non-self-membered set', 'well-founded set', 'ordinal'. There is a well-determined collection of all the ZF sets; and there is a domain for quantification over sets. Further,the Axiom of Choice is provable in von Neumann's system. Several issues, both technical and intuitive, have been reported with respect to this system. A discussion can be found in [242], and here we only mention the consequence of this theory, that the concept of class has no extension (based on the axioms of this system, there is no class of all classes, and therefore the problem has just been pushed back).

An alternative approach involving "extensions" was suggested for the resolution if Russell's paradox. The extension of a predicate is the set of tuples of values that, used as arguments, satisfy the predicate (a truth valued function). Such a set of tuples is a relation. But this has been shown to be a pathological

[14] Schroder (1890) and Cantor (1899), cited in van Heijenoort (1967, p. 113), copied from Simmons (2000)

predicate logic case [242] with respect to universal extensions (Russell's paradox pushed back again). Therefore the resolution of this paradox remains unresolved.

In mathematical logic, it is suggested that problems that are essentially the same must be resolved by the same means, and similar paradoxes should be resolved by similar means. This is the principle of uniform solution[281]. Two paradoxes can be thought to be of the same kind when (at a suitable level of abstraction) they share a similar internal structure, or because of external considerations such as the relationships of the paradoxes[281]. The question rises as to the existence of other paradoxes that are of the same kind with Russell's paradox. Russell, focussed more on the underlying structure of the paradoxes and saw them all as paradoxes of impredicativity. The "inclosure schema" was proposed by Priest, as a formal schema that can be used to classify paradoxes[247]. Although the schema will not be analyzed in this work, the conclusion is very interesting: Russell's paradox is of one kind with the "sorites" paradox (the paradox of the "heap"). This paradox was introducd by to Eubulides of Miletus (4^{th} century BC), a pupil of Euclid, and appears when one considers a heap of sand, from which grains are removed. Is it still a heap when only one grain remains? If not, when did it change from a heap to a non-heap? These two paradoxes are neighboring paradoxes, and it has been suggested that we should not just consider the internal structure of the paradoxes—although that is undoubtedly important—we also consider the external relationships—the relationships to other nearby paradoxes [281]. important. The way nearby neighbours (paradoxes of one kind) respond or fail to respond to proposed treatments tells us something about what makes the whole family tick and about their structural similarity[281].

The question "when is the cell dead?" indicates a confusion between cessation of organic coherence and cellular activity. When a cell irrevocably loses its organization, it's dead. The point when it becomes irrevocably damaged is related to the sorites problem. The sorites paradox appears in the conventional definition of amount of substance[248]. The amount of substance n is as a quantity proportional to

number of entities N. This implies that n is discrete for small N while n is considered to be continuous at the macroscopic scale, leading to a sorites paradox. A practical criterion has been proposed in [248] for distinguishing between amount of substance and number of entities, that is to resolve this case of the sorites paradox. In this study, the ideal gas equation $P \cdot V = n \cdot R \cdot T$ is derived as a combination of Boyle's law $P \propto 1/V$, of Charles law $V \propto T$, and Avogadro's law $N \propto V$. By substituting the molar gas constant by the Boltzman constant, a brief analysis of the resulting ideal gas equation $P \cdot V = N \cdot k_B \cdot T$ for the case $N = 1$ (the well known "particle in a box" situation) leads to quantization of energy, and therefore quantization of temperature. However, kinetic theory, assumes a large number of particles and this brings up the sorites paradox as the question of what is the scale at which we can consider temperature to be a continuous quantity of kinetic theory to be valid. An alternative metrological criterion for large N was poposed[248]:

- Consider a physical quantity that depends on the amount of substance: it will obviously also depend on the number of entities, and its numerical value can be expressed as f (x) where x is the numerical value of N .
- Consider a measurement of that quantity for $N = x$ and for $N = x + 1$. These measurements will be associated with measurement uncertainties.
- If the difference between the two measurement results is significant with respect to the uncertainties in those measurement results, the quantity is considered to be discrete at $N = x$; if not, the quantity is treated as continuous for that measurement procedure at that scale.

In other words, if there is a significant difference in measurement result by adding a single entity the measurement is a count of number of entities; if there is no significant difference in measurement result on adding a single entity, it is a measurement of amount of substance. Temperature is one of

the uncertainty sources in precision dimensional measurement and probability density functions of temperature change are usually derived by mathematical models.

The Ehrenfest model of diffusion was originally proposed as a model for dissipation of heat and to explain the 2nd law of thermodynamics. The model is defined by a system of N particles in two containers, with particles independently change container. The stochastic process $X = (X_1, X_2, X_3, \ldots)$ of the state of the system is defined by $X(n) = X_n$, the number of particles in one container at time $n \in N$, and the state space is $S = \{0,1,2,3,\ldots,m\}$ where m is the total number of particles. The system evolves according to the transition probability $P(x, x-1) = \frac{x}{m}$, and $P(x, x+1) = \frac{m-x}{m}$, $x \in S$. A generalized form of this model is $P(x, x-1) = \lambda \cdot x$ and $P(x, x+1) = \lambda \cdot (m-x)$, where λ is the transition rates. This last Markov process methods can be used in dynamic probabilistic systems to make sequential predictions, where the system can be in a finite number of states and the decision-making process involves a choice of several actions in each of those states. Solution techniques for Markov decision problems rely on exact knowledge of the transition rates, which may be difficult or impossible to obtain and therefore current studies focus on the quantification of the range of the uncertainty of the transition rates[249]. Despite of this, one can observe that the transition probabilities can be thought of as the measurable "physical quantity" that depends on the amount of substance, the number of entities. These measurements are indeed associated with measurement uncertainties , the source of which is the transition rates. The metrological criterion that was introduced aboved can be applied here, indicating the presence of the sorites problem for discreteness vs continuity in the definition of the probability. Moreover, it is known that continuous time Markov processes, are used for the formulation of stochastic predator prey models that are based on withing individual variation [250], [251], [252]. Within individual

variation refers to the fact that no considerations are taken of characteristics of an individual that affect its chance of dying. Death is treated as an intrinsically withing individual phenomenon [250]. For example, chance effects may lead to death of some individuals and these outcomes are likely regardless of the characteristics of the individuals involved. The variation is unique to the individual, but is unpredictable, given any particular characteristics.

Within individual variation, used under the name of “demographic stochasticity”, has been used in the theory of adaptive dynamics. The theory of adaptive dynamics aim at describing the dynamics of the dominant trait in a population, that is called the ’fittest’ trait. The main approach is through stochastic, or individual centered models which in the limit of large population, can be transformed into integro-differential equations or partial differential equations[253] [254, 255]. Stochastic simulations, using a finite size population, involve extinction phenomenon operating through demographic stochasticity (which is another name for the “within individual variation”) which acts drastically on small populations[253]. These simulations involve a unit for minimal survival population size, which corresponds to a single individual. In general though, typical stochastic and deterministic simulations do not fit and give rather different behaviors in terms of branching patterns. It has been observed that the notion of demographic stochasticity does not occur in general in deterministic population models, and an alternative proposed has been proposed in order to include a similar notion in these models: the notion of a survival threshold[256], which allows some phenotypical traits of the population to vanish when represented by too few individuals. In particular, through the investigations of simple and standard Lotka Volterra systems that describe the time of the distribution of phenotypic traits in time, it is shown that the inadequacy of determinsitc models to handle extinction phenomena through demographic stochasticity, can be corrected by the introduction of a survival threshold, leading to a mimicking effect of the extinction probability due to demographic stochastcity in small sub-populations, while hardly influences the

dynamics of large sub-populations [253]. In this framework, the above principle implies (at the extreme) that densities corresponding to less that one individual are undesirable[253], indicating that the link between the continuous (large populations) and the discrete (small sub populations), between the existence (survival) and the vanishing (extinction – demographic stochasticity), between the deterministic approach (differential equations) and the stochastic approach is correlated with the existence of a survival threshold in the model, originating from the discreteness part of this duality model.

Furthermore, this hybrid approach of survival, as continuous-discrete function with a survival threshold assigned to a population, raises the following question: Is there an internal quantization scheme that relates the continuous models for large populations with survival thresholds to small populations discrete models? As mentioned above, the one is in agreement with the other in the appropriate limits, but the presence of the limit involves the external operation of rescaling, which is related according to our previous discussion to the sorites paradox. In particular, the existence of both features, of continuity and quantization in a single process , appears in the study of the conditional survival probabilities of a firm (the computation of the conditional survival probability of the firm from an investor's point of view, i.e., given the "investor information"). Callegaro and Sagna used a quantization procedure, to analyze and compare the spread curves under complete and partial information in new and more general settings in their work on applications to credit risk of optimal quantization methods for nonlinear filtering. The theory of quantization probability they used was based on an earlier study of local quantization behavior of absolutely continuous probabilities [257]. This study analyzes the L^r quantization error estimates for $L^r(P)$ codebooks for absolutely continuous probabilities P and and Voronoi partitions satisfying specific conditions. But the origins of the theory developed there can be traced back to electrical engineering and image processing and in particular in

digitizing analog signals and compressing digital images[258]. Therefore, in the heart of the study of survival probabilities we find a theory for the quantization as analog-to-digital conversion and as data compression. Analog signal is a continuous signal which transmits information as a response to changes in physical phenomenon and uses continuous range of values to represent information, where digital signals are discrete time signals generated by digital modulation and Use discrete or discontinuous values to represent information. The quality of a quantizer can be measured by the goodness of the resulting reproduction of a signal in comparison to the original. This is accomplished with the definition of a distortion measure that quantifies cost or distortion resulting from reproducing the signal, and the consideration of the average distortion as a measure of the quality of a system, with smaller average distortion meaning higher quality[258]. The design and analysis of practical quantization techniques can be tracked in three paths[258]

- Fixed-rate scalar quantization, which adds linear processing to scalar quantization in order to exploit source redundancy, and variable-rate quantization (it uses Shannon's lossless source coding techniques[259] to reduce rate). Lossless codes were originally called noiseless.
- Vector quantization, including the seminal work of Shannon and Zador, in which vector quantization appears more to be a paradigm for analyzing the fundamental limits of quantizer performance than a practical coding technique.

This is precisely the framework we have adopted earlier in this work to study and analyze the process of cell survival during treatment (in our framework). This suggests an organic connection among an axiomatic system foundation, a predator prey rate equation and information theoretic signal processing.

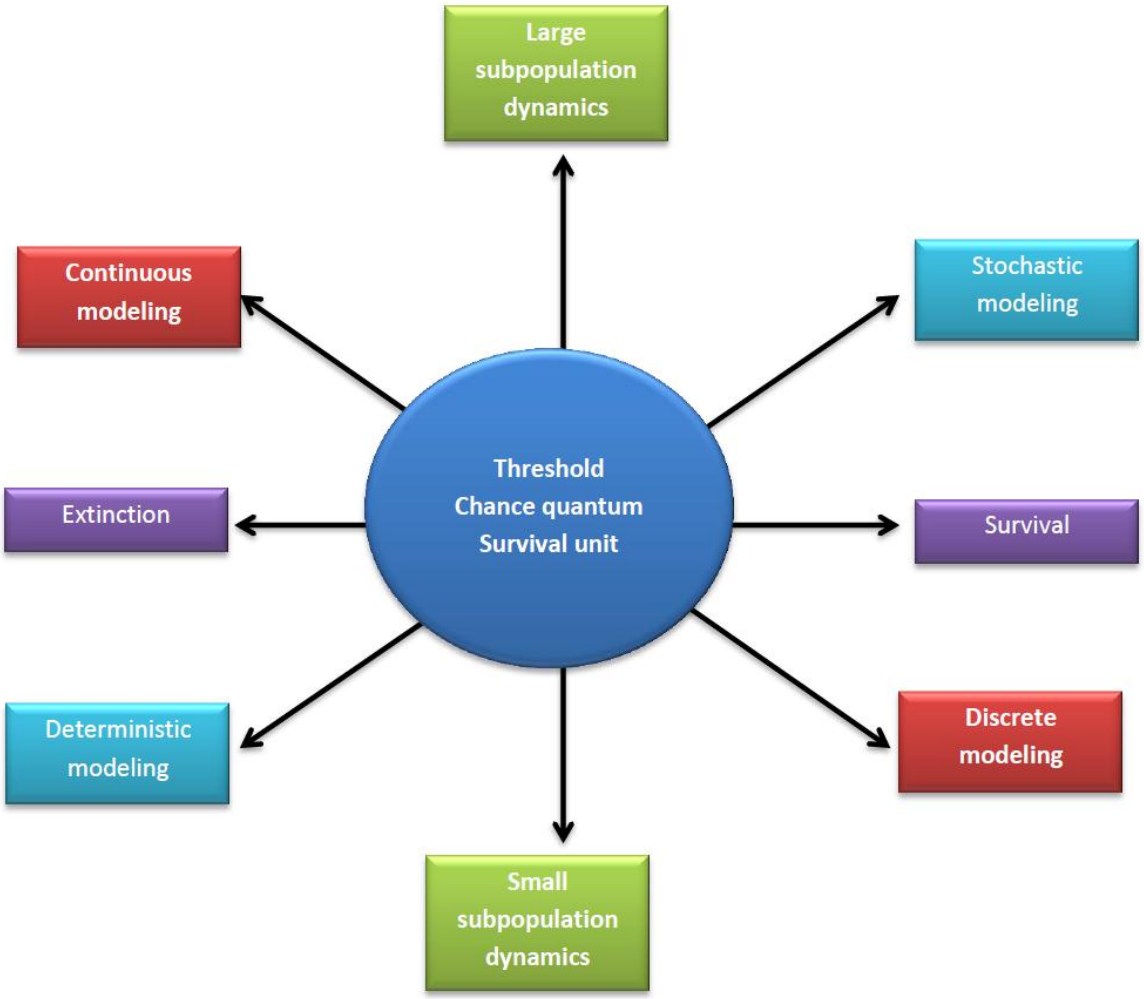

Figure 5.2.2. The existence of threshold as the link between different aspects of the modeling process.

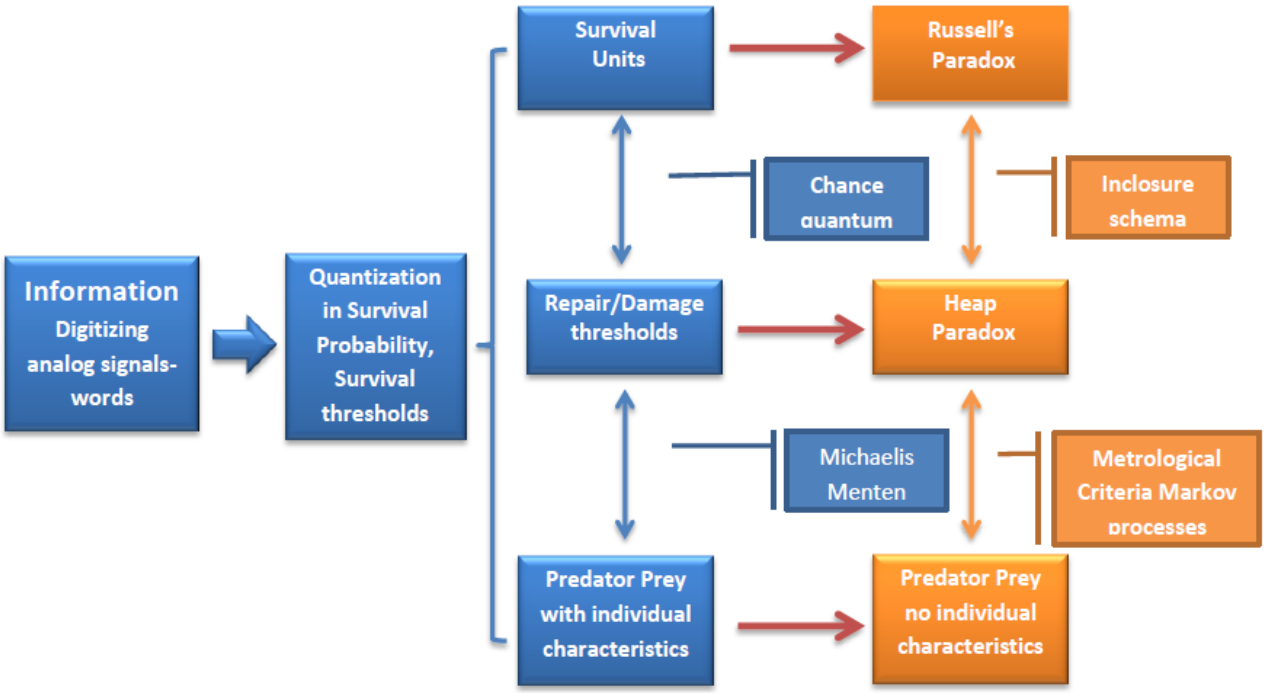

Figure 5.2.3. Logical design of the steps that may lead to an organic connection of different components of modeling (information, axioms, rate equations) as the new approach to current issues in the foundations of mathematics.

Quantized proptoplasm. Each water molecule represented by the formula, H_2O, contains two hydrogen atoms and one oxygen atom, arranged in such a manner that one end of the water molecule is positively charged while the other end if negatively charged. In other words, each water molecule may be seen as a dipolar molecule[260]. In the framework of the new theory of Association Induction (AI) by G.Ling, induction (the mutual electrical polarization that results in induced dipole moments, either through interaction with a neighboring water molecule) is not present only between pairs of water molecules but among all the interacting protein-water-small molecules/ion assembly that makes up the living cell. This is what makes the different components of the cell, *functionally coherent and discrete cooperative assemblies*. Cardinal adsorbents are defined as the biologically potent molecules that demonstrate an on or off action and shift an assembly from one resting-living-cooperative state to an

active-living-cooperative state. Electrical polarization, or induction, thus brings about the association of all or virtually all water molecules in the cells[260]. if alternating positively charged P sites and negatively charged N sites are arranged in two dimensions at suitable distance apart like a checkerboard (an NP system), or if two such NP surfaces are face-to-face in close juxtaposition (an NP-NP system) or if alternating N and P sites are carried on linear chains among a matrix of similar chains (an NP-NPNP system), the interaction with and among the water molecules will be intensified. The interplay of induction and association can produce a stable and yet highly flexible, three-dimensional dynamic structure of polarized multilayers of water molecules[261]. The theory of polarized multilayers as well as the association induction theory, is a continuation of the studies of Thomas Huxley (1 825-1 895) that suggested that the living cell is the basic unit of all life, and that the substance of living cells called the "protoplasm", is "the physical basis of life". In these two complementary theories, being alive means that the components of the cell substance, proteins, water and small molecules and ions are associated in a specific spatial relationship and in the high (negative) energy-low entropy state, called the living state (a cooperative state that allows for neighbor-to-neighbor electronic interaction among the individual elements). This idea leads to a view of the living cell as an essentially an electronic machine, where the electronic perturbations are not carried out through long-range ohmic conduction of free electrons along electric wires but by a falling-domino-like propagated short-range interaction. In the dead state, water and ions are to a large extent liberated and exist as free water and free ions, with a large entropy gain. In death, the proteins enter an internally neutralized state[262]. The minimal structural unit of protoplasm that preserves the basic physical properties of the whole living cell, is constituted by protein molecules with bound ATP, water and potassium ions and the vital activity of the cell is reduced to transitions between two states[15]:

[15] http://vladimirmatveev.ru/mainprinciples.html

$$protein(ATP)_m(H_2O)_n(K^+)_q \leftrightarrow protein + mADP + mPi + nH_2O + qK^+ . \quad (5.2.1)$$

We need to mention here that the goald of AI hypothesis is to interpret all microscopic cell physiological manifestations in terms of properties and activities of microscopic molecules, atoms, ions, and electrons. In this direction, cell nuclei, cell mebranes and other subcellular structures are made up of different variaties of macroscopic protoplasm. Although there is great diversity in form and function among these components, all macroscopic protoplasms have one thing in common: They all comprise a vast number of of similar microscopic units called nanoprotoplasm (NP) which is claimed to be the smallest unit and ultimate physical basis of life[263]

$$nanoprotoplasm = (A_1B_mC_n...Z_1)(H_2O)_{a\times1000}(K^+)_{b\times10}(ATP)_c \quad (5.2.2)$$

Where a, b, c, l, m, n are all positive integers each of the symbols, $A, B, C, ..., Z$ represents a different component protein. NP unit may contain just a single protein molecule characteristic of that particular protoplasm like (red blood cell cytoplasmic protoplasm), and in more complex protoplasm, each NP unit may contain two or more protein molecules of different kinds and number[263]. As an example, in the case of a red blood cell, the nanorpotoplasm unit is composed of one hemoglobin molecule, contains some seven thousand water molecules, twenty K^+, a single molecule of ATP, all directly or indirectly attached to the single hemoglobin molecule: $(Hb)_1(H_2O)_{7000}(K^+)_{20}(ATP)_1$ A quick calculation shows that for a spherical nanoprotoplasm unit model, the diameter would be in the range of nano-meters(roughly 8.6 nm) [263]. The fundamental characteristics of the dynamic structure (of chemical entities) shared by all nano-protoplasm can be summarized as [263]:

- The universal possession of a long and a partially resonating polypeptide chain.

- The universal possession of two kinds of proximal functional groups: the β-, and γ-carboxyl groups and the backbone NHCO groups and their access to alternative partners, K+, Na+ or fixed cations (for the β-, and γ-carboxyl groups) and CONH groups belonging to the third amino-acid residues up and down the polypeptide chain or massive number of water molecules (for the backbone NHCO groups).
- The universal presence of principle, auxiliary and pseudocardinal sites and the right kind of cardinal adsorbent for each of them.

The distinction among different units is associated with the type and sequential order of amino-acid residues of their protein components, with location the unit occupies in the cell, with the way these components associate with one another in space and in energy [263]. It is considered that fixed β-, and γ-carboxyl groups as **the highways of information and energy transfer,** where Information in this context is any kind of event that affects the state of a dynamic system. Using terminology from computer science, a nanoprotoplasm assembly unit or better "nanoprotoplasm assembler" is a "utility" program that converts an assembly language (a low-level symbolic code, with low abstraction) into executable machine code (the biochemical type of nanoprotoplasm as given by the molecular formula above; what this code does, is to alternate the chemical composition between two states, resting and active living state (or dead), and to determine the mutual spatial and energetic relationships among its components and in relation to the rest of the macroscopic protoplasm [263]). We conjecture that the low level symbolic code corresponds to a survival unit. Moreover, a compiler is a computer program (or set of programs) that transforms a source code from one language to another. In the framework of a cell, this compiler represents the quantization of the cell survival to survival units, and the source code is cell survival of cell life. The physical basis for the survival unit is the nanoprotoplasm.

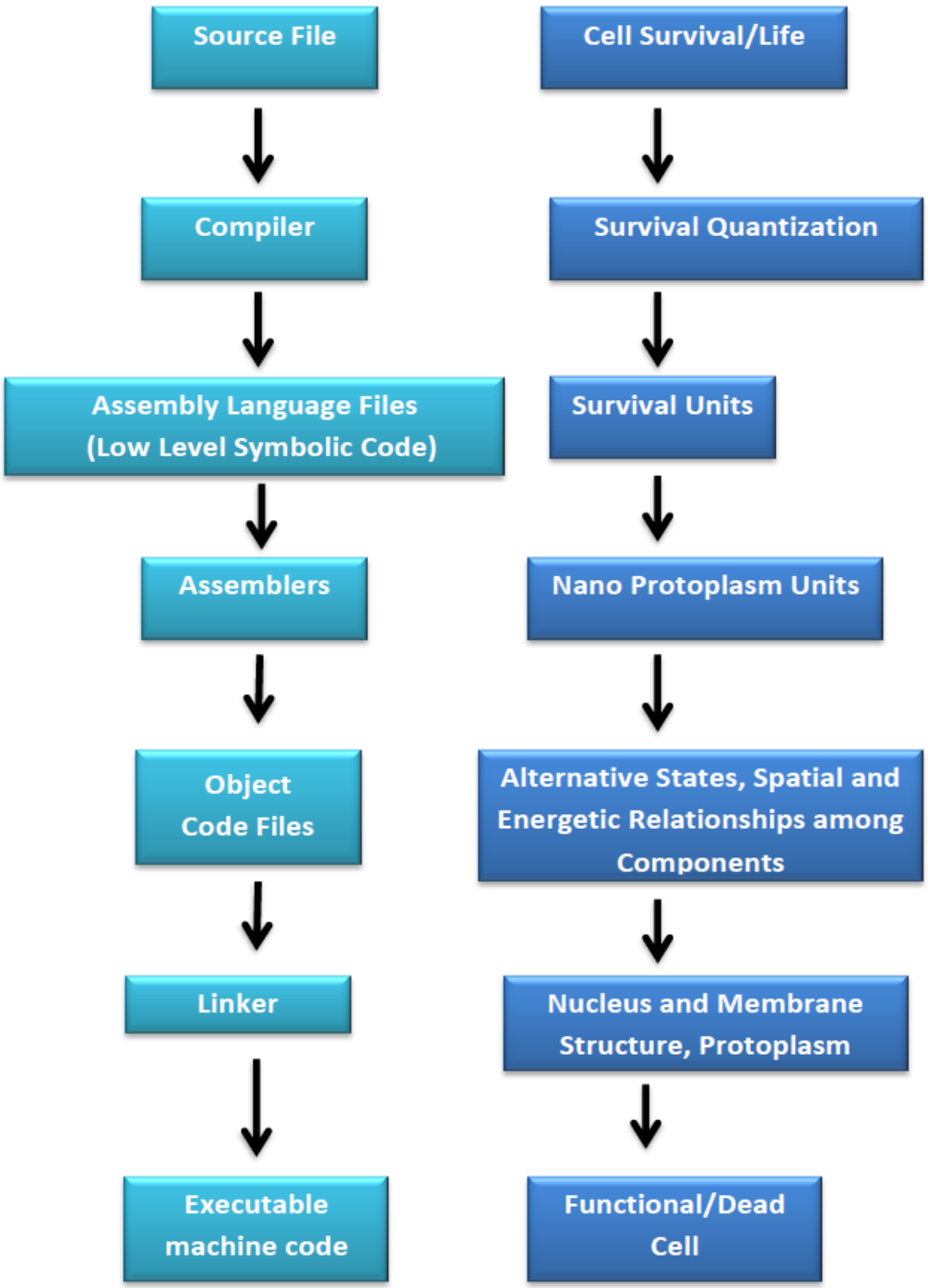

Figure 5.2.4. Cell as a programmable device. The compiler translates the higher level language into assembly language. The assembler translates assembly language into object code. The linker builds an executable program from object modules and any library modules required.

Life of a cell as prey and molecules as predators. We would like to introduce a new approach to study the photodynamic cell killing by investigating the continuous, functionally coupled biochemical and signaling differential equations of apoptosis, necrosis and autophagy. The predator-prey model is interesting in this context both in terms of modeling the different pathways of cell killing and in terms of time-domain study of treatment of the cells. The framework of a predator-prey interaction is employed using the concept of life unit cellular density as the prey and molecules inducing potential cell death as the predators. Hybridization by normalization of all concentrations underlies the predation. Each isolated pathway of cell death operates according to the underlying biochemical reaction or signaling mechanism. The resulting cell death is obtained by coupling of all death pathways through their molecular effectors such as ROS according to the underlying mechanism described earlier in the modeling section. Some molecules contribute to both cell proliferation and cell death. Cancer cells suppress cell apoptosis activities, but they do not disable the entire signaling cascade [264] which is evidence of the existence of molecules that contribute to both processes of cellular proliferation and cell death*. Bcl2 family members are some of these molecules that have a dual role in cell death.* In particular, the Bcl2 family members known as BH3-only molecules, lacking domains BH1 are known to have a pro-apoptotic character. Some members of this subfamily are Bad, Bid, Bim_{EL}, Bmf, and $Mcl\text{-}_{1S}$.Some of the anti-apoptotic members of the Bcl-2 family are Bax, Bok/Mtd, Bak, and $Bcl\text{-}_{XS}$ and they all contain at least one BH1 and BH2 domain . The pro-apoptotic Bcl2 members have been considered to play a role in the coupling of apoptosis and cell cycle arrest [264] .

Experimental verification of MM term*.* Holling was able to experimentally verify and derive the form of this nonlinear response, which is the famous “disk equation”, identical to the Michaelis Menten term of enzyme kinetics,

$$\frac{Vx}{K+x} \tag{5.2.1}$$

where in the predator prey context, V is the maximum predator attack rate, K is prey density where the attack rate is half-saturated. . To accommodate the difference in the time scale of predators (fast behavioral time scale) and the prey population (usually slower time scale), and to overcome the problem of incongruent time scaling, the nonlinear functional response should be expressed in terms of the ratio or prey to predator [265]. This expression ,when inserted in the prey equation ,solves the paradoxes of enrichment and biological control[266] [265].

5.3 The Survival Equation Model

This equation does not account for any predation by other molecular inducers. The effect of potentially competing predators on a single limited prey has been studied extensively [267] [268] [269]. For example, it has been shown that if the interference coefficient is small between two predators is small, then the winner competes its rival successfully and if the interference coefficient is large enough, then the competition outcome depends on the initial population of predator species [270]. As mentioned earlier, a suitable predator-prey theory should be based on the so-called ratio-dependent theory, in which the per capita prey growth rate should be function of the ratio of prey to predator abundance, and should have the form of an empirical Michaelis-Menten ratio-dependent predator-prey functional response system. With this in mind we write the equations:

$$\frac{dN}{dt} = r([^3O_2], p53, N) - \sum_{i=1}^{n} \frac{V_i \cdot [inducer_i] \cdot N}{K_i N + w_i [inducer]_i} \tag{5.3.1}$$

Which in a first simple approach can be written as:

$$\frac{dN}{dt} = r[p53]N - \frac{V_{cPARP}[cPARP]N}{K_{cPARP}N + w_{cPARP}[cPARP]} -$$

$$- \frac{V_{ROS}[ROS]N}{K_{ROS}N + w_{ROS}[ROS]} - \frac{V_{BECN1}[BECN1]N}{K_{BECN1}N + w_{BECN1}[BECN1]} \quad (5.3.2)$$

The double role of factors as the p53 molecule and hypoxia, points to internal system instability of the precise prediction of the deterministic cell death pathways as described by the biochemical and signaling differential equations. The p53 regulation in the modeling we scheme we use is described in the differential equations (down regulation of Bcl2, etc.). The observed quiescence and cell cycle arrest, as well as the maintenance of the cell cycle by molecules of p53 during the attack of the death inducing molecules (which might also be triggered by p53), we conjecture that it is a net effect of reproduction and loss of survival units which happens during the attack due to treatment, and is independent of the biochemical effects of the death inducers, but is rather a “fake death” (quiescence) mechanism of cancerous cells, that decrease their cell survival units as manifested by the arrest of the cell cycle, and at the same time preserve the wholeness of their viability and cell life, contained in its fullness in each remaining life unit. We project to test this model or variations of this model against PDT cell survival curves and with curve fitting to determine the constants of this model. This is work in progress.

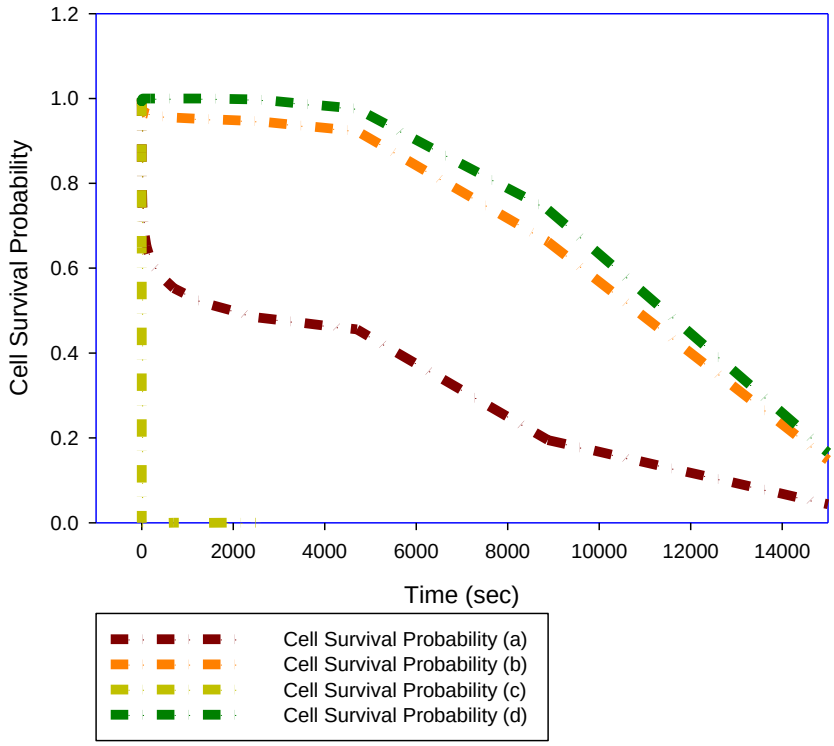

Fig.5.3.1. A sample of survival curves for the equation (4) of the cell model. Value of the parameters Survival curve (a) $V_1 = 10^{-2}$, $V_1 = 10^{4}$, $V_3 = 10^{-6}$, $R = 10^{-10}$, $K_1 = 10$, $K_2 = 10$, $K_3 = 10^{-7}$, $w_1 = 10^{-15}$, $w_2 = 1$, $w_3 = 2 \times 10^{4}$. Survival curve (b) $V_1 = 10^{-1}$, $V_1 = 10^{4}$, $V_3 = 10^{-6}$, $R = 10^{-10}$, $K_1 = 10$, $K_2 = 10$, $K_3 = 10^{-7}$, $w_1 = 10^{-15}$, $w_2 = 1$, $w_3 = 2 \times 10^{4}$. Survival curve (c) $V_1 = 10^{-3}$, $V_1 = 10^{4}$, $V_3 = 10^{-6}$, $R = 10^{-10}$, $K_1 = 10$, $K_2 = 10$, $K_3 = 10^{-7}$, $w_1 = 10^{-15}$, $w_2 = 1$, $w_3 = 2 \times 10^{4}$. Survival curve (d) $V_1 = 10, V_2 = 1, V_3 = 10^{-3}, R = 10^{-8}, K_1 = 10^{-2}, K_2 = 10^{-3}, K_3 = 10^{-4}$, $w_1 = 1$, $w_2 = 1$, $w_3 = 1$.

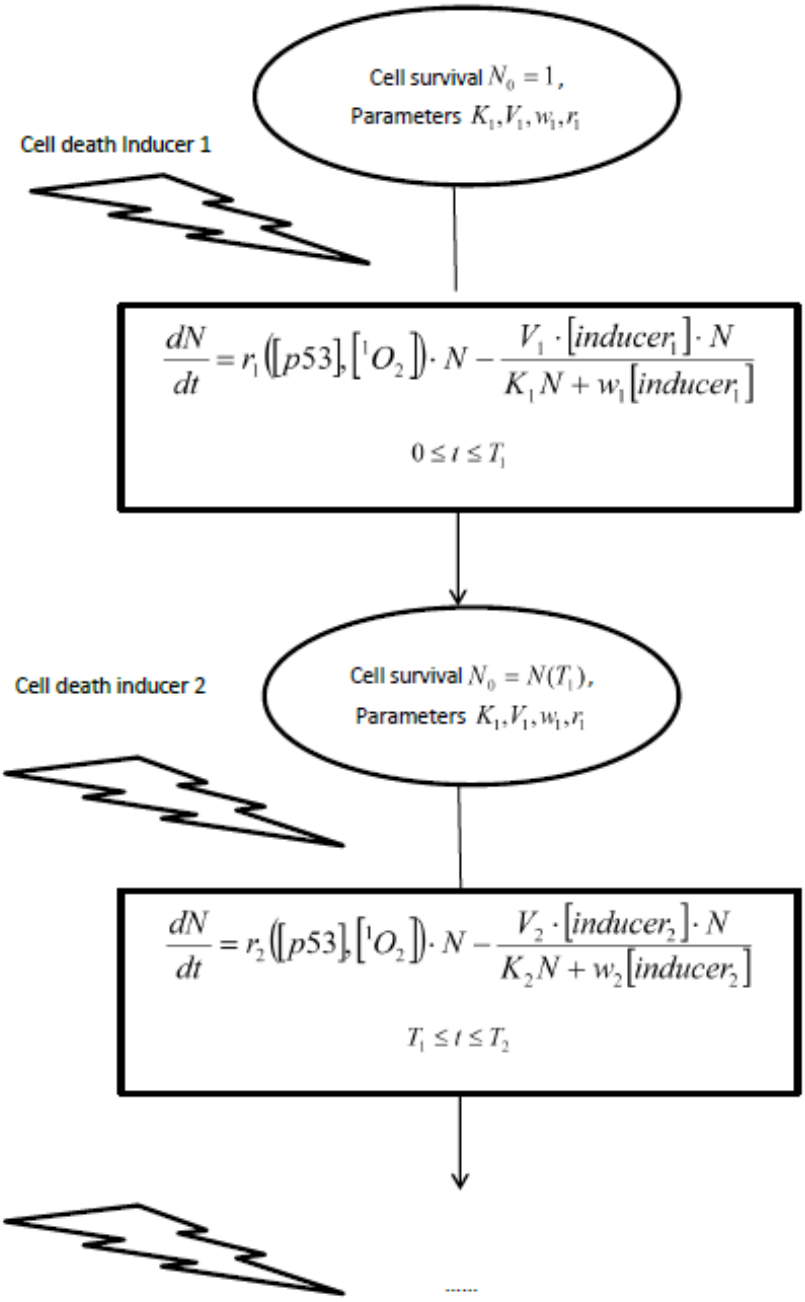

Fig.5.3.2 An logical design application of the Predator-Prey equations for different time domains where different cell death inducers are activated. In a cellular automaton, it will be possible to determine the route of damage. Necrotic and apoptotic cell death proceed in different time scales. Necrosis is a form

of cell death that occurs rapidly (minutes) in response to severe insult. Apoptosis is a slower form of death lasting for many hours or days.

5.4 Conclusion

We have developed a phenomenological modeling framework for cell decision making. The purpose is to provide a systematic method for discovering and expressing correlations in experimental data o cell survival curves and detailed biochemical pathways. The modeling framework is based on network modeling dynamics for cellular biochemical reactions, coupled to "signal transmission rules" which describe certain features of the mechanism of cell decision making. As an example of the application of our methodology to a specific biological system, it is shown in detail how to derive a testable model of the molecular network and mechanism leading to cell death in a point like model for a PDT treated cancer cell. The framework presented here is designed to discover and express correlation in data, even when knowledge of underlying mechanisms is incomplete[195]. Our approach is feasible and has predictive value. As it can be shown with the use of the Blahut Arimoto algorithm, there is large variability in the decision mechanism and it depends on the distortion function. Despite of this there is some agreement of the derived graphs with existing data on survival curves, from hydrogen peroxide treatment of cells (work in preparation). Due to the normalization of the concentrations in the phase space of stimuli, an expected variation for different initial conditions of the photosensitizer and different molecular oxygen concentrations is not evident. This is a coding disadvantage of linking the biochemical reaction equations to the cell decision mechanism. In other words, how the process of modeling the bio molecular reaction is integrated into the entire cell decision process is essential for a fully quantifiable prediction and numerical simulation of this complex physical system. Despite of this, our model ,

- develops an understanding of the physical system of a cell and the process of decision making when the cell is treated with photo-chemo therapy (conceptual model).
- translates biophysics describing our understanding into a mathematical system (mathematical model)
- develops a solution of the mathematical model using numerical, analytic and graphical techniques (numerical model).

In [87], a method is provided for the accurate determination of the distortion function. If the conditional probability $p_{Y|X}(y,x)$ minimizes the mutual information $I(X,Y)$, then it satisfies the equations mentioned above, and this fact can be used to compute the distortion function around which a given pathway $p_{Y|X}(y,x)$ is optimized. More precisely, after algebraic rearrangements of the equations of the decision algorithm the equation gives the distortion measure in this reference, is:

$$d(x, y = survival) = -\frac{1}{s} \cdot \log\left[\frac{p_{Y|X}(y = death|x)\, p_Y(y = survival)}{p_{Y|X}(y = survival|x)\, p_Y(y = death)} \right] + d(x, y = death) \qquad (5.4.1)$$

Where $d(x, y = death) = g(x)$ is a function such that

$$\min\{d(x, y = death), d(x, y = survival)\} = 0 \qquad (5.4.2)$$

$p_{Y|X}(y,x)$ is calculated experimentally, and the actual distortion function is then computed with the use of these equations, where S becomes just a scaling factor. This method can be applied in our modeling scheme where $x \to (x_1, x_2, x_3)$. The required function is the $p_{Y|X}(y,x)$ that it remains to be determined by experiments on the PDT cell survival.

To summarize our study, we have extended a previous rate-equation model in time domain with oxygen diffusion in a spherical cell. Different oxygen diffusion mechanisms through cell membrane and inside the cell have been investigated within the context of PDT. We have found that the widely accepted cell model of oxygen diffusion using the Michaelis–Menten term can be significantly improved and investigated the range of parameters of the rate equations for modeling of photobleaching and cell killing.

We have also provided a mathematical model of the mechanism for making binary fate decisions about cell death or survival, during and after type II photodynamic therapy (PDT) treatment, and supplied the logical design for this decision mechanism as an application of rate distortion theory to the biochemical processing of information by the physical system of a cell. Based on system biology models of the molecular interactions involved in the PDT processes previously established, and regarding a cellular decision-making system as a noisy communication channel, we use rate distortion theory to design a time dependent three dimensional Blahut-Arimoto algorithm where the input is a stimulus vector composed of the time dependent concentrations of three PDT related cell death signaling molecules and a cell fate decision as output. The molecular concentrations are determined by a group of rate equations. The output is the cell decision with a probability of cell survival or death. The optimality of the cell decision strategy is assessed by the cell survival probability, which might be modified to account for heterogeneous cell resistance to therapy.

The model of the detailed molecular pathways and biochemical events induced by Type II PDT treatment leading to cell death that can occur through a multiplicity of different mechanisms such as apoptosis, autophagy, and necrosis, presented in this study, is based on corrected previous biological knowledge related with PDT, and a new cell survival probability equation is also proposed based on a

predator prey model as a measure of the PDT tumor cell killing, which can be difficult to quantify through experimental verification of the molecular concentrations of the cytotoxic agents.

With these models at hand, one can proceed to cellular automata designs. Building appropriate numerical algorithms for a functional automaton that can simulate the tumor environment starts with the determination of occupation status on the grid points of a given automaton (normal cell, cancer cell, empty space , or vessel) , cell status (proliferative or quiescent state), local (intracellular) molecular concnetrations , and prescribed local rules that update a given element on the basis of its own state and those of its neighbors at a previous time step. These rules will originate by generic features of tumor growth such as the ability of cancer to elude the control mechanisms which maintain stasis in normal tissues. The cancer cells can be endowed with the ability to survive hypoxia longer than normal cell. The cell decision making process, as well as the survival probabilities, are the first steps in this direction.

The hard work is yet to be done: researchers will need to formulate and verify models, estimate kinetic parameters, make non-obvious predictions and test them by quantitative experimental measurements[101]. It is a matter of time before effective, integrated models of regulatory networks in cancer cells is used as an informational supplement for the next wave of experiments and therapies

CHAPTER 6: SUMMARY

The primary goal of this thesis was the assessment of cell killing by photodynamic therapy and the application of logical and computational-theoretic techniques to better understand the foundational nature of cell decision making for cell fate determination (mainly cell death/survival) during treatment. Looking for the link between the cellular decisions due to photochemical treatment and the biochemical dynamics in signal transduction occuring on a time scale of minutes to hours, is a powerful way to gain insights. The establishment of principles that describe observed patterns in PDT cell killing, should lead to predictions that can be tested. Although experimental verification of these predictions can be difficult, if not impossible, our system demonstrates the generative principle of an experiment-based modeling method that reflects an understanding of the experimental results, formalizes essential processes and puts in adequate equations visible and hidden parameters[16]. A model based analysis of the photochemical interactions involved in PDT and the corresponding distributions was carried out, for illumination times and drug concentrations found in current literature. This is important since, therapy design can be integrated into a predictive treatment planning model for PDT cancer therapy.

We develop a reaction diffusion system by considering the oxygen diffusion in a spherical cell which consists of a surface membrane. This is an analytic model of diffusion in a biological system which is developed and examined through numerical simulations. Two mechanisms of PDT cytotoxicity are evaluated and a differential equation for comparison of the spheroid cell survival data to existing experiments is introduced. We obtain the cell survival ratio as a function of light fluence or initial photosensitizer concentration with different photon density or irradiance of incident light and other parameters of oxygen transport. The results show that this model of Type-II PDT yields a powerful tool

[16] Serguei Sokol 2007-09-06, BioPlot user's guide,
http://biopuce.insa toulouse.fr/ExperimentExplorer/doc/BioPlot/node2.html

to quantify various events underlying PDT at the molecular and cellular levels and to interpret experimental results of in vitro cell studies [117].

Based on existing system biology models, we have developed a detailed molecular PDT model that includes 70 types of molecules and their corresponding interactions, pathways and biochemical events induced by PDT treatment. Molecular interactions, rate equations, reaction constants and initial concentrations have been identified in the literature and used in the composition of the (up to our knowledge) first explicit PDT system. The biochemical equations are represented by the general mass-action paradigms and the protein regulatory network paradigms. Then, the decision making process is analyzed using the framework of rate distortion theory. The benefit of this approach is that it provides a perspective on decision making regarding these several cell tasks as a single process. The cell is considered as an information quantizer that processes information through biochemical signaling and generates a cell fate. The average mutual information as the mean amount of information that knowledge of the value assumed by the input supplies about the value assumed by the output, is used to assess the reliability molecular signaling and cell fate determination. The mathematical analysis uses the methods of the Lagrange and an augmented functional of mutual information is minimized. The computational solutions are determined with the development of a time dependent Blahut Arimoto algorithm and cell survival curves are obtained that match patterns observed in cell killing studies.

Several disciplines have contributed to the development of PDT [271]: chemistry in the development of new photosensitizing agents, biology in the elucidation of cellular processes involved in PDT, pharmacology and physiology in identifying the mechanisms of distribution of photosensitizers in an organism, and physics in the development of better light sources, construction of imaging devices, etc. to briefly mention just a few from a large set of applications. These are all important parameters for optimally effective PDT. The present study gives way to one more discipline for contribution: information. The field of information and

mathematics that studies the technical process of information is communication theory [259] and in particular the branch of rate distortion theory, is used as a theoretical foundation for lossy data compression.

The link between the cell survival probbaility and the rate distortion theory is the idea of *quantization of probability* that is reflected in the *predator prey* form of the cell survival equation. Starting from cell survival differential equation, we identify the similarities to the dynamic energy budget models that study the "*strategy*" that an organism might develop to optimize its overall fitness, measured, for example, by a net reproductive output. The probability of survival for an individual organism is determined by the principal hazard for most creatures which is *predation*, and the risk of predation is dependent on the size of the organism. This is the link between predator prey theory and the idea of the development of a strategy. Then, we observe that this idea which has been used in applications of linear circuits to adequately predict circuit performance as a function of components tolerances. This is the link between quantized probability and communication channels. Linking quantized probability to predator prey theory implies the link between the development of a strategy and the existence of a communication channel, which in turn, implies the use of rate distortion theory according to Shannon's program. A new set theoretic approach is also introduced through the definition of cell survival units or cell survival units indicating the use of "proper classes" according to the Zermelo–Fraenkel set theory and the axiom of choice, as the mathematics appropriate for the development of biological theory of cell survival.

Cancer cells grow and divide at an unregulated pace. There are several differences between normal cells and cancer cells[17]. With respect to structure, normal cells have DNA in their genes and chromosomes that functions normally and they divide in an orderly way to produce more cells only when the body needs them. Cancer cells develop an aberrant DNA or gene structure or acquire abnormal numbers of chromosomes and continue to be created without control or order. This leads to an excess cells form a mass of tissue called a tumor. With respect to energy, normal cells derive most of their energy from a process called the Krebs cycle and only a small amount from from the process of glycolysis, and the means to derive these energies is oxygen. The opposite is true for cancer cells. With respect to blood vessels, normal cells have a built in blood vessel system, something that cancer cells are lacking. With respect to functions, normal cells have enzymes and hormones that behave in a balanced manner, where instead, cancer cells have either overactive or underactive enzymes and hormones. With respect to tumors, benign tumors of normal cells are not cancerous. They do not invade nearby tissues or spread to other parts of the body. Can be removed and are not a threat to life. Malignant tumors of cancer cells are cancerous and can invade and damage nearby tissues and organs and can break away and enter the bloodstream to form new tumors in other parts of the body, a process called metastasis. With these observations in mind, the modeling techniques we introduced are or will be (in the frame of cellular automata) suitable for testing of several hypotheses such as:

- Reactive oxygen species (ROS) function as signaling molecules in many aspects of growth factor-mediated angiogenesis. Changes in oxygen concentrations regulate neo-vascularization through induction of vascular endothelial growth factors (VEGF).

[17] Healthy Cells vs. Cancer Cells, A.P. John Institute for Cancer Researchhttps://www.apjohncancerinstitute.org/frequently-asked-questions/healthy-cells-vc-cancer-cells

- Post operative PDT causes oxygen related stimulation of immune response that under certain conditions can provoke tumor remission.
- PDT produces its tumoricidal effect through the generation of singlet oxygen and other oxygen species, which are toxic to cells and might also lead to destruction of the tumor microvasculature.

This present modeling approach can be developed further through coupling with extisting models of tumor neovascularization and the oxygen regulated tumor-immune dynamics with angiogenesis taken into account, to study the effect of type II PDT oxygen diffusion in the tumor macroenvironment with a small remnant of tumor tissue left after surgical resection as the initial condition. This way, it can be used as a platform to examine the potential applications of PDT for post-operational treatment to eliminate or manage the tumor regression and reformation of tumor vasculature. Moreover, the problem can be enriched by other prameters such as the effect of heating tissue using during PDT treatment, which decreases the viscosity of fluid elements, increases metabolic rate, increases blood flow which assists in the reduction of swelling, stimulates the immune system. All these factors might play a significant role in the final outcome.

Hopefully, utilization of this optimization model will initiate a program that will enable a physician to evaluate photochemical tumor treatment and to better design a patient-specific therapy to achieve maximum destruction of the tumor and injury minimization of healthy tissue by controlling time, fluence and drag concnetrations in tissue.

APPENDIX A

THE SET OF VALUES OF THE COEFFICIENTS ADOPTED IN THE MODEL OF CHAPTER 3

Table 1

The following coefficients are used to solve the differential equations, their sources were given in Table 1 of Reference[7] unless noted otherwise.

v	**Light speed in tissue**	**2.17×10^{10}cm/s**
σ_{psa}	Cross section of light absorption of cells containing S_0	$5.0\times10^{-13}cm^2$
τ_1	Relaxation time of S_1 to S_0	10 ns
τ_3	Relaxation time of T to S_0	30 μs
τ_0	Relaxation time of $^1O_2$ to $^3O_2$	30 ns
η_{10}	Quantum yield of S_1 to S_0	0.20
η_{13}	Quantum yield of S_1 inter-system crossing to T	0.80
η_{30}	Quantum yield of T to S_0	0.30
α_s	Efficiency factor for energy transfer from T to $^3O_2$	1×10^{-17}
η_0	Quantum yield of $^1O_2$ transition to $^3O_2$	0.30
k_{pb}	Photo bleaching rate	$2.0\text{x}10^{-10}$ cm^3s^{-1}
k_{cx}	Cytotoxicity rate	$2.0\text{x}10^{-9}$ cm^3s^{-1}
$[C]_i$	Initial concentration of oxygen scavengers	$1.0\text{x}10^3$ cm^{-3}
K_m	Michaelis constant for oxygen uptake	1.5×10^{17} cm^{-3}
$[R]_i$	Initial concentration of unoxdized receptors	5.0×10^{17} cm^{-3}
β_0	Rate coefficient of cell killing by oxidized receptors	1.0×10^{-2}
V_c	Maximum rate of cell killing by single oxygen	$4.0\text{x}10^{-3}$ cm^3s^{-1}
K_c	Michaelis constant for singlet oxygen uptake in cell killing	2.0×10^9 cm^{-3}

THE SET OF ORDINARY DIFFERENTIAL EQUATIONS AND PARAMETERS ADOPTED IN THE MODEL OF CHAPTER 4

Table 2

State	Variable	Initial concentration cm^{-3}	Initial concentration (Molarity)	Initial concentration ($\frac{molecules}{cell}$)	Reference
$[L]$	x_1	3.1x10^{12} cm^{-3}	5.1x10^{-9}	$(alt_{1a} \times \rho) \times (alt_{1b} \times [S_0]$ $(3x10^3)$	[100]
$[R]$	x_2	$2.05 \times 10^{11} cm^{-3}$	3.4x10^{-10}	2x10^2	[100]
$[L{:}R]$	x_3	0	0	0	[100]
$[R^*]$	x_4	0	0	0	[100]
$[flip]$	x_5	1.02x10^{11} cm^{-3}	1.7x10^{-10}	10^2	[100]
$[flip{:}R^*]$	x_6	0	0	0	[100]
$[C8]$	x_7	2.05x10^{13}cm^{-3}	3.4x10^{-8}	2x10^4	[100]
$[C8{:}R^*]$	x_8	0	0	0	[100]
$[C8^*]$	x_9	0	0	0	[100]
$[Bar]$	x_{10}	1.02x10^{12} cm^{-3}	1.7x10^{-9}	10^3	[100]
$[C8^*{:}Bar]$	x_{11}	0	0	0	[100]
$[C3]$	x_{12}	1.02x10^{13} cm^{-3}	1.7x10^{-8}	10^4	[100]
$[C8^*{:}C3]$	x_{13}	0	0	0	[100]
$[C3^*]$	x_{14}	0	0	0	[100]
$[C6]$	x_{15}	1.02x10^{13} cm^{-3}	1.7x10^{-8}	10^4	[100]
$[C3^*{:}C6]$	x_{16}	0	0	0	[100]
$[C6^*]$	x_{17}	0	0	0	[100]
$[C6^*{:}C8]$	x_{18}	0	0	0	[100]
$[XIAP]$	x_{19}	1.02x10^{14} cm^{-3}	1.7x10^{-7}	10^5	[100]
$[XIAP{:}C3^*]$	x_{20}	0	0	0	[100]
$[PARP]$	x_{21}	1.02x10^{15} cm^{-3}	1.7x10^{-6}	10^6	[100]
$[C3^*{:}PARP]$	x_{22}	0	0	0	[100]
$[cPARP]$	x_{23}	0	0	0	[100]
$[Bid]$	x_{24}	5.0x10^{13} cm^{-3}	6.6x10^{-8}	4x10^4	[100]
$[C8^*{:}Bid]$	x_{25}	0	0	0	[100]
$[tBid]$	x_{26}	0	0	0	[100]
$[Bcl2_C]$	x_{27}	2.05x10^{13}cm^{-3}	3.4x10^{-8}	2x10^4	[100]
$[tBid{:}Bcl2_C]$	x_{28}	0	0	0	[100]
$[Bax]$	x_{29}	1.02x10^{14} cm^{-3}	1.7x10^{-7}	10^5	[100]
$[tBid{:}Bax]$	x_{30}	0	0	0	[100]
$[Bax^*]$	x_{31}	0	0	0	[100]

$[Bax_m^*]$	x_{32}	0	0	0	[100]
$[Bcl2]$	x_{33}	2.89x10^{14}cm^{-3}	4.8x10^{-7}	2x10^{4}	[100]
$[Bax_m^*: Bcl2]$	x_{34}	0	0	0	[100]
$[Bax_2]$	x_{35}	0	0	0	[100]
$[Bax_2: Bcl2]$	x_{36}	0	0	0	[100]
$[Bax_4]$	x_{37}	0	0	0	[100]
$[Bax_4: Bcl2]$	x_{38}	0	0	0	[100]
$[M]$	x_{39}	7.22x10^{15}cm^{-3}	1.2x10^{-5}	5x10^{5}	[100]
$[Bax_4: M]$	x_{40}	0	0	0	[100]
$[M^*]$	x_{41}	0	0	0	[100]
$[CyC_m]$	x_{42}	7.22x10^{15}cm^{-3}	1.2x10^{-5}	5x10^{5}	[100]
$[M^*: CyC_m]$	x_{43}	0	0	0	[100]
$[CyC_r]$	x_{44}	0	0	0	[100]
$[Smac_m]$	x_{45}	1.44x10^{15}cm^{-3}	2.4x10^{-6}	10^{5}	[100]
$[M^*: Smac_m]$	x_{46}	0	0	0	[100]
$[Smac_r]$	x_{47}	0	0	0	[100]
CyC	x_{48}	0	0	0	[100]
$[Apaf]$	x_{49}	1.02x10^{14} cm^{-3}	1.7x10^{-7}	10^{5}	[100]
$[Apaf: CyC]$	x_{50}	0	0	0	[100]
$[Apaf^*]$	x_{51}	0	0	0	[100]
$[C9]$	x_{52}	1.02x10^{14} cm^{-3}	1.7x10-7	10^{5}	[100]
$[Apop]$	x_{53}	0	0	0	[100]
$[Apop: C3]$	x_{54}	0	0	0	[100]
$[Smac]$	x_{55}	0	0	0	[100]
$[Apop: XIAP]$	x_{56}	0	0	0	[100]
$[Smac: XIAP]$	x_{57}	0	0	0	[100]
$[C3_{Ub}^*]$	x_{58}	0	0	0	[100]
$[S_0]$	x_{59}	2x10^{10}(cm^{-3}) OR 2x10^{14}cm^{-3}	3.3x10^{-11} 3.3x10^{-7}	2x10^{1} 2x10^{5}	[102]
$[S_1]$	x_{60}	0	0	0	[102]
$[T]$	x_{61}	0	0	0	[102]
$[^3O_2]$	x_{62}	6x10^{17} cm^{-3}	10^{-4}	6x10^{7}	[102]
$[^1O_2]$	x_{63}	0	0	0	[102]
[R]	x_{64}	5x10^{17}cm^{-3}	8.3x10^{-4}	4.5x10^{8}	[102]
$[DAPK]$	x_{65}	7.5x10^{12} 7.5x10^{12}	12.5x10^{-9} 12.5x10^{-8}	7.5x10^{3}	[272]
$[IRE1]$	x_{66}	6.022x10^{13}	10^{-7}	6x10^{4}	[273]
$[BECNP]$	x_{67}	9.0x10^{13}	1.5x10^{-7}	9x10^{4}	[7]
$[Ca_2^+]$	x_{68}	6.022x10^{12} or 6.022x10^{13}	10^{-8} to 10^{-7}	6x10^{4}	[8]
$[JNK]$	x_{69}	6.022x10^{13}	10^{-7}	6x10^{4}	
$[p53]$	x_{73}	2.4x10^{18}	4x10^{-3}	2.4x10^{9}	[152, 274]

Table 3

Number	Rate Equation	Reference
(1)	$\frac{dx_1}{dt} = -k_1x_1x_2 + k_{-1}x_3$	[100]
(2)	$\frac{dx_2}{dt} = -k_1x_1x_2 + k_{-1}x_3$	[100]
(3)	$\frac{dx_3}{dt} = k_1x_1x_2 - k_{-1}x_3 - \kappa_1x_3$	[100]
(4)	$\frac{dx_4}{dt} = \kappa_1x_3 - k_2x_4x_5 + k_{-2}x_6 - k_3x_4x_7 + k_{-3}x_8 + \kappa_3x_8$	[100]
(5)	$\frac{dx_5}{dt} = -k_2x_4x_5 + k_{-2}x_6$	[100]
(6)	$\frac{dx_6}{dt} = k_2x_4x_5 - k_{-2}x_6$	[100]
(7)	$\frac{dx_7}{dt} = -k_3x_4x_7 + k_{-3}x_8 - k_7x_7x_{17} + k_{-7}x_{18}$	[100]
(8)	$\frac{dx_8}{dt} = k_3x_4x_7 - k_{-3}x_8 - \kappa_{-3}x_8$	[100]
(9)	$\frac{dx_9}{dt} = \kappa_{-3}x_8 - k_4x_9x_{10} + k_{-4}x_{11} - k_5x_9x_{12} + k_{-5}x_{13} + \kappa_5x_{13} + \kappa_7x_{18} - k_{10}x_9x_{24} + +k_{-10}x_{25} + \kappa_{10}x_{25}$	[100]
(10)	$\frac{dx_{10}}{dt} = -k_4x_9x_{10} + k_{-4}x_{11}$	[100]
(11)	$\frac{dx_{11}}{dt} = k_4x_9x_{10} - k_{-4}x_{11}$	[100]
(12)	$\frac{dx_{12}}{dt} = -k_5x_9x_{12} + k_{-5}x_{13} - k_{25}x_{12}x_{53} + k_{-25}x_{54}$	[100]
(13)	$\frac{dx_{13}}{dt} = k_5x_9x_{12} - k_{-5}x_{13} - \kappa_5x_{13}$	[100]
(14)	$\frac{dx_{14}}{dt} = \kappa_5x_{13} + \kappa_{25}x_{54} - k_6x_{14}x_{15} + k_{-6}x_{16} + \kappa_6x_{16} - k_8x_{14}x_{19} + k_{-8}x_{20} - k_9x_{14}x_{21} + k_{-9}x_{22} + \kappa_9x_{22}$	[100]
(15)	$\frac{dx_{15}}{dt} = -k_6x_{14}x_{15} + k_{-6}x_{16}$	[100]
(16)	$\frac{dx_{16}}{dt} = k_6x_{14}x_{15} - k_{-6}x_{16} - \kappa_6x_{16}$	[100]
(17)	$\frac{dx_{17}}{dt} = \kappa_6x_{16} - k_7x_7x_{17} + k_{-7}x_{18} + \kappa_7x_{18}$	[100]
(18)	$\frac{dx_{18}}{dt} = \kappa_7x_7x_{17} - k_{-7}x_{18} - \kappa_7x_{18}$	[100]
(19)	$\frac{dx_{19}}{dt} = \kappa_6x_{16} - k_8x_{14}x_{19} + k_{-8}x_{20} + \kappa_8x_{20} - k_{27}x_{19}x_{53} + k_{-27}x_{56} - k_{28}x_{19}x_{55} + k_{-28}x_{57}$	[100]
(20)	$\frac{dx_{20}}{dt} = k_8x_{14}x_{19} - k_{-8}x_{20} - \kappa_8x_{20}$	[100]
(21)	$\frac{dx_{21}}{dt} = -k_9x_{14}x_{21} - k_{-9}x_{22}$	[100]
(22)	$\frac{dx_{22}}{dt} = k_9x_{14}x_{21} - k_{-9}x_{22} - \kappa_9x_{22}$	[100]
(23)	$\frac{dx_{23}}{dt} = \kappa_9x_{22}$	[100]

(24)	$$\frac{dx_{24}}{dt} = -k_{10}x_9x_{24} - k_{-10}x_{25}$$	[100]
(25)	$$\frac{dx_{25}}{dt} = k_{10}x_9x_{24} - k_{-10}x_{25} - \kappa_{10}x_{25}$$	[100]
(26)	$$\frac{dx_{26}}{dt} = \kappa_{10}x_{25} - k_{11}x_{26}x_{27} + k_{-11}x_{28} - k_{12}x_{26}x_{29} + k_{-12}x_{30} + \kappa_{12}x_{30}$$	[100]
(27)	$$\frac{dx_{27}}{dt} = -k_{11}x_{26}x_{27} + k_{-11}x_{28}$$	[100]
(28)	$$\frac{dx_{28}}{dt} = k_{11}x_{26}x_{27} + k_{-11}x_{28}$$	[100]
(29)	$$\frac{dx_{29}}{dt} = -k_{12}x_{26}x_{29} + k_{-12}x_{30} + c_1\frac{1 + x_{70}^4}{x_{70}^4 + thr^4}$$	[100] [152]
(30)	$$\frac{dx_{30}}{dt} = k_{12}x_{26}x_{29} - k_{-12}x_{30} - \kappa_{12}x_{30}$$	[100]
(31)	$$\frac{dx_{31}}{dt} = -k_{13}x_{31} + k_{-13}x_{32} + \kappa_{12}x_{30}$$	[100]
(32)	$$\frac{dx_{32}}{dt} = k_{13}x_{31} - k_{-13}x_{32} - \frac{1}{v}k_{14}x_{32}x_{33} + k_{-14}x_{34} - \frac{2}{v}k_{15}k_{32}^2 + 2k_{-15}x_{35}$$	[100]
(33)	$$\frac{dx_{33}}{dt} = -\frac{1}{v}k_{14}x_{32}x_{33} + k_{-14}x_{34} - \frac{1}{v}k_{16}x_{33}x_{35} + k_{-16}x_{36} - \frac{1}{v}k_{18}x_{33}x_{37} + k_{-18}x_{38} - dx_{33}x_{63} + c_2\frac{x_{70}^4}{x_{70}^4 + thr^4}$$	[100] [192] [152]
(34)	$$\frac{dx_{34}}{dt} = \frac{1}{v}k_{14}x_{32}x_{33} - k_{-14}x_{34}$$	[100]
(35)	$$\frac{dx_{35}}{dt} = \frac{1}{v}k_{15}k_{32}^2 - k_{-15}x_{35} - \frac{1}{v}k_{16}x_{33}x_{35} + k_{-16}x_{36} - \frac{2}{v}k_{17}k_{35}^2 + 2k_{-17}x_{37}$$	[100]
(36)	$$\frac{dx_{36}}{dt} = \frac{1}{v}k_{16}x_{33}x_{35} - k_{-16}x_{36}$$	[100]
(37)	$$\frac{dx_{37}}{dt} = \frac{1}{v}k_{17}k_{35}^2 - k_{-17}x_{37} - \frac{1}{v}k_{18}x_{33}x_{37} + k_{-18}x_{38} - \frac{1}{v}k_{19}x_{39}x_{37} + k_{-19}x_{40}$$	[100]
(38)	$$\frac{dx_{38}}{dt} = \frac{1}{v}k_{18}x_{33}x_{37} - k_{-18}x_{38}$$	[100]
(39)	$$\frac{dx_{39}}{dt} = -\frac{1}{v}k_{19}x_{39}x_{37} + k_{-19}x_{40}$$	[100]
(40)	$$\frac{dx_{40}}{dt} = \frac{1}{v}k_{19}x_{39}x_{37} - k_{-19}x_{40} - \kappa_{19}x_{40}$$	[100]
(41)	$$\frac{dx_{41}}{dt} = \kappa_{19}x_{40} - \frac{1}{v}k_{20}x_{41}x_{42} + k_{-20}x_{43} + \kappa_{20}x_{43} - \frac{1}{v}k_{21}x_{41}x_{45} + k_{-21}x_{46} + \kappa_{21}x_{46}$$	[100]
(42)	$$\frac{dx_{42}}{dt} = -\frac{1}{v}k_{20}x_{41}x_{42} + k_{-20}x_{43}$$	[100]
(43)	$$\frac{dx_{43}}{dt} = \frac{1}{v}k_{20}x_{41}x_{42} - k_{-20}x_{43} - \kappa_{20}x_{43}$$	[100]
(44)	$$\frac{dx_{44}}{dt} = \kappa_{20}x_{43} - k_{22}x_{44} - k_{-22}x_{48}$$	[100]
(45)	$$\frac{dx_{45}}{dt} = -\frac{1}{v}k_{21}x_{41}x_{45} + k_{-21}x_{46}$$	[100]

(46)	$\frac{dx_{46}}{dt} = \frac{1}{v} k_{21} x_{41} x_{45} - k_{-21} x_{46} - \kappa_{21} x_{46}$	[100]
(47)	$\frac{dx_{47}}{dt} = \kappa_{21} x_{46} - k_{26} x_{47} + k_{-26} x_{55}$	[100]
(48)	$\frac{dx_{48}}{dt} = k_{22} x_{44} - k_{-22} x_{48} - k_{23} x_{48} x_{49} + k_{-23} x_{50} + \kappa_{23} x_{50}$	[100]
(49)	$\frac{dx_{49}}{dt} = -k_{23} x_{48} x_{49} + k_{-23} x_{50}$	[100]
(50)	$\frac{dx_{50}}{dt} = k_{23} x_{48} x_{49} - k_{-23} x_{50} + \kappa_{-23} x_{50}$	[100]
(51)	$\frac{dx_{51}}{dt} = \kappa_{23} x_{50} - k_{24} x_{51} x_{52} + k_{-24} x_{53}$	[100]
(52)	$\frac{dx_{52}}{dt} = -k_{24} x_{51} x_{52} + k_{-24} x_{53}$	[100]
(53)	$\frac{dx_{53}}{dt} = k_{24} x_{51} x_{52} - k_{-24} x_{53} - k_{25} x_{12} x_{53} + k_{-25} x_{54} + \kappa_{25} x_{54} - k_{27} x_{19} x_{53} + k_{-27} x_{56}$	[100]
(54)	$\frac{dx_{54}}{dt} = k_{25} x_{12} x_{53} + k_{-25} x_{54} - \kappa_{25} x_{54}$	[100]
(55)	$\frac{dx_{55}}{dt} = k_{26} x_{47} - k_{-26} x_{55} - k_{28} x_{19} x_{55} + k_{-28} x_{57}$	[100]
(56)	$\frac{dx_{56}}{dt} = k_{27} x_{19} x_{53} - k_{-27} x_{56}$	[100]
(57)	$\frac{dx_{57}}{dt} = k_{28} x_{19} x_{55} - k_{-28} x_{57}$	[100]
(58)	$\frac{dx_{58}}{dt} = \kappa_8 x_{20}$	[100]
(59)	$\frac{dx_{59}}{dt} = a_1 x_{59} x_{63} - a_2 \frac{1}{1 + e^{b(t-a)}} x_{59} + a_3 x_{60} + a_4 x_{61} + a_5 x_{61} x_{62}$	[102]
(60)	$\frac{dx_{60}}{dt} = -a_6 x_{60} + a_2 \frac{1}{1 + e^{b(t-a)}} x_{59}$	[102]
(61)	$\frac{dx_{61}}{dt} = -a_4 x_{61} - a_5 x_{61} x_{62} + a_7 x_{60}$	[102]
(62)	$\frac{dx_{62}}{dt} = -a_5 x_{61} x_{62} + a_8 x_{63} + 10^{12} - \frac{V_m x_{62}}{K_m + x_{62}}$	[102]
(63)	$\frac{dx_{63}}{dt} = -a_1 x_{59} x_{63} - a_9 x_{63} x_{64} - 10^{-6} x_{63} - a_8 x_{63} + a_5 x_{61} x_{62}$	[102]
(64)	$\frac{dx_{64}}{dt} = -a_9 x_{64} x_{63} - a_9 x_{63} x_{64} + U$	[102]
(65)	$\frac{dx_{65}}{dt} = A_1 \left(\frac{1}{1 + e^{-A_2(A_3 + A_4 x_{63})}} - x_{65} \right)$	[275]
(66)	$\frac{dx_{66}}{dt} = A_5 \left(\frac{1}{1 + e^{-A_2(A_6 + A_7 x_{TBD})}} - x_{66} \right)$	[275]
(67)	$\frac{dx_{67}}{dt} = A_8 \left(\frac{A_9}{1 + e^{-A_2(A_{10} + A_{12} x_{65})}} - x_{67} \right)$	[275]
(68)	$\frac{dx_{68}}{dt} = A_{12} A_{13} (A_{14} - x_{68}) - A_{15} x_{68}$	[275]
(69)	$\frac{dx_{69}}{dt} = A_{16} \left(\frac{A_9}{1 + e^{-A_2(A_{17} + A_{18} x_{66} + A_{19} A_{20})}} - x_{69} \right)$	[275]

(70)	$\frac{dx_{70}}{dt} = q_1 - q_2 \frac{x_{62}x_{70}}{D + x_{62}}$	[274]

Table 4

Constant	Units (molecules/CC)	Reference	Constant	Units	Reference
k_1	4×10^{-7}	[100]	k_{15}	10^{-6}	[100]
k_2	10^{-6}	[100]	k_{16}	10^{-6}	[100]
k_3	10^{-6}	[100]	k_{17}	10^{-6}	[100]
k_4	10^{-6}	[100]	k_{18}	10^{-6}	[100]
k_5	10^{-5}	[100]	k_{19}	10^{-6}	[100]
k_6	10^{-6}	[100]	k_{20}	2×10^{-6}	[100]
k_7	10^{-8}	[100]	k_{21}	2×10^{-6}	[100]
k_8	2×10^{-6}	[100]	k_{22}	0.01	[100]
k_9	10^{-6}	[100]	k_{23}	5×10^{-7}	[100]
k_{10}	10^{-7}	[100]	k_{24}	5×10^{-8}	[100]
k_{11}	10^{-6}	[100]	k_{25}	5×10^{-9}	[100]
k_{12}	10^{-7}	[100]	k_{26}	0.01	[100]
k_{13}	0.01	[100]	k_{27}	2×10^{-6}	[100]
k_{14}	10^{-6}	[100]	k_{28}	7×10^{-6}	[100]

Constant	Units (molecules/CC)	Reference	Constant	Units	Reference
k_{-1}	10^{-3}	[100]	k_{-15}	10^{-3}	[100]
k_{-2}	10^{-3}	[100]	k_{-16}	10^{-3}	[100]
k_{-3}	10^{-3}	[100]	k_{-17}	10^{-3}	[100]
k_{-4}	10^{-3}	[100]	k_{-18}	10^{-3}	[100]
k_{-5}	10^{-3}	[100]	k_{-19}	10^{-3}	[100]
k_{-6}	10^{-3}	[100]	k_{-20}	10^{-3}	[100]
k_{-7}	10^{-3}	[100]	k_{-21}	10^{-3}	[100]
k_{-8}	10^{-3}	[100]	k_{-22}	10^{-2}	[100]
k_{-9}	10^{-2}	[100]	k_{-23}	10^{-3}	[100]
k_{-10}	10^{-3}	[100]	k_{-24}	10^{-3}	[100]
k_{-11}	10^{-3}	[100]	k_{-25}	10^{-3}	[100]
k_{-12}	10^{-3}	[100]	k_{-26}	10^{-3}	[100]
k_{-13}	10^{-2}	[100]	k_{-27}	10^{-3}	[100]
k_{-14}	10^{-3}	[100]	k_{-28}	10^{-3}	[100]

Constant	Units (molecules/CC)	Reference	Constant	Units	Reference
κ_1	10^{-5}	[100]	κ_{15}	0	[100]
κ_2	0	[100]	κ_{16}	0	[100]
κ_3	1	[100]	κ_{17}	0	[100]
κ_4	0	[100]	κ_{18}	0	[100]

κ_5	1	[100]	κ_{19}	1	[100]
κ_6	1	[100]	κ_{20}	10	[100]
κ_7	1	[100]	κ_{21}	10	[100]
κ_8	0.1	[100]	κ_{22}	0	[100]
κ_9	1	[100]	κ_{23}	1	[100]
κ_{10}	1	[100]	κ_{24}	0	[100]
κ_{11}	0	[100]	κ_{25}	1	[100]
κ_{12}	1	[100]	κ_{26}	0	[100]
κ_{13}	0	[100]	κ_{27}	0	[100]
κ_{14}	0	[100]	κ_{28}	0	[100]

Constant	Units (molecules/CC)	Reference	Constant	Units	Reference
k_1	4×10^{-7}	[100]	k_{15}	10^{-6}	[100]
k_2	10^{-6}	[100]	k_{16}	10^{-6}	[100]
k_3	10^{-6}	[100]	k_{17}	10^{-6}	[100]
k_4	10^{-6}	[100]	k_{18}	10^{-6}	[100]
k_5	10^{-5}	[100]	k_{19}	10^{-6}	[100]
k_6	10^{-6}	[100]	k_{20}	2×10^{-6}	[100]
k_7	10^{-8}	[100]	k_{21}	2×10^{-6}	[100]
k_8	2×10^{-6}	[100]	k_{22}	0.01	[100]
k_9	10^{-6}	[100]	k_{23}	5×10^{-7}	[100]
k_{10}	10^{-7}	[100]	k_{24}	5×10^{-8}	[100]
k_{11}	10^{-6}	[100]	k_{25}	5×10^{-9}	[100]
k_{12}	10^{-7}	[100]	k_{26}	0.01	[100]
k_{13}	0.01	[100]	k_{27}	2×10^{-6}	[100]
k_{14}	10^{-6}	[100]	k_{28}	7×10^{-6}	[100]

Constant	Value	Reference	Constant	Units	Reference
α	$2800\ sec$	treatment	a_4	$0.3 \times I_3$	[102]
β	10^{10}	Steepness	a_5	$10^{-17} \times I_3$	[102]
ρ	$10^6 cm^{-3}$	[102]	a_6	I_1	[102]
τ_0	$3 \times 10^{-8} sec$	[102]	a_7	$0.8 \times I_1$	[102]
τ_1	$10^{-8} sec$	[102]	a_8	$0.3 \times I_0$	[102]
τ_3	$3 \times 10^{-4} sec$	[102]	a_9	$2 \times 10^{-18} \frac{cm^3}{sec}$	[102]
V_M	3×10^{18}	[102]	v	0.07	[100]
K_M	1.5×10^{17}	[102]	q_1	16×10^{-3}	[274]
I_0	$1/\tau_0$	[102]	q_2	16×10^{-3}	[274]
I_1	$1/\tau_1$	[102]	D	3.3×10^{-5}	[274]
I_3	$1/\tau_3$	[102]	$alt1_a$	$6 \times 10^4/10^6$	
a_1	$2 \times 10^{-10} \frac{cm^3}{sec}$	[102]	$alt1_b$	(6×10^4) $/(5 \times 10^{13})$	
a_2	2.17×10^{10} $\times 5 \times 10^{-13}$ $\times \rho\ sec^{-1}$	[102]	$alt2_a$	$3 \times 10^3/10^6$	

a_3	$0.2 \times I_1 sec^{-1}$	[102]	$alt2_b$	(3×10^3) $/(5 \times 10^{13})$

References

[1] T. M. Busch, S. M. Hahn, S. M. Evans *et al.*, "Depletion of tumor oxygenation during photodynamic therapy: Detection by the hypoxia marker EF3 [2-(2-nitroimidazol-1[H]-yl)-N-(3,3,3-trifluoropropyl)acetamide]," *Cancer Res,* vol. 60, no. 10, pp. 2636-2642, May 15, 2000.

[2] B. J. Tromberg, A. Orenstein, S. Kimel *et al.*, "In vivo tumor oxygen tension measurements for the evaluation of the efficiency of photodynamic therapy," *Photochemistry and Photobiology,* vol. 52, no. 2, pp. 375-85, Aug, 1990.

[3] M. G. Nichols, and T. H. Foster, "Oxygen diffusion and reaction kinetics in the photodynamic therapy of multicell tumour spheroids," *Phys Med Biol,* vol. 39, no. 12, pp. 2161-81, Dec, 1994.

[4] I. Georgakoudi, and T. H. Foster, "Singlet oxygen- versus nonsinglet oxygen-mediated mechanisms of sensitizer photobleaching and their effects on photodynamic dosimetry," *Photochemistry and Photobiology,* vol. 67, no. 6, pp. 612-25, Jun, 1998.

[5] S. Gubarev, A. Makhanek, and Z. Shul'man, "Model of photodynamic therapy of skin tumors," *Journal of Engineering Physics and Thermophysics,* vol. 80, no. 1, pp. 81-88, 2007.

[6] J. P. Henning, R. L. Fournier, and J. A. Hampton, "A Transient Mathematical-Model of Oxygen Depletion during Photodynamic Therapy," *Radiat Res,* vol. 142, no. 2, pp. 221-226, May, 1995.

[7] X. H. Hu, Y. Feng, J. Q. Lu *et al.*, "Modeling of a type II photofrin-mediated photodynamic therapy process in a heterogeneous tissue phantom," *Photochem Photobiol,* vol. 81, no. 6, pp. 1460-8, Nov-Dec, 2005.

[8] I. Golding, "Decision Making in Living Cells: Lessons from a Simple System," *Annual Review of Biophysics, Vol 40,* vol. 40, pp. 63-80, 2011.

[9] M. Ptashne, A. D. Johnson, and C. O. Pabo, "A genetic switch in a bacterial virus," *Sci Am,* vol. 247, no. 5, pp. 128-30, 132, 134-40, Nov, 1982.

[10] A. Jemal, F. Bray, M. M. Center *et al.*, "Global cancer statistics," *CA Cancer J Clin,* vol. 61, no. 2, pp. 69-90, Mar-Apr, 2011.

[11] P. Anand, A. B. Kunnumakara, C. Sundaram *et al.*, "Cancer is a Preventable Disease that Requires Major Lifestyle Changes," *Pharmaceutical Research,* vol. 25, no. 9, pp. 2097-2116, Sep, 2008.

[12] P. Romestaing, Y. Lehingue, C. Carrie *et al.*, "Role of a 10-Gy boost in the conservative treatment of early breast cancer: results of a randomized clinical trial in Lyon, France," *Journal of clinical oncology,* vol. 15, no. 3, pp. 963, 1997.

[13] F. A. Critz, R. S. Tarlton, and D. A. Holladay, "Prostate specific antigenâ€monitored combination radiotherapy for patients with prostate cancer. Iâ€125 implant followed by externalâ€beam radiation," *Cancer,* vol. 75, no. 9, pp. 2383-2391, 1995.

[14] C. A. Regueiro, F. J. Valcarcel, J. Romero *et al.*, "Treatment of conjunctival lymphomas by beta-ray brachytherapy using a strontium-90-yttrium-90 applicator," *Clinical Oncology,* vol. 14, no. 6, pp. 459-463, 2002.

[15] K. J. Russell, R. J. Caplan, G. E. Laramore *et al.*, "Photon versus fast neutron external beam radiotherapy in the treatment of locally advanced prostate cancer: results of a randomized prospective trial," *International Journal of Radiation Oncology* Biology* Physics,* vol. 28, no. 1, pp. 47-54, 1994.

[16] H. J. Frischbier, and K. Thomsen, *Treatment of cancer of the vulva with high energy electrons*, Univ., Hamburg, 1971.

[17] J. D. Slater, C. J. Rossi, L. T. Yonemoto *et al.*, "Proton therapy for prostate cancer: the initial Loma Linda University experience* 1," *International Journal of Radiation Oncology* Biology* Physics,* vol. 59, no. 2, pp. 348-352, 2004.

[18] J. C. Kennedy, R. H. Pottier, and D. C. Pross, "Photodynamic therapy with endogenous protoporphyrin:: IX: Basic principles and present clinical experience," *Journal of Photochemistry and Photobiology B: Biology,* vol. 6, no. 1-2, pp. 143-148, 1990.

[19] A. A. Gage, "Cryosurgery in the treatment of cancer," *Surgery, gynecology & obstetrics,* vol. 174, no. 1, pp. 73, 1992.

[20] J. H. Schiller, D. Harrington, C. P. Belani *et al.*, "Comparison of four chemotherapy regimens for advanced nonâ€"small-cell lung cancer," *New England Journal of Medicine,* vol. 346, no. 2, pp. 92-98, 2002.

[21] J. Stromberg, A. Martinez, J. Gonzalez *et al.*, "Ultrasound-guided high dose rate conformal brachytherapy boost in prostate cancer: treatment description and preliminary results of a phase I/II clinical trial," *International journal of radiation oncology, biology, physics,* vol. 33, no. 1, pp. 161, 1995.

[22] U. HÃ¤feli, *Scientific and clinical applications of magnetic carriers*: Springer Us, 1997.

[23] M. Triesscheijn, P. Baas, J. H. M. Schellens *et al.*, "Photodynamic therapy in oncology," *Oncologist,* vol. 11, no. 9, pp. 1034-1044, 2006.

[24] G. Balazsi, A. van Oudenaarden, and J. J. Collins, "Cellular decision making and biological noise: from microbes to mammals," *Cell,* vol. 144, no. 6, pp. 910-25, Mar 18, 2011.

[25] M. D. Daniell, and J. S. Hill, "A history of photodynamic therapy," *Aust N Z J Surg,* vol. 61, no. 5, pp. 340-8, May, 1991.

[26] T. J. Dougherty, J. E. Kaufman, A. Goldfarb *et al.*, "Photoradiation therapy for the treatment of malignant tumors," *Cancer Res,* vol. 38, no. 8, pp. 2628-35, Aug, 1978.

[27] Y. Hayata, H. Kato, C. Konaka *et al.*, "Hematoporphyrin derivative and laser photoradiation in the treatment of lung cancer," *Chest,* vol. 81, no. 3, pp. 269-77, Mar, 1982.

[28] A. Dahlman, A. G. Wile, R. G. Burns *et al.*, "Laser photoradiation therapy of cancer," *Cancer Res,* vol. 43, no. 1, pp. 430-4, Jan, 1983.

[29] J. Moan, and Q. Peng, "An outline of the hundred-year history of PDT," *Anticancer Research,* vol. 23, no. 5A, pp. 3591-3600, Sep-Oct, 2003.

[30] R. L. Lipson, and E. J. Baldes, "The photodynamic properties of a particular hematoporphyrin derivative," *Arch Dermatol,* vol. 82, pp. 508-16, Oct, 1960.

[31] W. Jerjes, T. Upile, S. Akram *et al.*, "The surgical palliation of advanced head and neck cancer using photodynamic therapy," *Clin Oncol (R Coll Radiol),* vol. 22, no. 9, pp. 785-91, Nov, 2010.

[32] M. G. Bredell, E. Besic, C. Maake *et al.*, "The application and challenges of clinical PD-PDT in the head and neck region: a short review," *J Photochem Photobiol B,* vol. 101, no. 3, pp. 185-90, Dec 2, 2010.

[33] S. M. Hahn, and E. Glatstein, "The emergence of photodynamic therapy as a major modality in cancer treatment," *Reviews in Contemporary Pharmacotherapy,* vol. 10, no. 1, pp. 69-74, 1999.

[34] I. Wang, N. Bendsoe, C. A. Klinteberg *et al.*, "Photodynamic therapy vs. cryosurgery of basal cell carcinomas: results of a phase III clinical trial," *Br J Dermatol,* vol. 144, no. 4, pp. 832-40, Apr, 2001.

[35] H. C. Wolfsen, "Carpe luz--seize the light: endoprevention of esophageal adenocarcinoma when using photodynamic therapy with porfimer sodium," *Gastrointest Endosc,* vol. 62, no. 4, pp. 499-503, Oct, 2005.

[36] S. M. Hahn, D. L. Fraker, R. Mick *et al.*, "A phase II trial of intraperitoneal photodynamic therapy for patients with peritoneal carcinomatosis and sarcomatosis," *Clin Cancer Res,* vol. 12, no. 8, pp. 2517-25, Apr 15, 2006.

[37] J. J. Wilson, H. Jones, M. Burock *et al.*, "Patterns of recurrence in patients treated with photodynamic therapy for intraperitoneal carcinomatosis and sarcomatosis," *Int J Oncol,* vol. 24, no. 3, pp. 711-7, Mar, 2004.

[38] T. R. Nathan, D. E. Whitelaw, S. C. Chang *et al.*, "Photodynamic therapy for prostate cancer recurrence after radiotherapy: A phase I study," *Journal of Urology,* vol. 168, no. 4, pp. 1427-1432, Oct, 2002.

[39] G. R. Prout, Jr., C. W. Lin, R. Benson, Jr. *et al.*, "Photodynamic therapy with hematoporphyrin derivative in the treatment of superficial transitional-cell carcinoma of the bladder," *N Engl J Med,* vol. 317, no. 20, pp. 1251-5, Nov 12, 1987.

[40] A. P. Berger, H. Steiner, A. Stenzl *et al.*, "Photodynamic therapy with intravesical instillation of 5-aminolevulinic acid for patients with recurrent superficial bladder cancer: a single-center study," *Urology,* vol. 61, no. 2, pp. 338-41, Feb, 2003.

[41] T. L. Moskal, T. J. Dougherty, J. D. Urschel *et al.*, "Operation and photodynamic therapy for pleural mesothelioma: 6-year follow-up," *Ann Thorac Surg,* vol. 66, no. 4, pp. 1128-33, Oct, 1998.

[42] K. Furuse, M. Fukuoka, H. Kato *et al.*, "A prospective phase II study on photodynamic therapy with photofrin II for centrally located early-stage lung cancer. The Japan Lung Cancer Photodynamic Therapy Study Group," *J Clin Oncol,* vol. 11, no. 10, pp. 1852-7, Oct, 1993.

[43] P. Agostinis, K. Berg, K. A. Cengel *et al.*, "Photodynamic therapy of cancer: an update," *CA Cancer J Clin,* vol. 61, no. 4, pp. 250-81, Jul-Aug, 2011.

[44] J. R. Starkey, A. K. Rebane, M. A. Drobizhev *et al.*, "New Two-Photon Activated Photodynamic Therapy Sensitizers Induce Xenograft Tumor Regressions after Near-IR Laser Treatment through the Body of the Host Mouse," *Clinical Cancer Research,* vol. 14, no. 20, pp. 6564-6573, Oct 15, 2008.

[45] M. S. Mathews, E. Angell-Petersen, R. Sanchez *et al.*, "The Effects of Ultra Low Fluence Rate Single and Repetitive Photodynamic Therapy on Glioma Spheroids," *Lasers in Surgery and Medicine,* vol. 41, no. 8, pp. 578-584, Oct, 2009.

[46] S. Kim, T. Y. Ohulchanskyy, H. E. Pudavar *et al.*, "Organically modified silica nanoparticles co-encapsulating photosensitizing drug and aggregation-enhanced two-photon absorbing fluorescent dye aggregates for two-photon photodynamic therapy," *Journal of the American Chemical Society,* vol. 129, no. 9, pp. 2669-2675, Mar 7, 2007.

[47] J. Moan, H. B. Steen, K. Feren *et al.*, "Uptake of hematoporphyrin derivative and sensitized photoinactivation of C3H cells with different oncogenic potential," *Cancer Lett,* vol. 14, no. 3, pp. 291-6, Dec, 1981.

[48] J. Moan, and Q. Peng, "An outline of the hundred-year history of PDT," *Anticancer Res,* vol. 23, no. 5A, pp. 3591-600, Sep-Oct, 2003.

[49] J. Moan, "Porphyrin photosensitization and phototherapy," *Photochem Photobiol,* vol. 43, no. 6, pp. 681-90, Jun, 1986.

[50] J. Moan, and K. Berg, "Photochemotherapy of cancer: experimental research," *Photochem Photobiol,* vol. 55, no. 6, pp. 931-48, Jun, 1992.

[51] J. Moan, K. Berg, H. Anholt *et al.*, "Sulfonated aluminium phthalocyanines as sensitizers for photochemotherapy. Effects of small light doses on localization, dye fluorescence and photosensitivity in V79 cells," *Int J Cancer,* vol. 58, no. 6, pp. 865-70, Sep 15, 1994.

[52] J. Moan, and K. Berg, "The photodegradation of porphyrins in cells can be used to estimate the lifetime of singlet oxygen," *Photochem Photobiol,* vol. 53, no. 4, pp. 549-53, Apr, 1991.

[53] K. Berg, J. Moan, J. C. Bommer *et al.*, "Cellular inhibition of microtubule assembly by photoactivated sulphonated meso-tetraphenylporphines," *Int J Radiat Biol,* vol. 58, no. 3, pp. 475-87, Sep, 1990.

[54] R. C. Yu, and S. M. Rappaport, "A lung retention model based on Michaelis-Menten-like kinetics," *Environmental Health Perspectives,* vol. 105, no. 5, pp. 496-503, May, 1997.
[55] H. X. Zhou, G. N. Rivas, and A. P. Minton, "Macromolecular crowding and confinement: Biochemical, biophysical, and potential physiological consequences," *Annual Review of Biophysics,* vol. 37, pp. 375-397, 2008.
[56] W. W. Chen, M. Niepel, and P. K. Sorger, "Classic and contemporary approaches to modeling biochemical reactions," *Genes & Development,* vol. 24, no. 17, pp. 1861-1875, Sep 10, 2010.
[57] J. L. Casti, and S. Wolfram, "A new kind of science," *Nature,* vol. 417, no. 6887, pp. 381-382, May 23, 2002.
[58] S. Wolfram, "Cellular Automata as Models of Complexity," *Nature,* vol. 311, no. 5985, pp. 419-424, 1984.
[59] M. Burgin, and A. Klinger, "Three aspects of super-recursive algorithms and hypercomputation or finding black swans," *Theoretical Computer Science,* vol. 317, no. 1-3, pp. 1-11, Jun 4, 2004.
[60] M. S. Burgin, and Y. M. Borodyanskii, "Infinite Processes and Super-Recursive Algorithms," *Doklady Akademii Nauk Sssr,* vol. 321, no. 5, pp. 876-879, 1991.
[61] Y. Benenson, B. Gil, U. Ben-Dor *et al.*, "An autonomous molecular computer for logical control of gene expression," *Nature,* vol. 429, no. 6990, pp. 423-429, May 27, 2004.
[62] E. Shapiro, "A mechanical Turing machine: blueprint for a biomolecular computer," *Interface Focus,* vol. 2, no. 4, pp. 497-503, Aug 6, 2012.
[63] L. M. Adleman, "Molecular Computation of Solutions to Combinatorial Problems," *Science,* vol. 266, no. 5187, pp. 1021-1024, Nov 11, 1994.
[64] J. Von Neumann, and A. W. Burks, *Theory of self-reproducing automata*, Urbana,: University of Illinois Press, 1966.
[65] M. Denton, *Evolution : a theory in crisis*, 1st U.S. ed., Bethesda, Md.: Adler & Adler, 1986.
[66] J. D. Watson, and F. H. C. Crick, "Molecular Structure of Nucleic Acids - a Structure for Deoxyribose Nucleic Acid," *Nature,* vol. 171, no. 4356, pp. 737-738, 1953.
[67] M. Mccarty, and O. T. Avery, "Studies on the Chemical Nature of the Substance Inducing Transformation of Pneumococcal Types .2. Effect of Desoxyribonuclease on the Biological Activity of the Transforming Substance," *Journal of Experimental Medicine,* vol. 83, no. 2, pp. 89-96, 1946.
[68] S. Brenner, "Life's code script," *Nature,* vol. 482, no. 7386, pp. 461-461, Feb 23, 2012.
[69] D. E. Dolmans, D. Fukumura, and R. K. Jain, "Photodynamic therapy for cancer," *Nat Rev Cancer,* vol. 3, no. 5, pp. 380-7, May, 2003.
[70] T. J. Dougherty, C. J. Gomer, B. W. Henderson *et al.*, "Photodynamic therapy," *J Natl Cancer Inst,* vol. 90, no. 12, pp. 889-905, Jun 17, 1998.
[71] M. Korbelik, and G. J. Dougherty, "Photodynamic therapy-mediated immune response against subcutaneous mouse tumors," *Cancer Res,* vol. 59, no. 8, pp. 1941-6, Apr 15, 1999.
[72] J. Crank, *The mathematics of diffusion*, 2d ed., Oxford, Eng: Clarendon Press, 1975.
[73] T. H. Foster, R. S. Murant, R. G. Bryant *et al.*, "Oxygen consumption and diffusion effects in photodynamic therapy," *Radiat Res,* vol. 126, no. 3, pp. 296-303, Jun, 1991.
[74] M. L. Agarwal, M. E. Clay, E. J. Harvey *et al.*, "Photodynamic therapy induces rapid cell death by apoptosis in L5178Y mouse lymphoma cells," *Cancer Res,* vol. 51, no. 21, pp. 5993-6, Nov 1, 1991.
[75] I. M. Belousova, N. G. Mironova, and M. S. Yur'ev, "A mathematical model of the photodynamic fullerene-oxygen action on biological tissues," *Optics and Spectroscopy,* vol. 98, no. 3, pp. 349-356, Mar, 2005.

[76] G. Canti, O. Marelli, L. Ricci *et al.*, "Haematoporphyrin-treated murine lymphocytes: in vitro inhibition of DNA synthesis and light-mediated inactivation of cells responsible for GVHR," *Photochem Photobiol,* vol. 34, no. 5, pp. 589-94, Nov, 1981.

[77] B. W. Henderson, S. M. Waldow, T. S. Mang *et al.*, "Tumor destruction and kinetics of tumor cell death in two experimental mouse tumors following photodynamic therapy," *Cancer Res,* vol. 45, no. 2, pp. 572-6, Feb, 1985.

[78] M. Korbelik, "Induction of tumor immunity by photodynamic therapy," *J Clin Laser Med Surg,* vol. 14, no. 5, pp. 329-34, Oct, 1996.

[79] S. J. Singer, and G. L. Nicolson, "The fluid mosaic model of the structure of cell membranes," *Science,* vol. 175, no. 4023, pp. 720-31, Feb 18, 1972.

[80] G. A. Sod, "A numerical study of oxygen diffusion in a spherical cell with the Michaelis-Menten oxygen uptake kinetics," *J Math Biol,* vol. 24, no. 3, pp. 279-89, 1986.

[81] J. Glimm, "Solutions in Large for Nonlinear Hyperbolic Systems of Equations," *Communications on Pure and Applied Mathematics,* vol. 18, no. 4, pp. 697-&, 1965.

[82] J. E. Bailey, "Biochemical-Engineering Fundamentals," *Abstracts of Papers of the American Chemical Society,* vol. 202, pp. 223-BIOT, Aug 25, 1991.

[83] M. C. Regalbuto, and W. Strieder, "Upper and Lower Bounds from the Maximum Principle - Intracellular Diffusion with Michaelis-Menten Kinetics," *Bulletin of Mathematical Biology,* vol. 51, no. 3, pp. 325-335, 1989.

[84] M. J. Mahon, M. Donowitz, C. C. Yun *et al.*, "Na+/H+ exchanger regulatory factor 2 directs parathyroid hormone 1 receptor signalling," *Nature,* vol. 417, no. 6891, pp. 858-861, Jun 20, 2002.

[85] S. Waldherr, J. B. Wu, and F. Allgower, "Bridging time scales in cellular decision making with a stochastic bistable switch," *Bmc Systems Biology,* vol. 4, Aug 9, 2010.

[86] J. D. Halley, F. R. Burden, and D. A. Winkler, "Stem cell decision making and critical-like exploratory networks," *Stem Cell Research,* vol. 2, no. 3, pp. 165-177, May, 2009.

[87] J. R. Porter, B. W. Andrews, and P. A. Iglesias, "A framework for designing and analyzing binary decision-making strategies in cellular systems," *Integr Biol (Camb),* vol. 4, no. 3, pp. 310-7, Mar, 2012.

[88] T. J. Perkins, and P. S. Swain, "Strategies for cellular decision-making," *Mol Syst Biol,* vol. 5, pp. 326, 2009.

[89] E. Ziv, I. Nemenman, and C. H. Wiggins, "Optimal signal processing in small stochastic biochemical networks," *PLoS One,* vol. 2, no. 10, pp. e1077, 2007.

[90] G. Tkacik, and A. M. Walczak, "Information transmission in genetic regulatory networks: a review," *J Phys Condens Matter,* vol. 23, no. 15, pp. 153102, Apr 20, 2011.

[91] P. Mehta, S. Goyal, T. Long *et al.*, "Information processing and signal integration in bacterial quorum sensing," *Mol Syst Biol,* vol. 5, pp. 325, 2009.

[92] B. W. Andrews, and P. A. Iglesias, "An information-theoretic characterization of the optimal gradient sensing response of cells," *PLoS Comput Biol,* vol. 3, no. 8, pp. e153, Aug, 2007.

[93] F. Tostevin, and P. R. ten Wolde, "Mutual information between input and output trajectories of biochemical networks," *Phys Rev Lett,* vol. 102, no. 21, pp. 218101, May 29, 2009.

[94] C. E. Shannon, "A Mathematical Theory of Communication," *Bell System Technical Journal,* vol. 27, no. 3, pp. 379-423, 1948.

[95] T. Berger, *Rate distortion theory; a mathematical basis for data compression*, Englewood Cliffs, N.J.,: Prentice-Hall, 1971.

[96] B. Ribba, T. Alarcon, K. Marron *et al.*, "The use of hybrid cellular automaton models for improving cancer therapy," *Cellular Automata, Proceedings,* vol. 3305, pp. 444-453, 2004.

[97] W. M. Sharman, C. M. Allen, and J. E. van Lier, "Role of activated oxygen species in photodynamic therapy," *Methods Enzymol,* vol. 319, pp. 376-400, 2000.

[98] E. Buytaert, M. Dewaele, and P. Agostinis, "Molecular effectors of multiple cell death pathways initiated by photodynamic therapy," *Biochim Biophys Acta,* vol. 1776, no. 1, pp. 86-107, Sep, 2007.

[99] E. Buytaert, G. Callewaert, J. R. Vandenheede *et al.*, "Deficiency in apoptotic effectors Bax and Bak reveals an autophagic cell death pathway initiated by photodamage to the endoplasmic reticulum," *Autophagy,* vol. 2, no. 3, pp. 238-40, Jul-Sep, 2006.

[100] J. G. Albeck, J. M. Burke, S. L. Spencer *et al.*, "Modeling a snap-action, variable-delay switch controlling extrinsic cell death," *PLoS Biol,* vol. 6, no. 12, pp. 2831-52, Dec 2, 2008.

[101] J. J. Tyson, W. T. Baumann, C. Chen *et al.*, "Dynamic modelling of oestrogen signalling and cell fate in breast cancer cells," *Nat Rev Cancer,* vol. 11, no. 7, pp. 523-32, Jul, 2011.

[102] I. Gkigkitzis, Y. Feng, C. Yang *et al.*, "Modeling of Oxygen Transport and Cell Killing in Type-II Photodynamic Therapy," *Photochem Photobiol*, Mar 24, 2012.

[103] I. Gkigkitzis, Y. Feng, C. Yang *et al.*, "Modeling of oxygen transport and cell killing in type-II photodynamic therapy," *Photochem Photobiol,* vol. 88, no. 4, pp. 969-77, Jul-Aug, 2012.

[104] J. S. Dysart, and M. S. Patterson, "Characterization of Photofrin photobleaching for singlet oxygen dose estimation during photodynamic therapy of MLL cells in vitro," *Phys Med Biol,* vol. 50, no. 11, pp. 2597-616, Jun 7, 2005.

[105] Y. F. Qin, D. Xing, S. M. Luo *et al.*, "Feasibility of using fluoresceinyl Cypridina luciferin analog in a novel chemiluminescence method for real-time photodynamic therapy dosimetry," *Photochem Photobiol,* vol. 81, no. 6, pp. 1534-1538, Nov-Dec, 2005.

[106] L. A. Sporn, and T. H. Foster, "Photofrin and Light Induces Microtubule Depolymerization in Cultured Human Endothelial-Cells," *Cancer Research,* vol. 52, no. 12, pp. 3443-3448, Jun 15, 1992.

[107] R. Hilf, "Mitochondria are targets of photodynamic therapy," *J Bioenerg Biomembr,* vol. 39, no. 1, pp. 85-9, Feb, 2007.

[108] J. L. Vincent, and D. De Backer, "Oxygen transport - the oxygen delivery controversy," *Intensive Care Medicine,* vol. 30, no. 11, pp. 1990-1996, Nov, 2004.

[109] I. Georgakoudi, and T. H. Foster, "Singlet oxygen- versus nonsinglet oxygen-mediated mechanisms of sensitizer photobleaching and their effects on photodynamic dosimetry," *Photochem Photobiol,* vol. 67, no. 6, pp. 612-625, Jun, 1998.

[110] T. J. Dougherty, G. Lawrence, J. H. Kaufman *et al.*, "Photoradiation in the Treatment of Recurrent Breast Carcinoma," *Journal of the National Cancer Institute,* vol. 62, no. 2, pp. 231-237, 1979.

[111] M. G. Nichols, and T. H. Foster, "Oxygen diffusion and reaction kinetics in the photodynamic therapy of multicell tumour spheroids," *Physics in Medicine and Biology,* vol. 39, no. 12, pp. 2161-81, Dec, 1994.

[112] B. J. Tromberg, A. Orenstein, S. Kimel *et al.*, "In vivo tumor oxygen tension measurements for the evaluation of the efficiency of photodynamic therapy," *Photochem Photobiol,* vol. 52, no. 2, pp. 375-85, Aug, 1990.

[113] T. S. Mang, T. J. Dougherty, W. R. Potter *et al.*, "Photobleaching of Porphyrins Used in Photodynamic Therapy and Implications for Therapy," *Photochem Photobiol,* vol. 45, no. 4, pp. 501-506, Apr, 1987.

[114] T. S. Mang, and T. J. Wieman, "Photodynamic Therapy in the Treatment of Pancreatic-Carcinoma - Dihematoporphyrin Ether Uptake and Photobleaching Kinetics," *Photochem Photobiol,* vol. 46, no. 5, pp. 853-858, Nov, 1987.

[115] S. Kimel, B. J. Tromberg, W. G. Roberts *et al.*, "Singlet oxygen generation of porphyrins, chlorins, and phthalocyanines," *Photochem Photobiol,* vol. 50, no. 2, pp. 175-83, Aug, 1989.

[116] I. Georgakoudi, M. G. Nichols, and T. H. Foster, "The mechanism of Photofrin photobleaching and its consequences for photodynamic dosimetry," *Photochem Photobiol,* vol. 65, no. 1, pp. 135-44, Jan, 1997.
[117] I. Gkigkitzis, C. Yang, Y. Feng *et al.*, "Modeling of PDT kinetics in cell killing," pp. 78860O-78860O, 2011.
[118] M. Price, N. Okan-Mensah, A. M. Santiago *et al.*, "The role of reactive oxygen species in PDT efficacy," pp. 716402-716402, 2009.
[119] Y. Luo, and D. Kessel, "Initiation of apoptosis versus necrosis by photodynamic therapy with chloroaluminum phthalocyanine," *Photochem Photobiol,* vol. 66, no. 4, pp. 479-83, Oct, 1997.
[120] M. Niedre, M. S. Patterson, and B. C. Wilson, "Direct near-infrared luminescence detection of singlet oxygen generated by photodynamic therapy in cells in vitro and tissues in vivo," *Photochem Photobiol,* vol. 75, no. 4, pp. 382-91, Apr, 2002.
[121] J. Moan, S. Sandberg, T. Christensen *et al.*, "Hematoporphyrin derivative: chemical composition, photochemical and photosensitizing properties," *Adv Exp Med Biol,* vol. 160, pp. 165-79, 1983.
[122] R. Pottier, and T. G. Truscott, "The photochemistry of haematoporphyrin and related systems," *Int J Radiat Biol Relat Stud Phys Chem Med,* vol. 50, no. 3, pp. 421-52, Sep, 1986.
[123] J. P. Henning, R. L. Fournier, and J. A. Hampton, "A Transient Mathematical-Model of Oxygen Depletion during Photodynamic Therapy," *Radiation Research,* vol. 142, no. 2, pp. 221-226, May, 1995.
[124] J. Moan, "On the Diffusion Length of Singlet Oxygen in Cells and Tissues," *Journal of Photochemistry and Photobiology B-Biology,* vol. 6, no. 3, pp. 343-347, Jul, 1990.
[125] I. Gkigkitzis, C. Austerlitz, and D. Campos, "The Effect of the Shape and Size of Gold Seeds Irradiated with Ultrasound on the Bio-heat Transfer in Tissue," *American Journal of Clinical Oncology-Cancer Clinical Trials,* vol. 35, no. 2, pp. 195-196, Apr, 2012.
[126] S. N. Olsen, "Applications of isothermal titration calorimetry to measure enzyme kinetics and activity in complex solutions," *Thermochimica Acta,* vol. 448, no. 1, pp. 12-18, Sep 1, 2006.
[127] A. P. Minton, "The influence of macromolecular crowding and macromolecular confinement on biochemical reactions in physiological media," *Journal of Biological Chemistry,* vol. 276, no. 14, pp. 10577-10580, Apr 6, 2001.
[128] M. R. King, "Apparent 2-D diffusivity in a ruffled cell membrane," *J Theor Biol,* vol. 227, no. 3, pp. 323-6, Apr 7, 2004.
[129] T. A. Massaro, and I. Fatt, "Oxygen diffusion in large single-celled organisms," *Bull Math Biophys,* vol. 31, no. 2, pp. 327-40, Jun, 1969.
[130] H. Pelicano, D. Carney, and P. Huang, "ROS stress in cancer cells and therapeutic implications," *Drug Resistance Updates,* vol. 7, no. 2, pp. 97-110, Apr, 2004.
[131] E. Hopf, "A Remark on Linear Elliptic Differential Equations of 2nd Order," *Proceedings of the American Mathematical Society,* vol. 3, no. 5, pp. 791-793, 1952.
[132] L. Nirenberg, "A Strong Maximum Principle for Parabolic Equations," *Communications on Pure and Applied Mathematics,* vol. 6, no. 2, pp. 167-177, 1953.
[133] A. Friedman, and B. Mcleod, "Blow-up of Solutions of Nonlinear Degenerate Parabolic Equations," *Archive for Rational Mechanics and Analysis,* vol. 96, no. 1, pp. 55-80, 1986.
[134] L. C. Evans, "A Strong Maximum Principle for Parabolic Systems in a Convex Set with Arbitrary Boundary," *Proceedings of the American Mathematical Society,* vol. 138, no. 9, pp. 3179-3185, Sep, 2010.
[135] D. L. McElwain, "A re-examination of oxygen diffusion in a spherical cell with Michaelis-Menten oxygen uptake kinetics," *J Theor Biol,* vol. 71, no. 2, pp. 255-63, Mar 20, 1978.
[136] L. A. Sporn, and T. H. Foster, "Photofrin and light induces microtubule depolymerization in cultured human endothelial cells," *Cancer Res,* vol. 52, no. 12, pp. 3443-8, Jun 15, 1992.

[137] J. S. Dysart, and M. S. Patterson, "Characterization of Photofrin photobleaching for singlet oxygen dose estimation during photodynamic therapy of MLL cells in vitro," *Physics in Medicine and Biology,* vol. 50, no. 11, pp. 2597-2616, Jun 7, 2005.

[138] J. Moan, and S. Sommer, "Oxygen dependence of the photosensitizing effect of hematoporphyrin derivative in NHIK 3025 cells," *Cancer Res,* vol. 45, no. 4, pp. 1608-10, Apr, 1985.

[139] B. W. Henderson, and V. H. Fingar, "Relationship of tumor hypoxia and response to photodynamic treatment in an experimental mouse tumor," *Cancer Res,* vol. 47, no. 12, pp. 3110-4, Jun 15, 1987.

[140] H. Pelicano, D. Carney, and P. Huang, "ROS stress in cancer cells and therapeutic implications," *Drug Resist Updat,* vol. 7, no. 2, pp. 97-110, Apr, 2004.

[141] J. L. Howland, *Introduction to cell physiology: information and control*, New York,: Macmillan, 1968.

[142] D. A. Gewirtz, S. E. Holt, and S. Grant, *Apoptosis and senescence in cancer chemotherapy and radiotherapy*, Totowa, N.J.: Humana Press, 2007.

[143] R. F. I. Cancho, and R. V. Sole, "Least effort and the origins of scaling in human language," *Proceedings of the National Academy of Sciences of the United States of America,* vol. 100, no. 3, pp. 788-791, Feb 4, 2003.

[144] R. Wallace, "A rate distortion approach to protein symmetry," *Biosystems,* vol. 101, no. 2, pp. 97-108, Aug, 2010.

[145] L. Gong, N. Bouaynaya, and D. Schonfeld, "Information-theoretic model of evolution over protein communication channel," *IEEE/ACM Trans Comput Biol Bioinform,* vol. 8, no. 1, pp. 143-51, Jan-Mar, 2011.

[146] E. Ben-Hur, and I. Rosenthal, "Factors affecting the photokilling of cultured Chinese hamster cells by phthalocyanines," *Radiat Res,* vol. 103, no. 3, pp. 403-9, Sep, 1985.

[147] N. Ramakrishnan, N. L. Oleinick, M. E. Clay *et al.*, "DNA lesions and DNA degradation in mouse lymphoma L5178Y cells after photodynamic treatment sensitized by chloroaluminum phthalocyanine," *Photochem Photobiol,* vol. 50, no. 3, pp. 373-8, Sep, 1989.

[148] I. Schulz, H. C. Mahler, S. Boiteux *et al.*, "Oxidative DNA base damage induced by singlet oxygen and photosensitization: recognition by repair endonucleases and mutagenicity," *Mutat Res,* vol. 461, no. 2, pp. 145-56, Oct 16, 2000.

[149] S. Tada-Oikawa, S. Oikawa, J. Hirayama *et al.*, "DNA damage and apoptosis induced by photosensitization of 5,10,15,20-tetrakis (N-methyl-4-pyridyl)-21H,23H-porphyrin via singlet oxygen generation," *Photochem Photobiol,* vol. 85, no. 6, pp. 1391-9, Nov-Dec, 2009.

[150] H. Sies, and C. F. Menck, "Singlet oxygen induced DNA damage," *Mutat Res,* vol. 275, no. 3-6, pp. 367-75, Sep, 1992.

[151] T. P. Devasagayam, S. Steenken, M. S. Obendorf *et al.*, "Formation of 8-hydroxy(deoxy)guanosine and generation of strand breaks at guanine residues in DNA by singlet oxygen," *Biochemistry,* vol. 30, no. 25, pp. 6283-9, Jun 25, 1991.

[152] E. Z. Bagci, Y. Vodovotz, T. R. Billiar *et al.*, "Bistability in apoptosis: roles of bax, bcl-2, and mitochondrial permeability transition pores," *Biophys J,* vol. 90, no. 5, pp. 1546-59, Mar 1, 2006.

[153] Y. Dogu, and J. Diaz, "Mathematical model of a network of interaction between p53 and Bcl-2 during genotoxic-induced apoptosis," *Biophys Chem,* vol. 143, no. 1-2, pp. 44-54, Jul, 2009.

[154] D. Kessel, M. Antolovich, and K. M. Smith, "The role of the peripheral benzodiazepine receptor in the apoptotic response to photodynamic therapy," *Photochem Photobiol,* vol. 74, no. 2, pp. 346-9, Aug, 2001.

[155] A. D. Garg, D. Nowis, J. Golab *et al.*, "Photodynamic therapy: illuminating the road from cell death towards anti-tumour immunity," *Apoptosis,* vol. 15, no. 9, pp. 1050-71, Sep, 2010.

[156] T. Suzuki, M. Nakagawa, A. Yoshikawa *et al.*, "The first molecular evidence that autophagy relates rimmed vacuole formation in chloroquine myopathy," *J Biochem,* vol. 131, no. 5, pp. 647-51, May, 2002.
[157] R. Scherz-Shouval, E. Shvets, and Z. Elazar, "Oxidation as a post-translational modification that regulates autophagy," *Autophagy,* vol. 3, no. 4, pp. 371-3, Jul-Aug, 2007.
[158] R. Scherz-Shouval, E. Shvets, E. Fass *et al.*, "Reactive oxygen species are essential for autophagy and specifically regulate the activity of Atg4," *EMBO J,* vol. 26, no. 7, pp. 1749-60, Apr 4, 2007.
[159] N. L. Oleinick, R. L. Morris, and I. Belichenko, "The role of apoptosis in response to photodynamic therapy: what, where, why, and how," *Photochem Photobiol Sci,* vol. 1, no. 1, pp. 1-21, Jan, 2002.
[160] B. J. Padanilam, "Cell death induced by acute renal injury: a perspective on the contributions of apoptosis and necrosis," *Am J Physiol Renal Physiol,* vol. 284, no. 4, pp. F608-27, Apr, 2003.
[161] N. Tavernarakis, "Cardiomyocyte necrosis: alternative mechanisms, effective interventions," *Biochim Biophys Acta,* vol. 1773, no. 4, pp. 480-2, Apr, 2007.
[162] P. Golstein, and G. Kroemer, "Cell death by necrosis: towards a molecular definition," *Trends Biochem Sci,* vol. 32, no. 1, pp. 37-43, Jan, 2007.
[163] C. Scaffidi, I. Schmitz, J. Zha *et al.*, "Differential modulation of apoptosis sensitivity in CD95 type I and type II cells," *J Biol Chem,* vol. 274, no. 32, pp. 22532-8, Aug 6, 1999.
[164] C. Scaffidi, I. Schmitz, P. H. Krammer *et al.*, "The role of c-FLIP in modulation of CD95-induced apoptosis," *J Biol Chem,* vol. 274, no. 3, pp. 1541-8, Jan 15, 1999.
[165] C. Scaffidi, S. Kirchhoff, P. H. Krammer *et al.*, "Apoptosis signaling in lymphocytes," *Curr Opin Immunol,* vol. 11, no. 3, pp. 277-85, Jun, 1999.
[166] D. J. Granville, C. M. Carthy, H. Jiang *et al.*, "Rapid cytochrome c release, activation of caspases 3, 6, 7 and 8 followed by Bap31 cleavage in HeLa cells treated with photodynamic therapy," *FEBS Lett,* vol. 437, no. 1-2, pp. 5-10, Oct 16, 1998.
[167] D. J. Granville, H. Jiang, B. M. McManus *et al.*, "Fas ligand and TRAIL augment the effect of photodynamic therapy on the induction of apoptosis in JURKAT cells," *Int Immunopharmacol,* vol. 1, no. 9-10, pp. 1831-40, Sep, 2001.
[168] D. J. Granville, J. G. Levy, and D. W. Hunt, "Photodynamic therapy induces caspase-3 activation in HL-60 cells," *Cell Death Differ,* vol. 4, no. 7, pp. 623-8, Oct, 1997.
[169] D. J. Granville, B. M. McManus, and D. W. Hunt, "Photodynamic therapy: shedding light on the biochemical pathways regulating porphyrin-mediated cell death," *Histol Histopathol,* vol. 16, no. 1, pp. 309-17, Jan, 2001.
[170] D. J. Granville, D. O. Ruehlmann, J. C. Choy *et al.*, "Bcl-2 increases emptying of endoplasmic reticulum Ca2+ stores during photodynamic therapy-induced apoptosis," *Cell Calcium,* vol. 30, no. 5, pp. 343-50, Nov, 2001.
[171] J. He, C. M. Whitacre, L. Y. Xue *et al.*, "Protease activation and cleavage of poly(ADP-ribose) polymerase: an integral part of apoptosis in response to photodynamic treatment," *Cancer Res,* vol. 58, no. 5, pp. 940-6, Mar 1, 1998.
[172] M. Lam, N. L. Oleinick, and A. L. Nieminen, "Photodynamic therapy-induced apoptosis in epidermoid carcinoma cells. Reactive oxygen species and mitochondrial inner membrane permeabilization," *J Biol Chem,* vol. 276, no. 50, pp. 47379-86, Dec 14, 2001.
[173] L. J. Marnett, "The Role of Oxygen-Free Radicals in Carcinogenesis," *Japanese Journal of Toxicology and Environmental Health,* vol. 39, no. 2, pp. P28-P31, Apr, 1993.
[174] W. X. Zong, and C. B. Thompson, "Necrotic death as a cell fate," *Genes Dev,* vol. 20, no. 1, pp. 1-15, Jan 1, 2006.

[175] R. W. G. Watson, H. P. Redmond, J. H. Wang *et al.*, "Human Neutrophil Apoptosis Is Induced by an Oxygen-Dependent Mechanism," *British Journal of Surgery,* vol. 82, no. 5, pp. 703-704, May, 1995.
[176] P. Agostinis, E. Buytaert, H. Breyssens *et al.*, "Regulatory pathways in photodynamic therapy induced apoptosis," *Photochem Photobiol Sci,* vol. 3, no. 8, pp. 721-9, Aug, 2004.
[177] R. D. Almeida, B. J. Manadas, A. P. Carvalho *et al.*, "Intracellular signaling mechanisms in photodynamic therapy," *Biochim Biophys Acta,* vol. 1704, no. 2, pp. 59-86, Sep 20, 2004.
[178] R. D. Almeida, E. R. Gomes, A. P. Carvalho *et al.*, "Calpains are activated by photodynamic therapy but do not contribute to apoptotic tumor cell death," *Cancer Lett,* vol. 216, no. 2, pp. 183-9, Dec 28, 2004.
[179] M. R. Hamblin, and E. L. Newman, "On the mechanism of the tumour-localising effect in photodynamic therapy," *J Photochem Photobiol B,* vol. 23, no. 1, pp. 3-8, Apr, 1994.
[180] B. W. Henderson, and J. M. Donovan, "Release of prostaglandin E2 from cells by photodynamic treatment in vitro," *Cancer Res,* vol. 49, no. 24 Pt 1, pp. 6896-900, Dec 15, 1989.
[181] S. Evans, W. Matthews, R. Perry *et al.*, "Effect of photodynamic therapy on tumor necrosis factor production by murine macrophages," *J Natl Cancer Inst,* vol. 82, no. 1, pp. 34-9, Jan 3, 1990.
[182] U. O. Nseyo, R. K. Whalen, M. R. Duncan *et al.*, "Urinary cytokines following photodynamic therapy for bladder cancer. A preliminary report," *Urology,* vol. 36, no. 2, pp. 167-71, Aug, 1990.
[183] G. Canti, P. Franco, O. Marelli *et al.*, "Hematoporphyrin derivative rescue from toxicity caused by chemotherapy or radiation in a murine leukemia model (L1210)," *Cancer Res,* vol. 44, no. 4, pp. 1551-6, Apr, 1984.
[184] A. P. Castano, P. Mroz, and M. R. Hamblin, "Photodynamic therapy and anti-tumour immunity," *Nat Rev Cancer,* vol. 6, no. 7, pp. 535-45, Jul, 2006.
[185] S. Coutier, L. Bezdetnaya, S. Marchal *et al.*, "Foscan (mTHPC) photosensitized macrophage activation: enhancement of phagocytosis, nitric oxide release and tumour necrosis factor-alpha-mediated cytolytic activity," *Br J Cancer,* vol. 81, no. 1, pp. 37-42, Sep, 1999.
[186] M. Djavaheri-Mergny, M. C. Maiuri, and G. Kroemer, "Cross talk between apoptosis and autophagy by caspase-mediated cleavage of Beclin 1," *Oncogene,* vol. 29, no. 12, pp. 1717-9, Mar 25, 2010.
[187] W. Martinet, and G. R. De Meyer, "Autophagy in atherosclerosis: a cell survival and death phenomenon with therapeutic potential," *Circ Res,* vol. 104, no. 3, pp. 304-17, Feb 13, 2009.
[188] W. Martinet, P. Agostinis, B. Vanhoecke *et al.*, "Autophagy in disease: a double-edged sword with therapeutic potential," *Clin Sci (Lond),* vol. 116, no. 9, pp. 697-712, May, 2009.
[189] R. K. Amaravadi, and C. B. Thompson, "The roles of therapy-induced autophagy and necrosis in cancer treatment," *Clin Cancer Res,* vol. 13, no. 24, pp. 7271-9, Dec 15, 2007.
[190] A. L. Edinger, and C. B. Thompson, "Death by design: apoptosis, necrosis and autophagy," *Current Opinion in Cell Biology,* vol. 16, no. 6, pp. 663-669, 2004.
[191] R. B. Moore, Z. Xiao, J. Tulip *et al.*, "A comparison of susceptibility to photodynamic treatment between endothelial and tumor cells in vitro and in vivo," *Photodiagnosis and Photodynamic Therapy,* vol. 4, no. 3, pp. 160-169, 2007.
[192] X. Bao, J. Cui, Y. Wu *et al.*, "The roles of endogenous reactive oxygen species and nitric oxide in triptolide-induced apoptotic cell death in macrophages," *J Mol Med (Berl),* vol. 85, no. 1, pp. 85-98, Jan, 2007.
[193] H. R. Wilson, and J. D. Cowan, "Excitatory and Inhibitory Interactions in Localized Populations of Model Neurons," *Biophysical Journal,* vol. 12, no. 1, pp. 1-&, 1972.
[194] L. Glass, "Combinatorial and Topological Methods in Nonlinear Chemical-Kinetics," *Journal of Chemical Physics,* vol. 63, no. 4, pp. 1325-1335, 1975.

[195] E. Mjolsness, D. H. Sharp, and J. Reinitz, "A Connectionist Model of Development," *Journal of Theoretical Biology,* vol. 152, no. 4, pp. 429-453, Oct 21, 1991.
[196] J. J. Tyson, and B. Novak, "Functional Motifs in Biochemical Reaction Networks," *Annual Review of Physical Chemistry, Vol 61,* vol. 61, pp. 219-240, 2010.
[197] R. E. Blahut, "Computation of Channel Capacity and Rate-Distortion Functions," *Ieee Transactions on Information Theory,* vol. 18, no. 4, pp. 460-+, 1972.
[198] L. Hörmander, *The analysis of linear partial differential operators*, 2nd ed., Berlin ; New York: Springer-Verlag, 1990.
[199] A. Gersho, and R. M. Gray, *Vector quantization and signal compression*, Boston: Kluwer Academic Publishers, 1992.
[200] J. E. Ferrell, and E. M. Machleder, "The biochemical basis of an all-or-none cell fate switch in Xenopus oocytes," *Science,* vol. 280, no. 5365, pp. 895-898, May 8, 1998.
[201] C. P. Bagowski, J. Besser, C. R. Frey *et al.*, "The JNK cascade as a biochemical switch in mammalian cells: ultrasensitive and all-or-none responses," *Curr Biol,* vol. 13, no. 4, pp. 315-20, Feb 18, 2003.
[202] J. Winther, "Photodynamic therapy effect in an intraocular retinoblastoma-like tumour assessed by an in vivo to in vitro colony forming assay," *Br J Cancer,* vol. 59, no. 6, pp. 869-72, Jun, 1989.
[203] E. Ben-Hur, I. Rosenthal, and C. C. Leznoff, "Recovery of Chinese hamster cells following photosensitization by zinc tetrahydroxyphthalocyanine," *J Photochem Photobiol B,* vol. 2, no. 2, pp. 243-52, Sep, 1988.
[204] S. H. Selman, M. Kreimer-Birnbaum, K. Chaudhuri *et al.*, "Photodynamic treatment of transplantable bladder tumors in rodents after pretreatment with chloroaluminum tetrasulfophthalocyanine," *J Urol,* vol. 136, no. 1, pp. 141-5, Jul, 1986.
[205] J. Savickiene, G. Treigyte, C. Aleksandraviciene *et al.*, "Low-dose ionizing radiation effects on differentiation of HL-60 cells," *Central European Journal of Biology,* vol. 5, no. 5, pp. 600-612, Oct, 2010.
[206] B. Wilson, V. V. Tuchin, S. Tanev *et al.*, *Advances in biophotonics*, Amsterdam ; Washington, DC: IOS Press, 2005.
[207] J. Gunawardena, "Signals and systems: Towards a systems biology of signal transduction," *Proceedings of the Ieee,* vol. 96, no. 8, pp. 1386-1397, Aug, 2008.
[208] W. W. Chen, M. Niepel, and P. K. Sorger, "Classic and contemporary approaches to modeling biochemical reactions," *Genes Dev,* vol. 24, no. 17, pp. 1861-75, Sep 1, 2010.
[209] M. A. Smith, E. Blankman, M. L. Gardel *et al.*, "A zyxin-mediated mechanism for actin stress fiber maintenance and repair," *Dev Cell,* vol. 19, no. 3, pp. 365-76, Sep 14, 2010.
[210] D. C. Cabelof, S. Yanamadala, J. J. Raffoul *et al.*, "Caloric restriction promotes genomic stability by induction of base excision repair and reversal of its age-related decline," *DNA Repair (Amst),* vol. 2, no. 3, pp. 295-307, Mar 1, 2003.
[211] J. A. Stuart, B. Karahalil, B. A. Hogue *et al.*, "Mitochondrial and nuclear DNA base excision repair are affected differently by caloric restriction," *FASEB J,* vol. 18, no. 3, pp. 595-7, Mar, 2004.
[212] M. Dean, T. Fojo, and S. Bates, "Tumour stem cells and drug resistance," *Nature Reviews Cancer,* vol. 5, no. 4, pp. 275-284, Apr, 2005.
[213] Z. Zeng, T. Huang, and W. X. Zheng, "Multistability of recurrent neural networks with time-varying delays and the piecewise linear activation function," *IEEE Trans Neural Netw,* vol. 21, no. 8, pp. 1371-7, Aug, 2010.
[214] J. Dahle, S. Bagdonas, O. Kaalhus *et al.*, "The bystander effect in photodynamic inactivation of cells," *Biochimica Et Biophysica Acta-General Subjects,* vol. 1475, no. 3, pp. 273-280, Jul 26, 2000.

[215] J. Dahle, O. Kaalhus, T. Stokke *et al.*, "Bystander effects may modulate ultraviolet A and B radiation-induced delayed mutagenesis," *Radiation Research,* vol. 163, no. 3, pp. 289-295, Mar, 2005.

[216] J. Dahle, E. Angell-Petersen, H. B. Steen *et al.*, "Bystander effects in cell death induced by photodynamic treatment UVA radiation and inhibitors of ATP synthesis," *Photochem Photobiol,* vol. 73, no. 4, pp. 378-87, Apr, 2001.

[217] S. A. Lorimore, and E. G. Wright, "Radiation-induced genomic instability and bystander effects: related inflammatory-type responses to radiation-induced stress and injury? A review," *Int J Radiat Biol,* vol. 79, no. 1, pp. 15-25, Jan, 2003.

[218] C. Mothersill, and C. B. Seymour, "Cell-cell contact during gamma irradiation is not required to induce a bystander effect in normal human keratinocytes: evidence for release during irradiation of a signal controlling survival into the medium," *Radiat Res,* vol. 149, no. 3, pp. 256-62, Mar, 1998.

[219] H. Nikjoo, and I. K. Khvostunov, "A theoretical approach to the role and critical issues associated with bystander effect in risk estimation," *Hum Exp Toxicol,* vol. 23, no. 2, pp. 81-6, Feb, 2004.

[220] O. V. Belyakov, M. Folkard, C. Mothersill *et al.*, "A proliferation-dependent bystander effect in primary porcine and human urothelial explants in response to targeted irradiation," *Br J Cancer,* vol. 88, no. 5, pp. 767-74, Mar 10, 2003.

[221] J. E. Trosko, and R. J. Ruch, "Cell-cell communication in carcinogenesis," *Front Biosci,* vol. 3, pp. d208-36, Feb 15, 1998.

[222] H. Nikjoo, and I. K. Khvostunov, "Biophysical model of the radiation-induced bystander effect," *Int J Radiat Biol,* vol. 79, no. 1, pp. 43-52, Jan, 2003.

[223] W. J. McGill, "Multivariate Information Transmission," *Psychometrika,* vol. 19, no. 2, pp. 97-116, Jun, 1954.

[224] L. Leydesdorff, "Interaction information: linear and nonlinear interpretations," *International Journal of General Systems,* vol. 38, no. 6, pp. 681-685, 2009.

[225] A. Jakulin, and I. Bratko, "Analyzing attribute dependencies," *Knowledge Discovery in Databases: Pkdd 2003, Proceedings,* vol. 2838, pp. 229-240, 2003.

[226] N. J. Cerf, and C. Adami, "Entropic Bell inequalities," *Physical Review A,* vol. 55, no. 5, pp. 3371-3374, May, 1997.

[227] N. Brenner, S. P. Strong, R. Koberle *et al.*, "Synergy in a neural code," *Neural Computation,* vol. 12, no. 7, pp. 1531-1552, Jul, 2000.

[228] M. Grabisch, and M. Roubens, "An axiomatic approach to the concept of interaction among players in cooperative games," *International Journal of Game Theory,* vol. 28, no. 4, pp. 547-565, Nov, 1999.

[229] R. A. Morgan, "Live and Let Die: A New Suicide Gene Therapy Moves to the Clinic," *Mol Ther,* vol. 20, no. 1, pp. 11-13, 2012.

[230] A. Di Stasi, S. K. Tey, G. Dotti *et al.*, "Inducible apoptosis as a safety switch for adoptive cell therapy," *N Engl J Med,* vol. 365, no. 18, pp. 1673-83, Nov 3, 2011.

[231] G. Ledder, J. D. Logan, and A. Joern, "Dynamic energy budget models with size-dependent hazard rates," *Journal of Mathematical Biology,* vol. 48, no. 6, pp. 605-622, Jun, 2004.

[232] R. C. Burns, and A. D. Lawson, "Quantized Probability Circuit Design Principles Applied to Linear Circuits," *Ieee Transactions on Reliability,* vol. R 13, no. 2, pp. 16-&, 1964.

[233] Y. M. Lomsadze, "Relativistically Invariant Formulation of Theory of Quantized Probability Amplitude Field," *Nuclear Physics,* vol. 37, no. 1, pp. 147-&, 1962.

[234] B. Kuipers, "Qualitative Reasoning - Modeling and Simulation with Incomplete Knowledge," *Automatica,* vol. 25, no. 4, pp. 571-585, Jul, 1989.

[235] J. G. Miller, *Living systems*, Niwot, Colo.: University Press of Colorado, 1995.

[236] H. Gardner, *The mind's new science : a history of the cognitive revolution*, New York: Basic Books, 1985.
[237] R. E. Babe, *Information and communication in economics*, Boston: Kluwer Academic Publishers, 1994.
[238] J. Boyle, *Shamans, software, and spleens : law and the construction of the information society*, Cambridge, Mass.: Harvard University Press, 1996.
[239] !!! INVALID CITATION !!!
[240] G. Link, and ebrary Inc., "One hundred years of Russell's paradox mathematics, logic, philosophy," *De Gruyter series in logic and its applications 6*, Walter de Gruyter,, 2004, pp. ix, 662 p.
[241] J. Van Heijenoort, *From Frege to Gödel; a source book in mathematical logic, 1879-1931*, Cambridge,: Harvard University Press, 1967.
[242] K. Simmons, "Sets, classes and extensions: A singularity approach to Russell's paradox," *Philosophical Studies,* vol. 100, no. 2, pp. 109-149, Aug, 2000.
[243] W. V. Quine, "On the Consistency of New Foundations," *Proceedings of the National Academy of Sciences of the United States of America,* vol. 37, no. 8, pp. 538-540, 1951.
[244] E. P. Specker, "The Axiom of Choice in Quine New Foundations for Mathematical Logic," *Proceedings of the National Academy of Sciences of the United States of America,* vol. 39, no. 9, pp. 972-975, 1953.
[245] P. Vop*enka, *Mathematics in the alternative set theory*, 1. Aufl. ed., Leipzig: B. G. Teubner, 1979.
[246] J. von Neumann, "An axiomatization of set theory," *Aut Aut*, no. 280-81, pp. 107-123, Jul-Oct, 1997.
[247] G. Priest, *Beyond the limits of thought*, Oxford: Clarendon/Oxford University Press, 2002.
[248] N. Wheatley, "A sorites paradox in the conventional definition of amount of substance," *Metrologia,* vol. 48, no. 3, pp. L17-L21, Jun, 2011.
[249] S. Kalyanasundaram, E. K. P. Chong, and N. B. Shroff, "Markov decision processes with uncertain transition rates: Sensitivity and max hyphen min control," *Asian Journal of Control,* vol. 6, no. 2, pp. 253-269, Jun, 2004.
[250] P. Chesson, "Predator-Prey Theory and Variability," *Annual Review of Ecology and Systematics,* vol. 9, pp. 323-347, 1978.
[251] M. S. Bartlett, "On Theoretical Models for Competitive and Predatory Biological Systems," *Biometrika,* vol. 44, no. 1-2, pp. 27-42, 1957.
[252] P. H. Leslie, "A Stochastic Model for Studying the Properties of Certain Biological Systems by Numerical Methods," *Biometrika,* vol. 45, no. 1-2, pp. 16-31, 1958.
[253] B. Perthame, and M. Gauduchon, "Survival thresholds and mortality rates in adaptive dynamics: conciliating deterministic and stochastic simulations," *Mathematical Medicine and Biology-a Journal of the Ima,* vol. 27, no. 3, pp. 195-210, Sep, 2010.
[254] N. Champagnat, "A microscopic interpretation for adaptive dynamics trait substitution sequence models," *Stochastic Processes and Their Applications,* vol. 116, no. 8, pp. 1127-1160, Aug, 2006.
[255] R. Ferriere, J. L. Bronstein, S. Rinaldi *et al.*, "Cheating and the evolutionary stability of mutualisms," *Proceedings of the Royal Society B-Biological Sciences,* vol. 269, no. 1493, pp. 773-780, Apr 22, 2002.
[256] K. Masutani, "Effects of survival thresholds upon one-dimensional dynamics of single-species populations," *Bulletin of Mathematical Biology,* vol. 55, no. 1, pp. 1-13, 1993.
[257] S. Graf, H. Luschgy, and G. Pages, "The Local Quantization Behavior of Absolutely Continuous Probabilities," *Annals of Probability,* vol. 40, no. 4, pp. 1795-1828, Jul, 2012.
[258] R. M. Gray, and D. L. Neuhoff, "Quantization," *Ieee Transactions on Information Theory,* vol. 44, no. 6, pp. 2325-2383, Oct, 1998.

[259] C. E. Shannon, “A Mathematical Theory of Communication,” *Bell System Technical Journal,* vol. 27, no. 4, pp. 623-656, 1948.
[260] G. N. Ling, “The New Cell Physiology - an Outline, Presented against Its Full Historical Background, Beginning from the Beginning,” *Physiological Chemistry and Physics and Medical Nmr,* vol. 26, no. 2, pp. 121-203, 1994.
[261] G. N. Ling, “Physical State of Water in Living Cell and Model Systems,” *Annals of the New York Academy of Sciences,* vol. 125, no. A2, pp. 401-&, 1965.
[262] G. N. Ling, “A Physical Theory of the Living State - Application to Water and Solute Distribution,” *Scanning Microscopy,* vol. 2, no. 2, pp. 899-913, Jun, 1988.
[263] G. Ling, “Nano-protoplasm: the ultimate unit of life,” *Physiol Chem Phys Med NMR,* vol. 39, no. 2, pp. 111-234, 2007.
[264] S. Maddika, S. R. Ande, S. Panigrahi *et al.*, “Cell survival, cell death and cell cycle pathways are interconnected: implications for cancer therapy,” *Drug Resist Updat,* vol. 10, no. 1-2, pp. 13-29, Feb-Apr, 2007.
[265] R. Arditi, and L. R. Ginzburg, “Coupling in Predator Prey Dynamics - Ratio-Dependence,” *Journal of Theoretical Biology,* vol. 139, no. 3, pp. 311-326, Aug 9, 1989.
[266] R. Arditi, and A. A. Berryman, “The Biological-Control Paradox,” *Trends in Ecology & Evolution,* vol. 6, no. 1, pp. 32-32, Jan, 1991.
[267] H. I. Freedman, and P. Waltman, “Persistence in Models of 3 Interacting Predator-Prey Populations,” *Mathematical Biosciences,* vol. 68, no. 2, pp. 213-231, 1984.
[268] G. W. Harrison, “Global Stability of Predator-Prey Interactions,” *Journal of Mathematical Biology,* vol. 8, no. 2, pp. 159-171, 1979.
[269] D. Mitra, D. Mukherjee, A. B. Roy *et al.*, “Permanent Coexistence in a Resource-Based Competition System,” *Ecological Modelling,* vol. 60, no. 1, pp. 77-85, Jan, 1992.
[270] S. B. Hsu, “On a Resource Based Ecological Competition Model with Interference,” *Journal of Mathematical Biology,* vol. 12, no. 1, pp. 45-52, 1981.
[271] A. Juzeniene, K. P. Nielsen, and J. Moan, “Biophysical aspects of photodynamic therapy,” *Journal of Environmental Pathology Toxicology and Oncology,* vol. 25, no. 1-2, pp. 7-28, 2006.
[272] G. Shani, L. Marash, D. Gozuacik *et al.*, “Death-associated protein kinase phosphorylates ZIP kinase, forming a unique kinase hierarchy to activate its cell death functions,” *Mol Cell Biol,* vol. 24, no. 19, pp. 8611-26, Oct, 2004.
[273] M. M. Ali, T. Bagratuni, E. L. Davenport *et al.*, “Structure of the Ire1 autophosphorylation complex and implications for the unfolded protein response,” *EMBO J,* vol. 30, no. 5, pp. 894-905, Mar 2, 2011.
[274] T. Alarcon, H. M. Byrne, and P. K. Maini, “A multiple scale model for tumor growth,” *Multiscale Modeling & Simulation,* vol. 3, no. 2, pp. 440-475, 2005.
[275] J. J. Tyson, W. T. Baumann, C. Chen *et al.*, “Dynamic modelling of oestrogen signalling and cell fate in breast cancer cells,” *Nature Reviews Cancer,* vol. 11, no. 7, pp. 523-532, Jul, 2011.

[277] Goldsmith, Alfred N., “Quantized Probability” Physical Review, vol. 64, Issue 11-12, pp. 376-377
[278] Wang I,“Photodynamic therapy and laser-based diagnostic studies of malignant tumors”, Ph.D. Thesis. Lund: Lund University, 1999, ISBN: 9162833529, 210p .
[279] M.J. Mahon, et al. Nature (2002) “Na+/H+ exchanger regulatory factor 2 directs parathyroid hormone 1 receptor signalling.” Vol. 417:858-861.
[280] Georgakoudi, “Effects of photosensitizer bleaching and localization on Photodynamic Oxygen consumption and dosimetry”, Thesis, 1998
[281] Colyvan Mark,”Vagueness and Truth”, in H. Dyke (ed.), From Truth to Reality: New Essays in Logic and Metaphysics, Routledge, 2009, pp. 29–40.